The Henryk Niewodniczański
INSTITUTE OF NUCLEAR PHYSICS
Polish Academy of Sciences
ul. Radzikowskiego 152, 31-342, Kraków, Poland

Report No. 2040/PH

STRONG AND ELECTROMAGNETIC EFFECTS IN PERIPHERAL NUCLEUS-NUCLEUS COLLISIONS AT SPS ENERGIES

Andrzej Rybicki

Habilitation Thesis

Mojej żonie

Abstract

This paper deals with low momentum transfer ("soft") hadronic interactions which build up most of the total cross section in high energy collisions of hadrons or atomic nuclei. The quantitative features of these interactions cannot be predicted on the basis of the present theory of strong interactions, Quantum Chromodynamics. The understanding of these processes relies therefore mostly on experimental knowledge.

The main emphasis in this work is put on an attempt to extract new, quantitative information on the process of particle production in the reaction center-of-mass energy regime of several GeV per incoming hadron. This specifically concerns two issues: 1) the change induced in this process by transition from the elementary nucleon-nucleon collision to the nuclear heavy ion reaction, and 2) the possibility of obtaining novel information on the strong interaction on the basis of specific electromagnetic processes.

Both issues are studied by means of a new, high quality experimental dataset on π meson production in peripheral lead-lead collisions. This dataset is compared with equally precise reference data on elementary interactions, allowing for the disentanglement of several effects present in the nuclear collision. One of these effects, the electromagnetic interaction between produced particles and the highly charged nuclear remnant ("spectator system") is subsequently subject to a phenomenological analysis. The results of this analysis suggest that the latter electromagnetic effect can provide new information on the space-time evolution of the reaction.

Contents

Chapter 1

Introduction

This paper deals with the process of particle production in low momentum transfer ("soft") hadronic interactions. The work presented here concentrates on two main issues, namely: 1) the change induced in particle production by the transition from the elementary (nucleon-nucleon) interaction to the nuclear (heavy ion) collision, and 2) the possibility of using a specific electromagnetic effect as a probe of the space-time evolution of the nuclear reaction.

The main attention of this paper is devoted to peripheral collisions of lead ions (Pb+Pb) at the center-of-mass energy per incoming nucleon pair equal to $\sqrt{s_{NN}} = 17.3$ GeV. Here, a new high quality dataset on π meson production, obtained by the NA49 experiment at the CERN Super Proton Synchrotron (SPS) will be introduced. This dataset will serve as a basis for a comparative study of particle production in nuclear reactions relative to elementary collisions. This study will be put in a broader context of several other analyses.

Particular attention will be devoted to a specific phenomenon present in nuclear collisions, namely the electromagnetic interaction between produced particles and the highly charged nuclear remnant ("spectator system"). A phenomenological analysis of this effect will be presented, aimed at studying its possible usefulness as an independent source of information on the space-time evolution of particle production in soft hadronic interactions.

The present Chapter describes the motivation of this study in the general context of the present situation in soft hadronic physics. Subsequently, the strategy of the analysis and its main objectives are discussed. The contribution of the author is shortly enumerated.

1.1 Motivation: Soft Hadronic Physics

By *high energy hadronic and nuclear reactions* one usually means collisions of hadrons with hadrons, hadrons with atomic nuclei, and atomic nuclei with atomic nuclei at energies of several or more gigaelectronvolts (1 GeV=10^9 eV) per each incoming nucleon. These processes are the domain of the fundamental *strong interaction*, responsible also for such phenomena as, e.g., the *confinement* of quarks into hadrons and the existence of the atomic nucleus as a bound system of protons and neutrons.

An overwhelming majority of processes occurring in high energy hadronic and nuclear reactions involves strong interactions with low transfer of momentum between particles in the initial and the final state of the reaction. These so called "soft" processes have a specific feature which differentiates them from other physical phenomena. Indeed, they cannot be quantitatively described, nor predicted, on the basis of the present theory of the strong interaction, *Quantum Chromodynamics* (QCD). This is due to the large value of the strong coupling constant, α_s, which precludes the use of quantum mechanical perturbation theory.

This situation is different, and far more difficult, than for processes involving the electromagnetic interaction, where the coupling constant remains small. As a consequence, our knowledge of

high energy collisions of hadrons and nuclei, as well as many other processes, remains fundamentally limited. Since many decades, the scientific description of such soft (or non-perturbative) processes has been the domain of *phenomenology* rather then pure *theory*. To be more specific, the principal tool for this description have been *phenomenological models of soft processes*, most often based on QCD, but additionally supplemented with more or less arbitrary assumptions about the nature of the process under study. The general idea underlying such an approach was that experimental information (*experimental data*) could be used to differentiate the right assumptions from the wrong ones, and to eliminate the latter.

Taken most generally, the overall collection of phenomenological models that appeared on the market during, say, the last half-century makes a very large set, far beyond the scope of the present paper. It is nevertheless instructive to list here a few examples, be it only to illustrate the different approaches to the understanding of the soft interaction occurring in high energy collisions of hadrons and nuclei, as well as of the principal phenomenon which takes place in these reactions. This phenomenon is *the multiparticle final state*, that is, the production of many new particles, mostly π mesons, with typically low values of "transverse" momentum (momentum component perpendicular to the original collision axis).

An arbitrary, and somewhat naive, selection of phenomenological approaches would include first the Regge method, a very fruitful phenomenology prior to QCD, and based on the exchange of "Regge trajectories" [Białkowski71, Białkowski72, Perkins89]. The next class would be the statistical models, assuming the thermal emission of secondary particles in the course of the reaction. These start from Fermi [Fermi51]; an eminent example is the model of Hagedorn (see, e.g., [Hagedorn84]). Of prime importance are the parton models [Fiałkowski83], based on the general idea that the internal (quark-gluon) structure of the hadron will find its reflection is soft hadronic reactions. Here the Dual Parton Model (DPM, [Capella94]), based on colour exchange between the constituents of the colliding hadrons (nuclei), and subsequent fragmentation of "colour strings" should definitely be quoted. And finally, one should separately mention the very important "Wounded Nucleon Model" by Białas, Bleszyński and Czyż [Białas76], where particle production in nuclear (proton-nucleus, nucleus-nucleus) reactions is assumed to be proportional to the number of "wounded" nucleons which have undergone at least one inelastic nucleon-nucleon collision. In spite of its extreme simplicity, this model has numerous successful applications in nuclear collision studies, some of which will be addressed in subsequent Chapters.

For the author of the present paper (born in 1971), it is not that easy to exactly trace the evolution of the soft hadronic field over the many decades of its existence. Evidently during numerous years, studies of soft interactions in hadronic and nuclear reactions were a subject of prime importance in the general field of High Energy Physics, and were considered as very attractive still in 1983 [Fiałkowski83]. Subsequently, however, the majority of the High Energy Physics community turned towards other challenges (like e.g. e^+e^- physics at LEP at CERN), leaving the non-perturbative strong interaction field to a large extent out of the "main stream" of physics. This happened in spite of the fact that unambiguous, model-independent answers to numerous fundamental questions (like e.g., on the exact role of quark constituents of the hadron in particle production in hadronic reactions), were still missing, and that the existing experimental information on hadronic and nuclear reactions was doubtlessly versatile but very far from complete. It should be said, however, that one important exception to this somewhat "negative" picture of the evolution of the field existed. This exception was the search for the *Quark-Gluon Plasma*.

Most generally, the hypothesis of the Quark-Gluon Plasma (QGP, see very simple description in [Mrówczyński98]) postulated that in heavy ion collisions at high enough energies, a *phase transition* might occur from "normal" nuclear matter (quarks and gluons confined in protons and neutrons) into a new state of *deconfined* quarks and gluons. This unstable new state of matter would later expand, cool down and thus "come back" to the "normal" confined hadronic

multiparticle final state, but *preserving the memory of its intermediate, deconfined phase.* This way, the latter deconfined phase would become experimentally observable by a set of specific "signatures", that is, features of final state particle production which would be different from these characteristic to normal nuclear matter, available in e.g. proton-proton or proton-nucleus collisions[1].

Only in the last two decades, the search for the QGP motivated large projects involving a number of experiments: at the Alternating Gradient Synchrotron (AGS) at the Brookhaven National Laboratory (BNL), at the Super Proton Synchrotron (SPS) at CERN, at the Relativistic Heavy Ion Collider (RHIC) at BNL, and finally at the presently starting Large Hadron Collider (LHC) at CERN. It is worthwhile to mention that both the SPS and RHIC scientific communities have actually claimed to have discovered a state of matter which could be identified as the QGP, respectively in 2000 [Heinz00] and 2005 [Bnl05]. To what extent are such claims unambiguous is a very important subject for discussion [Fischer03, Trzupek06].

However, the study of strong and electromagnetic interactions made in the present paper touches the problem of Quark-Gluon Plasma formation only indirectly. In fact, the main motivation for this study is the conviction of the author that the *general* situation of the field of soft hadronic physics is quite unsatisfactory. While the issue of QGP production is certainly one of the most fundamental problems in science, with deep repercussions on the understanding of strong interactions, cosmology, etc., it seems that a more general, "wide-scope" investigation of soft interactions is at the present moment very highly indicated, be it only for the very considerable progress in detector and data processing techniques, which results in the possibility of obtaining much more complete and much more precise experimental information. Once gathered, this information could very considerably limit the uncertainties present at the moment in the soft hadronic sector, and possibly shed new light on the non-perturbative strong interaction. Thus, the present analysis constitutes an attempt to collect some of this information, and to study the potential possibilities of obtaining new information from specific processes present in heavy ion collisions.

Several main lines can be pointed which should be followed by the wide-scope study of soft interactions postulated above:

1. *Completeness of experimental information.* The present necessity of phenomenological models to rely on arbitrary assumptions can be strongly limited with properly complete, large statistics experimental datasets. Ideally, such datasets should cover the total range of phase space (p_x, p_y, p_z) available to final state particles. The latter particles should be precisely identified. This way, the role of the various assumed mechanisms over the phase space of each final state particle could be followed in detail.

2. *Versatility.* Further limitations on models can be brought if the new experimental data include a maximally versatile body of different reactions, like e.g., interactions involving different hadron projectiles and targets at different collision energies[2]. Special attention should be devoted to the *transition from the elementary to the nuclear reaction*, a subject of prime importance in view of any claim of a qualitatively new state of matter (like the QGP) being produced in heavy ion collisions. Here, the optimal information could be provided by a direct comparative study of hadron-hadron, hadron-nucleus and nucleus-nucleus reactions measured by the same detector in a similar, wide range of phase space, and at the same energy per incoming nucleon.

---

[1]A comprehensive description of the most important signatures of QGP formation can be found, e.g., in [Trzupek06].

[2]For clarity, this paper follows the historical convention originating from fixed target experiments, specifying the two colliding objects always as "projectile" and "target".

3. *Deeper insight into the mechanism of particle production.* Finally, attempts should be made at the extraction of model-independent information going deeper than just the final (p_x, p_y, p_z) state of the reaction observed in the experiment. For instance, any observable that could possibly provide direct, assumption-free information on the evolution of the process of particle production in space and time (x, y, z, t) should be most carefully examined. This specifically concerns electromagnetic phenomena present in the reaction which could preserve a "memory" of the evolution of non-perturbative processes. Account taken of our very precise knowledge of the electromagnetic force, this "memory" could then become directly accessible to analysis.

Although in principle focussed on π meson production in peripheral Pb+Pb collisions, the analysis presented here constitutes an attempt to respond to the postulates **1.**, **2.**, **3.** formulated above. As such, it is hoped to broaden the available experimental and phenomenological knowledge on soft hadronic interactions *in general*. It also hoped that the information extracted from peripheral heavy ion interactions will provide a basis to be possibly further exploited in analyses of other production phenomena as well as hadron-hadron and hadron-nucleus reactions. The precise strategy of this study as well as its detailed justification will be presented below.

1.2 Strategy

A large part of the present paper will be devoted to peripheral Pb+Pb collisions. The term "peripheral" requires some clarification. For the specific purpose of the present analysis, peripheral heavy ion reactions can be defined as these characterized by an impact parameter b, Fig. 1.1, typically comparable to twice the standard root-mean-square radius[3] of the colliding nuclei:

$$ b \ \approx \ 2 \cdot < r^2 >^{\frac{1}{2}} \tag{1.1} $$

For two colliding lead nuclei, this gives typical impact parameters of about 11 fm. A schematic illustration of such a reaction is drawn in Fig. 1.1. Several advantages suggest the use of such peripheral Pb+Pb reactions as a valuable source of versatile information on soft hadron production processes:

- As it will be explained in Chapters 2 and 3, such events correspond to typically 50-60 participating nucleons, each of them suffering on the average 2-3 elementary nucleon-nucleon collisions. This constitutes an optimal "intermediate stage" between the pure elementary process (two nucleons, each suffering one collision) and the most "central" heavy ion reaction ($\sim$350 nucleons, each suffering typically 4-5 collisions).

- On the other hand, the presence of two large surviving spectator systems of about 180 nucleons each offers the possibility of investigating interactions with the nuclear remnants as well as processes characteristic of the break-up of the latter spectator systems.

- Finally, the net charge of the spectator systems of about 70 elementary units results in a sizeable electromagnetic field which will modify the trajectories of the produced charged hadrons, in particular π^+ and π^- mesons. The presence of this electromagnetic field may possibly be exploited in order to obtain information on the space-time evolution of the hadron production process.

---

[3]The root-mean-square radius in Eq. (1.1) follows the definition $< r^2 >^{\frac{1}{2}} = \sqrt{\frac{\int r^2 \rho(r) dV}{\int \rho(r) dV}}$, where r is the radial distance from the nucleus' center, $\rho(r)$ is the nuclear density (or charge density), and dV is the infinitesimal volume element. For more details, see e.g. [Trzcińska01, Strzałkowski78, Fricke95].
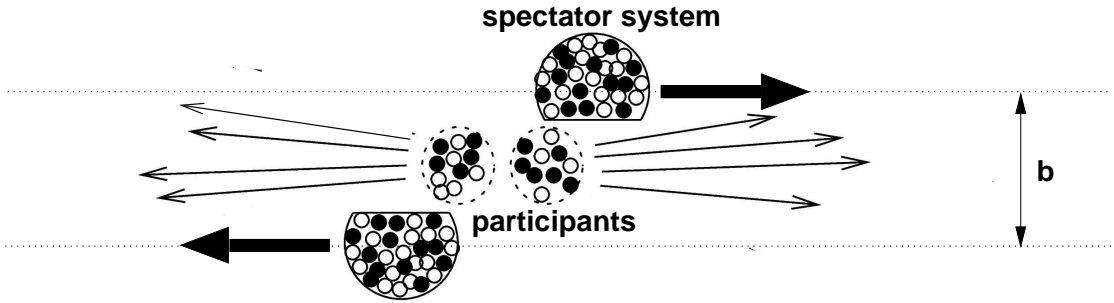
Figure 1.1: Schematic sketch of a peripheral Pb+Pb collision at high energy. Nucleons participating directly in the reaction are labelled "participants", while the two surviving remnants of the two nuclei are defined as "spectator systems". The particles produced in the participant zone are marked by thin arrows. The impact parameter b defines the distance between the centers of the two nuclei. Note: for simplicity, this plot neglects relativistic Lorentz contraction.

As such, and following the main lines **1.**, **2.**, **3.** postulated above, the present paper is aimed at the following objectives:

a) to construct a general methodological background for the present analysis of Pb+Pb reactions. This will consist of a selected set of experimental and phenomenological findings on soft hadronic interactions. These findings have been obtained in several precedent analyses which constitute the starting point for the present study.

b) to introduce a novel set of experimental data on π^+ and π^- production in peripheral Pb+Pb collisions, with a proper description of experimental aspects, corrections and data analysis up to, finally, the extraction of double differential cross sections for pion production covering a wide range of available phase space.

c) on the basis of equally complete and precise data on elementary proton-proton (p+p) as well as proton-nucleus (p+A) interactions, to perform an essentially model-independent comparative study of the change caused in pion production by the transition from the elementary to the nuclear collision. This will specifically include an attempt at the disentanglement of several different effects present in soft hadron production in Pb+Pb collisions.

d) to perform a phenomenological analysis of one of these effects, namely the final state electromagnetic ("Coulomb") interaction of the produced π^+ and π^- mesons with the highly charged spectator system and the resulting modification of charged pion spectra. This analysis will be done mostly in view of the possible sensitivity of the above effect to initial conditions characterising the process of pion production. It will be made in the hope to determine the usefulness of the spectator charge as a possible probe of the space-time (x, y, z, t) evolution of the nuclear reaction and of the non-perturbative hadron production process.

e) to discuss the significance of the knowledge gathered in b), c) and d) in the general context of non-perturbative phenomena in soft hadronic interactions, and to point at its specific applications in further analyses of elementary and nuclear interactions.

The outcome of the programme presented above will be a new set of experimental and phenomenological information on charged pion production at top energies available to the SPS accelerator ($\sqrt{s_{NN}} = 17.3$ GeV). This will cover a wide range of available phase space in a dense two-dimensional grid as a function of longitudinal and transverse momentum of the pion. Apart

from various manifestations of the strong interaction, this set will include a precise measurement of the electromagnetic effect induced by the spectator charge on two-dimensional charged pion momentum spectra. Within the NA49 experiment where the data are coming from, the experimental and subsequent phenomenological analysis of this specific effect constitutes a complete novelty, which has been introduced by the author of the present paper[4]. The detailed contribution of the author to the whole analysis will be presented in the next Section.

1.3 Author's Contribution

The work presented in this document is, in its majority, based on experimental data coming from the NA49 experiment at the SPS. As for any state-of-the-art experiment in high energy physics, this implies that it constitutes a result of a technical, software and data analysis effort of a number of people. It seems therefore indicated to specify the role of the author in the complete process of obtaining these results.

This role can be quantified as follows:

- As a member of the NA49 Collaboration since 1996, I participated to experimental data taking until the end of the active NA49 data taking period in 2003.

- On the technical level, I was responsible for the process of radioactive krypton gas calibration of four large volume Time Projection Chambers (TPC) which constitute the principal element of the NA49 detector. This procedure [Afanasiev99, Rybicki02] was an important part of the NA49 reconstruction process in view of optimal particle identification (PID) of charged particles via specific energy loss (dE/dx, see also Chapter 3). It was applied in all the NA49 experimental analyses relying on identified particles, including also all such NA49 results quoted in this paper. Later, under my supervision[5], this method was successfully transferred to the ALICE experiment at the LHC, where it presently constitutes an important element of the calibration of the ALICE TPC, see [Matyja09]. I was also involved in several other studies on further optimization of PID in NA49.

- On the physics analysis level, I was involved in various stages of the studies of hadron-hadron, hadron-nucleus and nucleus-nucleus interactions. This implies a contribution to various NA49 results discussed in Chapter 2 of this paper, including the data on baryon spectra in proton-nucleus collisions (Section 2.3.1), specific aspects of pion production studies (Section 2.3.2), as well as a part of the presented analysis of resonance production and its consequences (Section 2.3.3).

- I was also extensively involved in the analysis of pion production in peripheral Pb+Pb collisions which is the main subject of this paper. While preliminary and less detailed studies existed before in NA49 [Chvala04], the present extended analysis was directly triggered by my observation of electromagnetic effects induced by the presence of the spectator system (these issues are described in Section 2.3.4).

- Also on the experimental side, I was involved in the major and most demanding aspects of the data analysis of peripheral Pb+Pb reactions discussed in Chapter 3. This included either a complete realisation or a partial involvement in a number of tasks: the separation of Pb+Pb collisions from the background of beam-gas events (Section 3.2), PID work

---

[4]I am aware of only one existing measurement of this effect at SPS energies [Ambrosini99]. This was performed only in a very narrow range of acceptance. On the other hand, similar phenomena have been studied at lower collision energies. This subject will be touched upon in Chapter 4.

[5]Work done together with A. Matyja (INP, Kraków), the ALICE responsible for krypton calibration of the TPC.

(*ibid.*), the study of reaction geometry (*ibid.*), work on the beam-gas background correction (Section 3.3), pion decay correction (*ibid.*), weak decay feed down correction (*ibid.*), systematic error determination (Section 3.4), and integration of the obtained distributions (Section 3.5.2).

- Finally, the phenomenological studies of electromagnetic phenomena contained in Chapter 4 of the present paper constitute a separate, completely independent analysis. I am the main author of this complete analysis[6,7].

Various NA49 results on hadron-hadron, hadron-nucleus and nucleus-nucleus interactions discussed in this paper have been published or shown at international conferences. On the other hand, a part of the new experimental data on peripheral Pb+Pb reactions presented here have never been shown before; another part was shown, e.g., at the EPS Europhysics Conference on High Energy Physics [Rybicki09]. As far as the phenomenological analysis of electromagnetic effects contained in this paper is concerned, the bulk of it has been published and shown at conferences; some other results have never been shown before.

1.4   Outline of the Paper

The remainder of this paper is organized as follows:

Chapter 2 contains a discussion of selected aspects of soft hadronic interactions. This discussion serves as a methodological background for the subsequent analyses.

The experimental aspects of this study, including detector issues, data analysis of peripheral Pb+Pb reactions, up to the extraction of final state pion distributions, are explained in Chapter 3.

Chapter 4 contains a phenomenological study of electromagnetic effects induced by the presence of the spectator system in peripheral heavy ion collisions.

Chapter 5 includes a comparative analysis of pion production in proton-proton, proton-nucleus, and peripheral Pb+Pb interactions.

Finally, Chapter 6 terminates the paper with a basic summary of the knowledge gathered.

---

[6]Work performed together with A. Szczurek (INP, Kraków).

[7]Note: it should be underlined that some of the contributions listed above were realized in the framework of my Ph. D. Thesis [Rybicki02]. This specifically concerns my partial contributions to Sections 2.3.1 and 2.3.3, the development of krypton calibration for NA49, and most of datataking. While the present paper originates from a different phenomenological idea and is largely focussed on different phenomena, the quoted work [Rybicki02] will constitute one of the ingredients building up the more general methodology of this study (see Chapter 2).

Chapter 2

Selected Topics on Soft Hadronic Interactions

The aim of this Chapter is to show the present analysis in the broader context of several issues which the author believes to be important for the general understanding of high energy hadronic physics, and for related experimental studies. As such, this Chapter contains:

- a definition of kinematical and other variables used in this study;

- a general description of basic experimental aspects;

- a selection of experimental findings on soft interactions, with a special emphasis on the issues which directly inspired the present analysis.

2.1 Definition of Variables and Data Presentation

Kinematical variables[1]. The two principal kinematical variables used in the present paper are the scaled longitudinal momentum of the produced particle, namely the Feynman variable $x_F = 2p_L/\sqrt{s_{NN}}$, and the momentum component perpendicular to the collision axis, p_T. Both variables are given in the nucleon-nucleon collision c.m.s. where $\sqrt{s_{NN}}$ is the corresponding nucleon-nucleon interaction energy.

This situation is illustrated in Fig. 2.1 where these two orthogonal variables are shown in relation to a "simplest" soft hadronic interaction process, namely the elementary p+p collision. The choice of x_F and p_T can be related [Chvala06] to a basic feature of particle production in hadron collisions which is the "longitudinal phase space" [Brandt64], i.e., filling up of the available phase space in the longitudinal direction by produced particles[2], in contrast to a damping of the transverse momentum distribution. This is connected with such phenomena as the "Feynman scaling" [Feynman69] of the x_F spectrum of fast final state particles with interaction energy. The variable x_F is also suitable for studying phenomena related to the fragmentation of the projectile and corresponding comparative analyses of elementary and nuclear reactions, which occupy an important place in this paper.

A "technical" drawback of the choice of x_F as longitudinal variable is the lack of Lorentz invariance [Amsler08] of the corresponding distributions. The latter invariance is characteristic for the well known rapidity variable, $y = \frac{1}{2}\ln\left(\frac{E+p_L}{E-p_L}\right) = \ln\left(\frac{E+p_L}{m_T}\right)$, where E and $m_T = \sqrt{m^2 + p_T^2}$ are the energy and "transverse mass" of the particle of mass m and longitudinal momentum p_L.

---

[1]Section 2.1 is partially based on [Alt06, Amsler08, Chvala06, Szymański06, Trzupek06].

[2]Baryons will also be referred to as "produced" particles in this paper. Note that in the inelastic sector discussed here, the connection between the initial and final state baryon is unknown *a priori*.

p_T

θ

p_L

$x_F = 2p_L/\sqrt{s_{NN}}$

(1)   p+p   (2)

$x_F = 1$
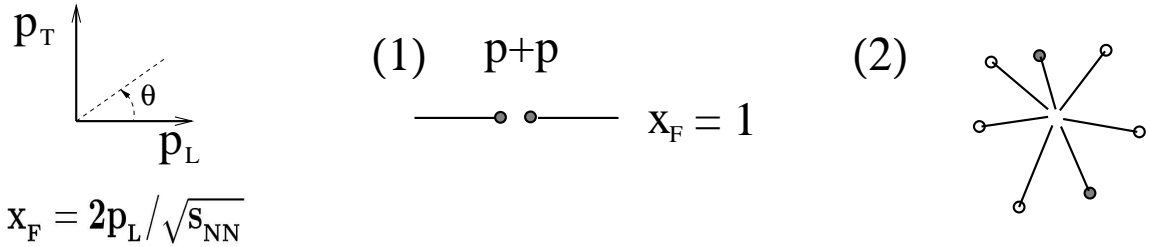
Figure 2.1: Definition of the longitudinal momentum p_L, the Feynman variable x_F, the transverse momentum p_T and the polar angle θ, drawn with respect to the initial **(1)** and final **(2)** state of the inelastic p+p collision. The incoming protons **(1)** have initial x_F closely equal to ± 1 while the final state particles **(2)** have extended distributions in x_F and p_T. Shaded circles define baryons before and after the collision (see discussion in Section 2.3.1). The plot is re-drawn from [Rybicki02].

Distributions drawn as a function of rapidity will also be shown in the present paper. The same is valid for its approximate, pseudorapidity, $\eta = -\ln\tan\left(\frac{\theta}{2}\right)$, obtained from the polar angle θ of the particle relative to the collision axis (also shown in Fig. 2.1).

Distributions. Most of the data presented in this paper will be contained in *single particle spectra* of *identified* final state particles, most often displayed as a function of the particle's x_F and p_T. These will be obtained either for inclusive inelastic (minimum bias) interactions, or for *constrained* data samples with an additional selection on e.g. the geometry (centrality) of the reaction.

For a multiparticle final state which is characteristic for all the reactions studied in this paper (Fig. 2.1), such a way of presenting the data constitutes an evident and dramatic simplification, and a very strongly reduced projection of their original multidimensional phase space. On one hand, this is imposed by experimental limitations and difficulties in interpretation of multidimensional structures [Szymański06]. On the other hand, this will be demonstrated to constitute already quite some progress in the interpretation of the data, if the latter are analysed over a large fraction of the total range of x_F and p_T available for final state particles.

Two principal quantities will be used for the presentation of two-dimensional particle spectra. The first will be the invariant single particle cross section:

$$f = E\frac{d^3\sigma}{dp^3} \tag{2.1}$$

where E and dp^3 are respectively the particle's energy and the infinitesimal volume element in three dimensional momentum space. This quantity will be typically used for minimum bias hadron-hadron and hadron-nucleus interactions. For constrained (e.g. centrality-selected) nuclear collisions, the corresponding used quantity will be the invariant single particle density:

$$d = E\frac{d^3n}{dp^3} \tag{2.2}$$

which will give the density (per single event) of particles d^3n falling into the volume element dp^3. While for a given type of identified particle, both quantities f and d are in principle functions of its three dimensional momentum vector, the azimuthal symmetry with respect to the rotation around the collision axis will make them practically only two dimensional functions of x_F and p_T. For all the inclusive inelastic reactions discussed here, d can be obtained from f as $d = f/\sigma_{inel}$, σ_{inel} being the total inelastic cross section. What follows from the above is that the p_T-integrated density of particles per unit of x_F, dn/dx_F, can always be readily obtained:

$$dn/dx_F = \int_0^{p_T^{\max}} \frac{d^2n}{dx_F dp_T} \, dp_T = \int_0^{p_T^{\max}} \left(\pi \, \sqrt{s_{NN}} \, \frac{p_T}{E} \, d \right) \, dp_T \qquad (2.3)$$

Here, the integrand $\frac{d^2n}{dx_F dp_T}$ is the non-invariant density per event for particles falling in the infinitesimal bin $dx_F dp_T$, and $p_T^{\max}$ is the x_F-dependent kinematic limit[3]. The density dn/dx_F will be the principal variable used in this paper to present one-dimensional distributions of produced particles. Analogous quantities, like $dn/d\eta$, will also be shown (in various quoted works the nomenclature dN/dx_F, $dN/d\eta$ will be in use). Additionally, the integral of Eq. (2.3) over the full x_F range will give the total multiplicity of particles of a given type produced per event. Finally, the x_F-dependence of the first moment of the $\frac{d^2n}{dx_F dp_T}$ distribution (the mean transverse momentum $<p_T>$) will also be occasionally studied in order to get a first idea on the evolution of particle production with, e.g., reaction type or centrality.

A useful observable which can be constructed on the basis of these introduced above is the *charged particle ratio*. In the present paper especially the ratio of densities of positive over negative pions (π^+/π^-) will be studied, either in two dimensions (as a function of x_F and p_T) or obtained from p_T-integrated spectra.

Data presentation. With rare exceptions, the error bars on the experimental data points presented in this paper will be only statistical. A discussion of systematic errors for the analysis of peripheral Pb+Pb reactions will be presented in Chapter 3; analogous discussions for several other presented datasets can be found in the enclosed bibliography. Unless explicitly specified, the curves drawn through the data points will serve merely to guide the eye.

2.2 Basic Experimental Aspects

2.2.1 General Considerations

The general postulates **1.**, **2.**, and **3.**, formulated in Chapter 1, Section 1.1 may readily serve to define an "ideal experiment" for the purpose of studying high energy soft hadronic interactions[4]. Following these requirements, such an experiment should:

- record large statistics data samples;

- cover the whole available phase space with a measurement of the final state particle momentum vector (p_x, p_y, p_z) as well as particle identification;

- cover a maximum variety of reactions and energies, including most of all a simultaneous measurement of hadron-hadron, hadron-nucleus and nucleus-nucleus interactions in the same detector.

One further asset to be added to the above is *impact parameter control* in nuclear collisions which will serve to establish the relation between particle production and the geometry (centrality) of the reaction as it was shown in Fig. 1.1. Among other issues (see Chapter 1 for comparison), this brings a valuable additional tool for probing the behaviour of the strong interaction as a function of the imposed nuclear medium, in particular of the size of the colliding system (number of participating nucleons) or of the depth of nuclear matter subject to the interaction (number of elementary nucleon-nucleon collisions suffered by each participant).

It should be remembered that even the "ideal experiment" will always remain limited to the initial and final state of the strong interaction as drawn in Fig. 2.1, with no possibility of

---

[3]In practice the kinematic limit is replaced by lower but large enough values of $p_T^{\max}$ (here typically 2-3 GeV/c).
[4]Note: Sections 2.2.1-2.2.3 are partially based on [Rybicki02].
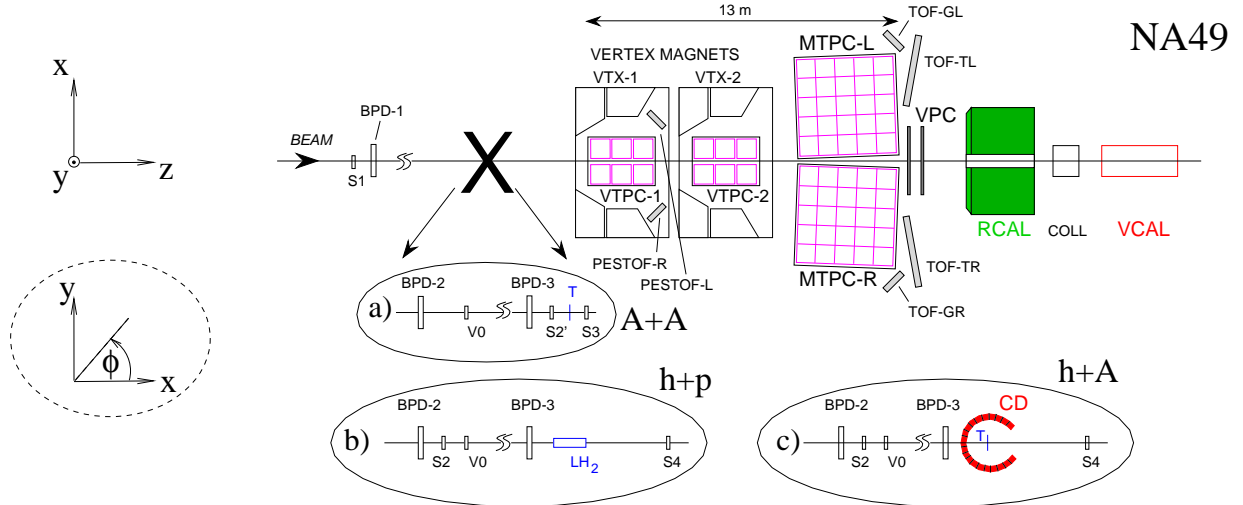
Figure 2.2: Set-up of the NA49 detector with different target arrangements for **a)** A+A, **b)** h+p, and **c)** h+A collisions. The Figure contains also the definition of the NA49 coordinate system and of the azimuthal angle ϕ. The plot comes from [Rybicki02].

direct measurement of the intermediate and most interesting stage of the collision. As a trivial example, none of the unstable strongly decaying particles (resonances) produced in hadronic reactions can be directly seen in the detector due to their extremely short lifetime of the order of fm/c. Thus, if the postulate **3.**, Section 1.1 is to be fulfilled, proper *indirect* methods must be applied. This subject will be further addressed in Chapter 4.

2.2.2 NA49 as an Example of a Soft Hadronic Experiment

It is illustrative to see how and to which extent the above ideal was realized in practice. For the purpose of the present discussion, the NA49 fixed target experiment at the SPS will serve as a good example of such a realisation, achieved by means of state-of-the-art detector techniques. This experiment completed active data taking in 2003 and is presently in the data analysis stage[5]. The set-up of the NA49 detector is shown in Fig. 2.2. It gives the possibility of studying hadron-proton (h+p), hadron-nucleus (h+A), and nucleus-nucleus (A+A) reactions. The four principal elements of the detector are the Time Projection Chambers (TPC): VTPC-1, VTPC-2, MTPC-L, and MTPC-R. These provide charged particle tracking and momentum vector determination, as well as particle identification via specific energy loss ("dE/dx") measurement [Afanasiev99]. The other components of the detector are the Time of Flight (TOF) scintillator arrays which improve the identification of charged particles in limited regions of phase space, a Ring Hadron Calorimeter (RCAL) for neutral particle identification, and a set of two Vertical Proportional Chambers (VPC), designed to differentiate charged from neutral particles. Three target configurations are available for the three reaction types. For hadron-proton interactions the target is a liquid hydrogen tube (LH$_2$). For hadron-nucleus and nucleus-nucleus collisions, nuclear targets of varying thickness are used (T). In the special case of hadron-nucleus reactions, a Centrality Detector (CD) surrounds the target, which allows for centrality triggering and determination on the basis of the number of measured low-momentum "grey" protons[6]. The number of these is commonly believed to be associated with the centrality of the hadron-nucleus collision. For

---

[5]The continuation of NA49, the NA61 experiment at the SPS, collected its first data in 2007.

[6]For NA49, these are protons in the lab momentum range from 0.15 to 1.2 GeV/c [Alt07]. The term "grey" originates from identification of such tracks in emulsion [Fredriksson84]. A discussion of the relation between grey tracks and the centrality of h+A collisions can also be found in e.g. [Chemakin99, Hegab81, Busza88, Babecki78].
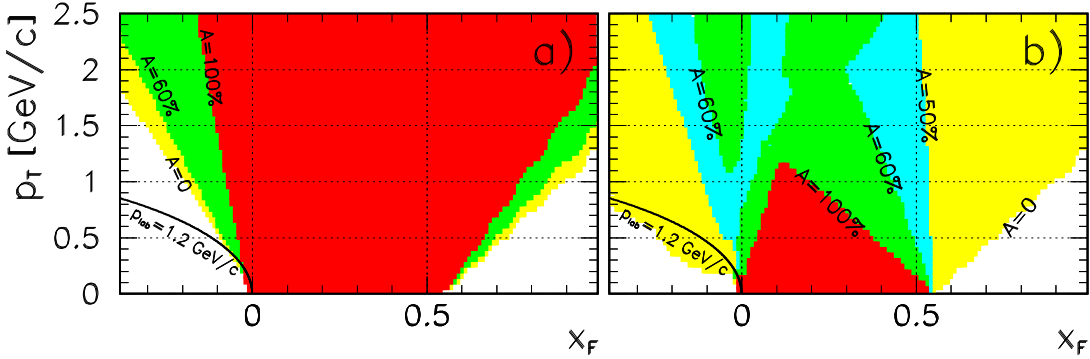
Figure 2.3: Geometrical acceptance A of the combined NA49 TPC system for positive pions **a)** averaged over azimuthal angle ϕ in the range $|\phi| < 50 \deg$, and **b)** averaged over the full azimuthal angle. The plot assumes a beam energy of 158 GeV/nucleon corresponding to $\sqrt{s_{NN}} = 17.3$ GeV; it is restricted to pions leaving at least 30 clusters in the TPC's. The solid curve ($p_{lab} = 1.2$ GeV/c) illustrates the range of total lab pion momenta for the c.m.s. target hemisphere ($x_F < 0$). The plot comes from [Rybicki02].

nucleus-nucleus collisions, centrality triggering and determination can be achieved on the basis of the energy deposit of nuclear fragments in the zero-degree Veto Calorimeter (VCAL). The measurement of charged particle multiplicity in the TPC system can also serve centrality determination in nucleus-nucleus reactions, see Chapter 3 for more details.

It is worthwhile to note that different reaction types are associated with different problems. For instance, the high ionization density of the ion beam used for heavy ion collisions forces the split configuration of the whole detector, Fig. 2.2, and results in a partial loss of forward acceptance. For hadron beams exclusively, this has been remedied by introducing a small "Gap" TPC in-between VTPC-1 and VTPC-2. This device (not shown in Fig. 2.2) extends the overall tracking acceptance of NA49 up to the kinematic limit [Alt06].

2.2.3 Coverage, Versatility, Statistics

The combined phase space coverage of the system of the four NA49 TPC's (Section 2.2.2) is shown in Fig. 2.3. Panel **(a)** displays the geometrical acceptance for positive pions drawn as a function of their x_F and p_T. This plot is restricted to pions leaving a minimum of 30 ionization electron clusters in the TPC system [Afanasiev99], in the azimuthal cone of $|\phi| < 50 \deg$ (see definition in Fig. 2.2). Acceptance with no azimuthal restriction is shown in panel **(b)**. As it follows from the two panels, acceptance varies as a function of ϕ, preserving however a comfortable area of full-azimuth coverage at positive x_F and lower p_T. This large coverage of the detector in the projectile hemisphere of the reaction ($x_F > 0$) is clearly an advantage of NA49. The situation is particularly favourable for single particle spectra which occupy the bulk of this paper: these can be measured in restricted cones in ϕ thanks to their azimuthal symmetry (Section 2.1). Up to above $x_F = 0.5$, the detector covers the whole region of available transverse momenta, starting sharp at $p_T = 0$. Apart from momentum vector measurement, particle identification is also available in this whole area. The coverage is worse in the target hemisphere ($x_F < 0$) which corresponds to low lab momenta in fixed target kinematics, see Fig. 2.3. Nevertheless, published pion measurements with PID exist at least down to $x_F = -0.1$ [Alt07].

For protons, the acceptance coverage will remain similar to pions at high values of x_F, but will extend further in the target hemisphere. For hadron-induced reaction measurements with the Gap TPC, the situation will be even better at high x_F.

Another important advantage of NA49 is the versatility of data collected by the experiment which include, among others, p+p, n+p, $\pi^{\pm}$+p, p+C, p+Pb, $\pi^{\pm}$+Pb, C+C, Si+Si, and Pb+Pb

reactions[7]. Such a wide versatility allows for extended comparative studies, some of which will be discussed in this paper. Data from all these reactions are available at 158 GeV/nucleon beam energy ($\sqrt{s_{NN}} = 17.3$ GeV); the overall beam energy span of all the collected NA49 datasets ranges from 20 to 250 GeV/nucleon corresponding to a range in $\sqrt{s_{NN}}$ from 6.3 to 21.7 GeV.

The collected statistics strongly varies as a function of reaction type and energy. It spans over a range of 0.1 to 5 million events both for hadron-induced reactions and for nucleus-nucleus data. It is to be remembered that the statistical significance of hadron-induced events is much lower due to a lower multiplicity of secondary particles produced per event[8]. Apart from the available beam time, the main limiting factor for the size of hadron-induced datasets was the relatively low NA49 data acquisition (DAQ) rate which was originally designed for central Pb+Pb events. It is to be underlined that this is the available statistics which effectively defines the upper limit of the p_T coverage discussed above. This limit varies between 1.8 and 4.5 GeV/c depending on given analysis and dataset.

Thus, although far from the ideal postulated above, NA49 offers specific experimental advantages in terms of coverage and data versatility. These will be largely exploited in this paper.

2.2.4 Comments on Other Experiments

It is instructive to see how the experimental advantages and limitations of the NA49 detector compare to other experiments in the field. This will be shown in a set of examples, given below.

Out of the four detectors at the RHIC collider (PHENIX [Adcox05], STAR [Adams05], PHOBOS [Back05], BRAHMS [Arsene05]), the coverage in simultaneous momentum measurement and particle identification is most extended for the case of the BRAHMS experiment. On the basis of [Arsene05, Brahms10], it can be concluded that at the top RHIC energy of $\sqrt{s_{NN}} = 200$ GeV, this coverage extends from $x_F \approx 0$ to $x_F \approx 0.12$ for typical pion transverse momenta. The coverage in x_F increases with increasing transverse momentum: it reaches only $x_F \approx 0.05$ at the lowest accessible value of $p_T = 0.2$ GeV/c, but goes up to $x_F \approx 0.25$ at $p_T = 0.9$ GeV/c.

The above-mentioned lowest limit of p_T-coverage has been considerably improved by the PHOBOS experiment, where a novel methodology has been developed [Trzupek06] extending this limit down to $p_T = 0.03$ GeV/c for pions (with PID but no charge differentiation). On the other hand, pseudorapidity distributions of non-identified charged particles obtained by the same experiment reach up to $\eta = \pm 5.4$ [Back05]. The resulting coverage in x_F is evidently a function of p_T. At top RHIC energy and $p_T = 0.5$ GeV/c, this corresponds to $x_F \approx \pm 0.55$. While it should be remembered that these are only *one-dimensional*, angular (pseudorapidity) rather than momentum measurements, an important advantage of these data is their simultaneous coverage of the projectile and target hemisphere of the collision ($x_F > 0$ and $x_F < 0$, respectively). This is particularly useful for studies of asymmetric systems like d+Au reactions, see also Section 2.3.2.

Compared to NA49, the versatility of RHIC datasets does not include e.g. pion-induced reactions, but nevertheless contains both elementary and nuclear collisions, in particular p+p, d+Au, Cu+Cu, and Au+Au interactions. Centrality control is available for all the measured nuclear reactions. The overall energy span of the collected datasets is a full order of magnitude in $\sqrt{s_{NN}}$, from 19.6 to 200 GeV. The statistics of the collected data exceeds by far that of NA49, with e.g. numerous PHOBOS datasets above one hundred million events each, in particular also for elementary collisions [Trzupek06].

Out of the four detectors at the LHC (LHCb, ATLAS, CMS, and ALICE), the latter three foresee large programs of heavy ion collision studies. To give the example of the ALICE experiment,

---

[7]The small, clean dataset on n+p collisions has been isolated from events induced by a deuteron beam.

[8]At beam energies of 158 GeV/nucleon, the typical charged multiplicity in p+p events is about 7, to be compared with some 1600 for central Pb+Pb events (see [Anticic10a] and [Bartke09], respectively).

most dedicated to the study of soft observables, the area of particle identification and tracking in the central ALICE detectors corresponds to $p_T > 0.1$ GeV/c and $|\eta| < 0.9$ [Alessandro06, Kowalski10]. At the top LHC energy which will be available to Pb+Pb collisions, $\sqrt{s_{NN}} \approx 5.5$ TeV, this gives a coverage in $|x_F|$ which remains below 0.001 up to $p_T \approx 2.7$ GeV/c. The range of multiplicity (pseudorapidity) measurements with Forward Multiplicity Detectors extends up to $\eta = 5$, which corresponds to $x_F \approx 0.03$ at $p_T = 1$ GeV/c. On the other hand, measurements of large x_F particles with Zero Degree Calorimeters ($0.3 < x_F < 0.64$ for charged particles) were proposed in p+p collisions at $\sqrt{s_{NN}} = 14$ TeV for "effective energy" studies [Alessandro06].

The total versatility of reactions measured by ALICE and the other LHC experiments includes a full set of high statistics p+p, proton-nucleus (p+A) and nucleus-nucleus data samples at different values of $\sqrt{s_{NN}}$, with nuclear reaction centrality control.

The differences between the coverage of the experiments discussed above and that of NA49, Section 2.2.3 should be commented upon. It is known that the higher c.m.s. energy generally available to collider experiments has to be paid for, among others, by construction limitations imposed by the two incoming beams [Szymański06]. This results in the difficulties in measurement of low p_T and high x_F particles. In principle, fixed target detectors should not suffer from such problems. This is for instance the case for the hadron beam configuration of NA49 where low-p_T tracking acceptance is available up to the kinematic limit, Section 2.2.2. For heavy ion collisions, the split between the four NA49 TPC's brings the situation slightly closer to that of collider experiments, as it becomes immediately apparent in Fig. 2.2. Finally, for LHC experiments, the larger incoming beam energy brings a further reduction in x_F coverage.

While it would be certainly interesting to extend the above comparison to the very large number of hadronic experiments done in the past, this exceeds the scope of this paper. A more complete overview of experiments and data on nuclear reactions can be found in, e.g., [Bartke09, Fredriksson84] and numerous references therein. Also, partial but very detailed discussions of elementary collision data can be found in [Alt06, Anticic10, Anticic10a].

2.3 A Few Results on Hadron-Hadron, Hadron-Nucleus and Nucleus-Nucleus Reactions

This Section presents a selected set of experimental findings on soft interactions. This is aimed at showing the study of peripheral Pb+Pb collisions made in this paper in a broader context of other analyses, with a clear emphasis on the issues that provided a direct inspiration for the present study. As such, the presented selection has no pretension to be neither fully general nor exhaustive, both being in fact far beyond the scope of this paper.

Nevertheless, the selection made here touches a set of different subjects - baryon, meson and resonance production - which allows to draw a basic picture of the soft interaction acting in high energy hadron-hadron, hadron-nucleus and nucleus-nucleus collisions.

2.3.1 Baryons and Baryon Number

Baryons play a special role in studies of hadronic collisions in the non-perturbative sector[9]. The basic reason for this is *baryon number conservation* which binds the total (net) baryon number in the collision to be equal in the initial and final states. At SPS energies where production of baryon/anti-baryon pairs gives only a small fraction of the total baryon yield, this imposes a relatively strong constraint on the dynamical scenarios of the reaction. The "usefulness" of this constraint can be illustrated by the example of the p+p reaction shown in Fig. 2.1. It is known

---

[9]Section 2.3.1 is mainly based on [Rybicki04], partially also on [Busza84, Rybicki02, Rybicki02a, Rybicki04a, Rybicki04b].
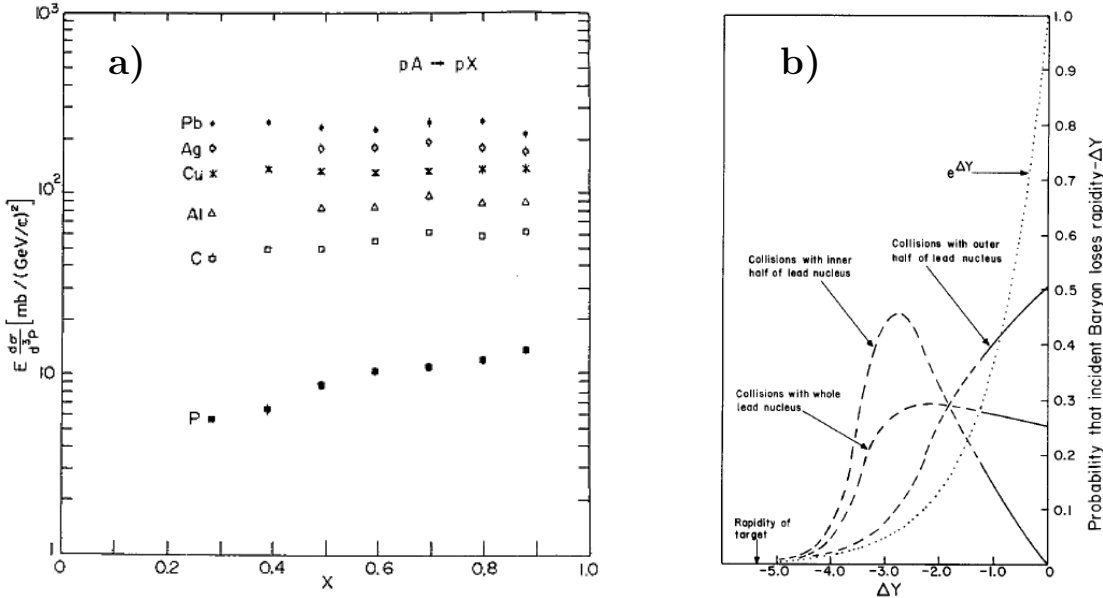
Figure 2.4: **a)** Inclusive invariant cross sections for final state protons in p+p and p+A reactions at 100 GeV beam energy, drawn at $p_T = 0.3$ GeV/c as a function of $x = [(E+p_L)_{(outgoing)}/(E+p)_{(incoming)}]$; E, p_L and p are the proton energy, longitudinal and total momentum. **b)** Probability distributions for rapidity loss ΔY of protons striking lead nuclei. The dashed lines indicate the extrapolated parts of the distributions. Both panels **(a, b)** are taken from [Busza84]; panel **(a)** was obtained from the data [Barton83].

that the incoming baryon number, originally positioned at $x_F = \pm 1$, in the final state spreads over a very wide longitudinal distribution. In particular, it may find itself at very low values of $|x_F|$. Any phenomenological model of the reaction should therefore provide a mechanism transporting the baryon number down to, say, $x_F = 0$, which in turn limits the freedom of possible scenarios for the overall dynamics.

In proton-nucleus collisions, the above effect of decreasing the final state momentum ("stopping") of the incoming proton is known to increase with the size of the target nucleus [Barton83]. It has been connected to such issues as the energy deposition in nuclei, as well as baryon and energy densities attainable in heavy ion collisions [Busza88, Daté85].

Among these works, one will be enlarged upon in view of the present discussion. On the basis of experimental data on fast proton production in p+p and p+A reactions at $p_T = 0.3$ GeV/c (Fig. 2.4a), and of several straight-forward considerations, Busza and Goldhaber deduced the complete probability distribution of the "loss in rapidity occurring when a baryon traverses the central part of a lead nucleus" [Busza84]. This is shown in Fig. 2.4b. As apparent in the Figure, the curve deduced for a proton passing through the inner half of the Pb nucleus corresponds to a much higher "loss in rapidity" relative to a peripheral or even inclusive p+Pb collision (also shown in the Figure). With decreasing impact parameter of the reaction, or increasing thickness of nuclear matter traversed by the projectile, the distribution is predicted to change shape and be steadily "pushed" in the negative (i.e. target) direction. The authors even give a quantitative estimate for the average "loss in rapidity" to be $\Delta Y = -2.4 \pm 0.5$ in the most central case. This value is not far from $x_F = 0$ in the nucleon-nucleon c.m.s., which at the energy of the dataset [Barton83] corresponds to $\Delta Y = -2.65$. It should be emphasized that the whole above analysis - in principle a very clever conjecture - was performed on the basis of experimental data without impact parameter control (Section 2.2.1), covering only a part of the available phase space.

A somewhat similar study was performed by the NA49 experiment at the beam energy of 158 GeV/nucleon. As a result of its high coverage and dataset versatility (Section 2.2.3), the fate
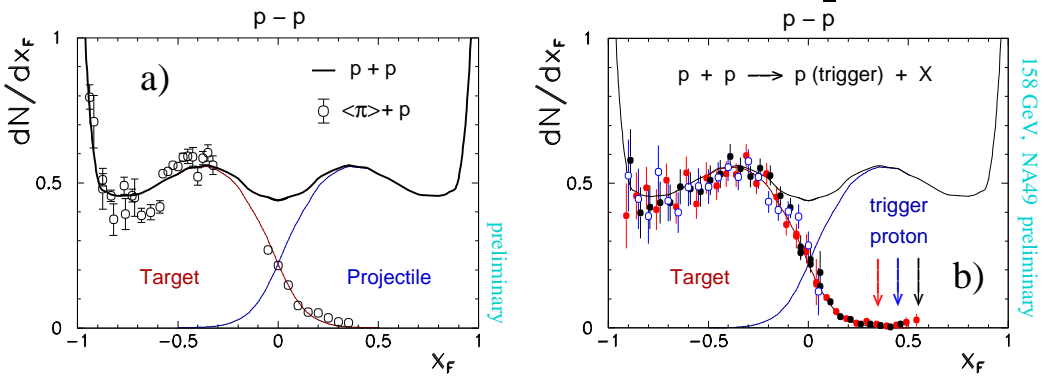
Figure 2.5: **a)** Net proton distribution in inclusive p+p reactions separated into target and projectile components, and net proton distribution in $<\pi>$+p reactions. **b)** The same target component compared to net proton distributions in semi-inclusive p+p collisions, obtained when fixing one of the protons respectively at x_F=0.35 (shaded dots), x_F=0.45 (open circles), and x_F=0.55 (black dots). Both panels are taken from [Rybicki04]. The presented data are described in more detail in [Fischer03, Varga04].

of projectile and target baryon number could be *disentangled*, essentially at the experimental level. This is shown in Fig 2.5. Panel **(a)** displays the x_F distribution of net protons $(p - \bar{p})$ produced in p+p collisions compared to average pion-proton ($<\pi> = \frac{\pi^+ + \pi^-}{2}$) reactions. As apparent in the Figure, the final state distribution in p+p collisions can be separated into two symmetric components, directly attributable to the projectile and target protons. The target proton component remains the same in pion-induced and proton-induced reactions. What is more, the same proton target component remains present in semi-inclusive p+p events where the projectile baryon is localised at a well defined value of x_F, panel **(b)**. This apparent independence of the projectile and target fragmentation into final state baryons has been given the name of the *two-component picture*[10] [Rybicki00]. These two components - the spectra of net protons coming from the fragmentation of the projectile and target - exhibit a characteristic shape. They remain mainly localised in their respective hemispheres in the collision c.m.s., but extend also into the opposite hemisphere, at least down to $x_F \approx -0.3$ and up to $x_F \approx +0.3$ for the projectile and target, respectively. This implies that an incoming proton moving *forward* may fragment into a baryon moving *backward* in the collision c.m.s.

The two-component picture explained above has brought important consequences for the interpretation of net proton spectra in *nuclear reactions*. In full analogy to the above, the distributions measured in p+Pb collisions have been split into respective target and projectile components, Fig. 2.6. The target component has been isolated experimentally by means of average pion-lead reactions, and the projectile component by subtracting the target contribution from the total $p - \bar{p}$ spectrum.

In a p+Pb collision, the projectile proton passes through a larger amount of nuclear matter relative to p+p reactions. It can be said to undergo *multiple collisions* with target nucleons. The resulting "response" of target nucleons is shown in Fig. 2.6a where the final state net proton spectrum in $<\pi>$+p interactions is compared to two experimental samples of $<\pi>$+Pb collisions. These two samples are characterized by a different centrality (impact parameter) of the collision, defined here by the mean number $<\nu>$ of target nucleons crossed by the proton projectile[11]. As it is apparent in the Figure, the net proton spectra originating from fragmen-

---

[10]Note: the two-component picture described above should not be mistaken for the one which was formulated in [Fiałkowski83] for inclusive particle and resonance production. In various other works [Fischer03, Rybicki04a, Anticic10] the equivalent term *factorization* was used.

[11]$<\nu>$ is deduced from grey proton measurement, Section 2.2.2, using the VENUS event generator [Werner93].
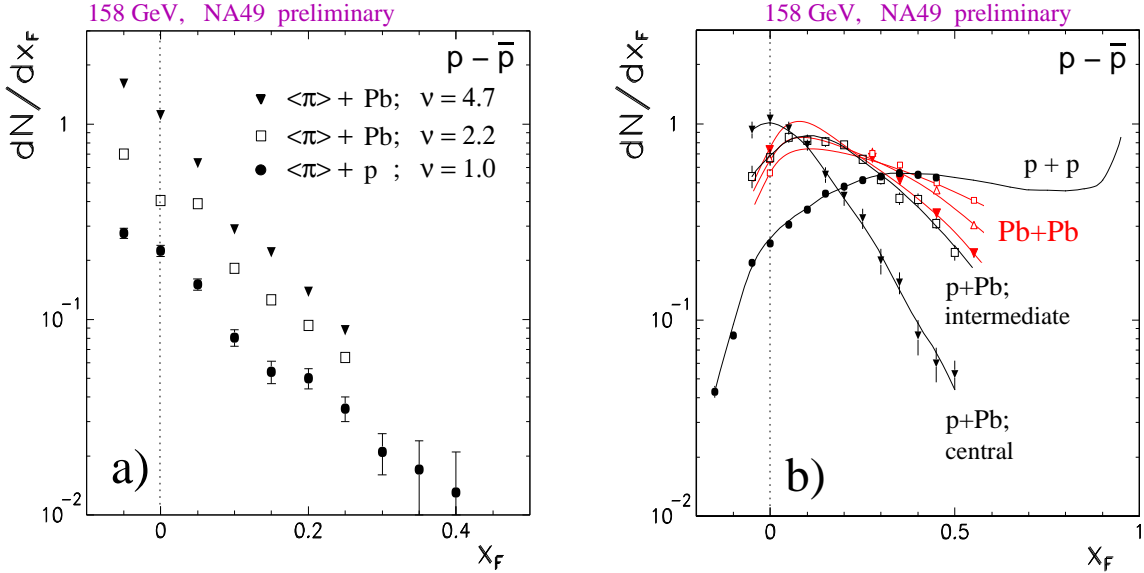
Figure 2.6: Target **(a)** and projectile **(b)** components of net proton spectra in p+p and centrality-selected p+Pb collisions. A comparison to Pb+Pb collisions is included in panel **(b)**. Both panels are taken from [Rybicki04].

tation of target nucleons approximately scale with $<\nu>$. This behaviour is indeed what is to be expected from a superposition of $<\nu>$ target nucleons, each being hit *once* by the projectile and therefore participating in one *elementary* collision.

On the other hand, the projectile component of net proton spectra is shown in Fig. 2.6b. In sharp contrast to target nucleons, the fragmentation of the projectile is strongly modified by multiple collisions which it suffers. When passing from elementary p+p interactions through intermediate to central p+Pb collisions, the distribution visibly changes shape, corresponding to an increased "push" of baryons towards $x_F = 0$. The resemblance of this picture to that resulting from the former analysis [Busza84], Fig. 2.4b, should be clearly pointed out.

Finally, a comparison to Pb+Pb collisions[12] is also included in Fig. 2.6b. It should be emphasized that following the discussion above, indeed *only the projectile component* of p+Pb reactions constitutes a good basis for comparison with Pb+Pb interactions as in the latter, *each* participating nucleon may undergo multiple collisions. The result of this comparison suggests a common trend which is a general "push backwards" of the distribution with increasing thickness of nuclear matter traversed by the projectile. In this trend, the "intermediate" position occupied even by central Pb+Pb collisions (shaded triangles in the Figure) could be at least partially understood from simple geometrical considerations: if seen as a superposition of nucleon+Pb reactions, a Pb+Pb collision will always correspond to a distribution of impact parameters, and will not reach the extreme degree of baryon stopping present in a selected sample of most central p+Pb interactions.

Altogether therefore, the following picture emerges from the data discussed above:

- the net baryon distribution in elementary collisions can be shown to be the sum of projectile and target fragmentation which are largely independent, in particular also of the opposite particle type;

---

[12]The author wishes to underline the preliminary character of the presented data, in particular also for Pb+Pb collisions which, in the somewhat "historical" comparative plot discussed in the text, come from a relatively early analysis [Bächler99]. This touches among others the different approaches to normalization and centrality determination in A+A reactions [Cooper99], which remain beyond the scope of the present paper.

- this *two-component picture*, when applied to hadron-nucleus collisions, shows that the target nucleons behave "passively", i.e. as if they would participate to single elementary interactions; this is very different from the "active" projectile suffering multiple collisions which strongly modify the corresponding final state distribution;

- following the above, only the projectile component of p+Pb reactions constitutes a good basis for comparison with Pb+Pb collisions. Once made, such a comparison displays overall similarities in the behaviour of p+Pb and Pb+Pb reactions.

Consequences of the above observations for comparative studies of production phenomena in p+p, p+A and A+A collisions will be addressed in subsequent Sections. However, a few remarks should still be made to complete the discussion on baryons. The two-component picture explained above is not inconsistent with data on spectra of fast scattered protons measured in γ^*+p reactions in the ZEUS experiment at HERA [Chekanov03]. As it is to be expected from the above considerations, these appear similar to high x_F proton spectra in p+p collisions [Anticic10]. The fragmentation of target nucleons into protons in the projectile hemisphere (Fig. 2.6a) was also measured by the ACCMOR experiment [Różańska91] in antiproton-nucleus collisions at $\sqrt{s_{NN}} \approx 15.1$ GeV, for various target nuclei (Be, Cu, Ag, W, and U). On the other hand, the evolution of the projectile distribution with multiple collisions (Fig. 2.6b) has been shown to be similar for final state protons and neutrons [Rybicki02a].

It is interesting to consider whether the above picture of two overlapping baryonic components would apply also to the much higher energies available at RHIC and LHC colliders. At RHIC, no analysis exactly similar to the above can be hoped for due to the lack of datasets on pion-induced interactions. However, it is true that the transport of baryon number down to $x_F = 0$ has been reported to be still present for nuclear reactions at $\sqrt{s_{NN}} = 200$ GeV, see e.g. [Bearden03]. An important question is whether at much higher energies available to the LHC, the region of $x_F \approx 0$ will finally become "baryon-free" as expected e.g. in [Bartke09]. At the present moment, data from p+p collisions at $\sqrt{s_{NN}} = 0.9$ and 7 TeV are becoming available from the ALICE experiment [Aamodt10]. The quoted paper reports that at $\sqrt{s_{NN}} = 7$ TeV, the yield of antiprotons produced at $x_F \approx 0$ becomes indeed compatible with that of protons. In the context of the considerations made above, the extension of these studies to nuclear reactions at LHC energies will clearly be a subject of very high interest.

2.3.2 Pion Production

The production of secondary π mesons can be safely regarded as the dominant phenomenon in any type of high energy hadronic collision ranging from elementary nucleon-nucleon up to central heavy ion reactions, possibly with the exception of the break-up process of the remnant nucleus in proton-nucleus or non-central nucleus-nucleus collisions. At the energy of $\sqrt{s_{NN}} = 17.3$ GeV considered here, a typical p+p collision yields as many as 5.4 charged pions (π^+, π^-) in the final state [Alt06]. In central Pb+Pb collisions this number can reach some 1250 [Afanasiev02]. A further contribution of about 50% has to be added to the above numbers to account for neutral π^0 mesons. It can therefore clearly be expected that the process of pion production will be linked to numerous theoretical and phenomenological ideas based on various corresponding observables. From all this rich phenomenology, only a few items directly influencing the present analysis will be discussed below.

In the precedent Section, the hypothesis of the two-component picture of baryon spectra was discussed. It is interesting to consider to what extent a similar concept could be applied to the case of pion production. For produced particles however, clear experimental and conceptual difficulties emerge due to the lack of a constraining factor analogous to baryon number
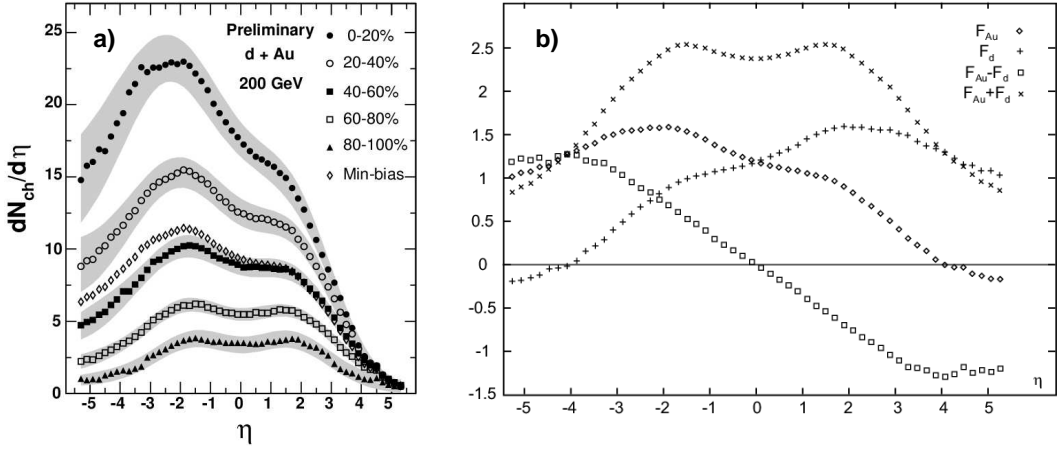
Figure 2.7: **a)** Pseudorapidity distributions of charged particles produced in d+Au reactions at $\sqrt{s_{NN}} = 200$ GeV, obtained in minimum bias collisions and in five centrality bins. The plot is taken from [Nouicer04]. **b)** Contribution to particle production from a single wounded nucleon belonging to the gold (F_{Au}, diamonds) or deuterium (F_d, crosses) nucleus, drawn as a function of pseudorapidity. The sum and difference of the two distributions are also shown in the Figure which is taken from [Białas05].

conservation in Section 2.3.1. It is in fact commonly believed that spectra of produced particles originate not only from projectile/target fragmentation but also from a central production component [Fiałkowski83].

On the other hand, at least two attempts in the above direction can be quoted since the advent of the present century. The first of these attempts started with the application of the Wounded Nucleon Model, Section 1.1, to pseudorapidity spectra of charged particles (mostly pions) produced in d+Au collisions, measured by the PHOBOS experiment at $\sqrt{s_{NN}} = 200$ GeV [Nouicer04] and shown in Fig. 2.7a. This resulted in the extraction of functions F_d and F_{Au}, responsible for the fragmentation of a single projectile (d) and target (Au) nucleon [Białas05]. The two functions are shown in Fig. 2.7b. They overlap and feed into the opposite hemispheres, in clear qualitative similarity to what was shown for the two baryonic components in Fig. 2.5. The range of this feed-over into the opposite hemisphere reaches about four units of pseudorapidity. At typical pion transverse momenta, this would roughly correspond to values of x_F between ± 0.1 and ± 0.15, to be compared with $x_F \approx \pm 0.3$ for baryons at SPS energies (Fig. 2.5).

It is worthwhile to add that the approach described above was later developed and extended by Białas and Bzdak in the framework of the two-constituent "Wounded Quark-Diquark" Model [Bzdak08]. This provided a good description of a number of phenomena in particle production at RHIC energies, in particular also of the centrality dependence of particle production in nucleus-nucleus reactions [Białas07].

The analysis discussed above obviously had to rely on the assumed scenario of particle production - the Wounded Nucleon Model. On the other hand, a completely independent attempt at the separation of pion spectra into projectile and target components was made at SPS energies[13] [Barr07]. This attempt did not need to rely on any specific model. Instead, it was based on accumulated experimental evidence. The starting point of this analysis were the NA49 experimental data on charged pions produced in inclusive inelastic p+p and p+C collisions [Alt06, Alt07]. These are shown in Fig. 2.8. Compared to PHOBOS distributions in Fig. 2.7, NA49 had the advantage of precise pion identification performed over an extended phase space coverage. What is more, it provided a two-dimensional, highly granular information both in the longitudinal and transverse directions (respectively x_F and p_T).

---

[13]The following part of Section 2.3.2 is, to a large extent, based on the quoted reference [Barr07].
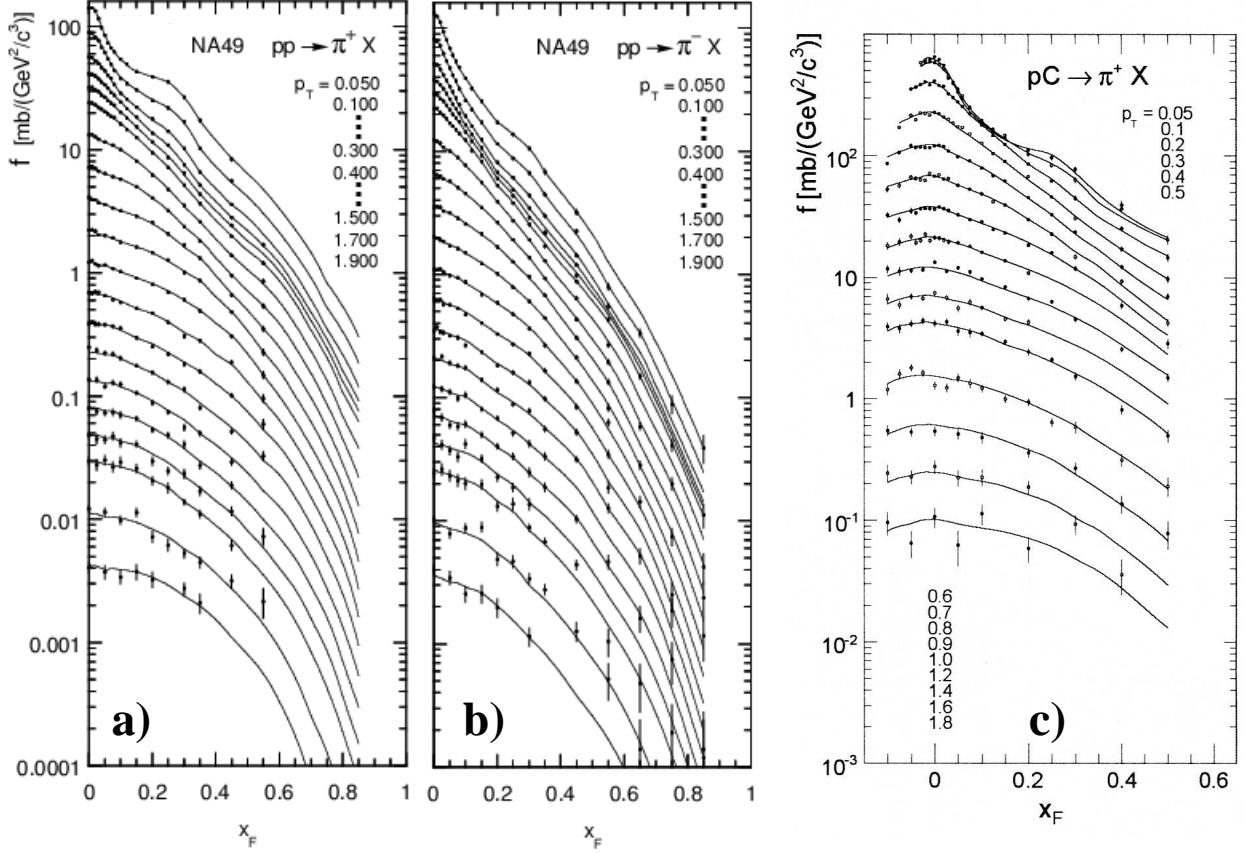
Figure 2.8: Invariant cross section drawn as a function of x_F at fixed p_T for identified positive and negative pions produced in inclusive inelastic p+p (a, b) and p+C (c) reactions at $\sqrt{s_{NN}} = 17.3$ GeV. The values of p_T given in the Figure are to be correlated to the respective distributions, from top to bottom. In panels (a, b), the steps in p_T are 50 MeV/c up to $p_T = 0.3$ GeV/c, then 100 MeV/c up to 1.5 GeV/c and finally 200 MeV/c, while data and lines for $p_T = 0.05$, 0.1, 0.15 GeV/c are respectively multiplied by 2.25, 1.5, 1.1, to allow for a better separation. The plots are taken from [Alt06, Makariev07].

The two-component picture of pion production in p+p collisions was then derived from a combination of independent experimental findings. These were [Barr07]:

- The absence of long range two-particle correlations between secondary hadrons produced in opposite hemispheres at $|x_F| > 0.2$ (see Fig. 2.9a);

- The presence of "forward-backward" multiplicity correlations between the two hemispheres (see Fig. 2.9b), which remains confined to the region $|x_F| < 0.1$ (see Fig. 2.9c);

- The x_F-dependence of the π^+/π^- ratio in $<\pi>$+p reactions, suggesting that the influence of the proton target when colliding with an isospin symmetric projectile again remains confined to the region $x_F < 0.1$ (see Fig. 2.9d).

As a result, the two-component picture deduced from the above is shown in Fig. 2.9e for the case of the averaged charged pion dn/dx_F distribution (i.e., the mean of the dn/dx_F distributions obtained for π^+ and π^- mesons, respectively). The two contributions, from the projectile and the target nucleon, dominate in the corresponding hemispheres, then feed-over into the opposite hemispheres dying out at $x_F = -0.1$ and $x_F = +0.1$, respectively. It may be worthwhile to note that this limiting value of x_F comes close to that quoted for the Wounded Nucleon Model above. Altogether, the overall similarity of results obtained by two different methods speaks
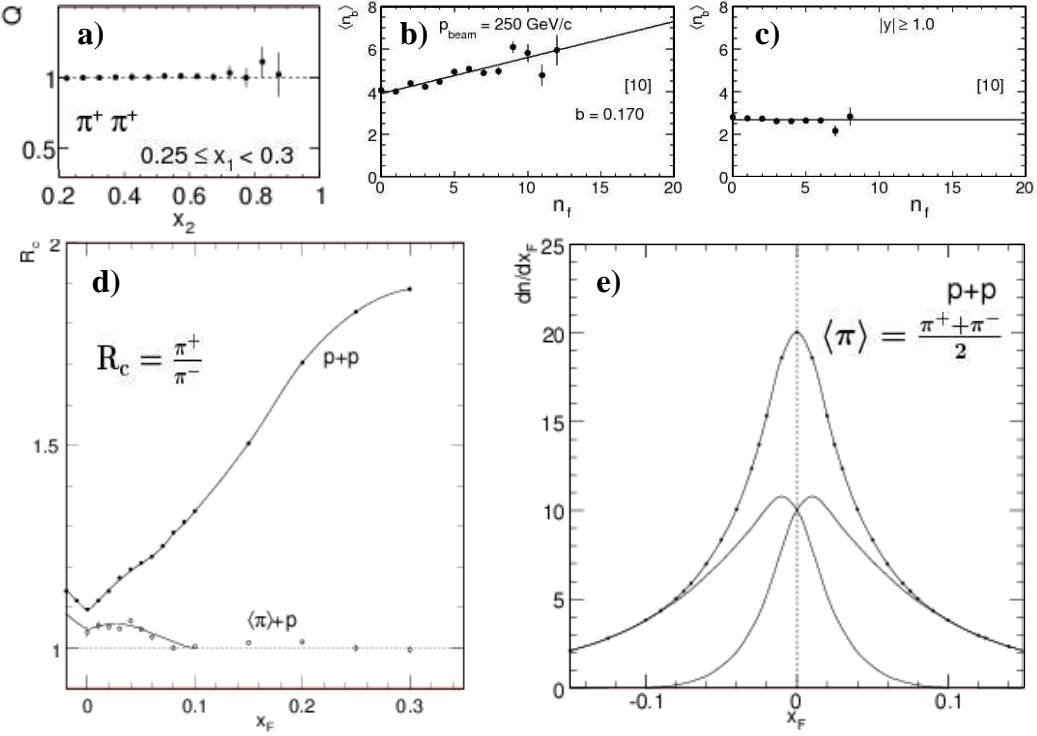
Figure 2.9: Study of two-component picture of pion production in p+p collisions. **a)** Absence of long-range correlation between $\pi^+\pi^+$ pairs. The two pions have Feynman-x values x_1, x_2 selected in opposite hemispheres of the collision; $Q(x_1, x_2)$ is the correlation quotient. **b)** Correlation between the average backward (target hemisphere) charged multiplicity $<n_b>$ and the forward (projectile hemisphere) charged multiplicity n_f. **c)** The correlation from panel (b) vanishes once a cut on particle rapidity is applied, corresponding to $|x_F| = 0.04$-0.06 for typical values of p_T [Barr07]. **d)** x_F-dependence of p_T-integrated π^+/π^- ratio measured in $<\pi>$+p and p+p reactions. **e)** Resulting two-component picture of the averaged charged pion spectrum in p+p reactions. Note: all the plots come from [Barr07] where a more detailed description of the corresponding correlation analyses [Bobbink82, Aivazian89] can also be found.

for the validity of the two-component hypothesis, also when applied to production of secondary pions rather than baryons.

The transition from the *elementary* to the *nuclear* reaction was subsequently investigated by means of p+C data from Fig. 2.8c. In a first step, the relevant *geometrical aspects* of the p+C reaction were studied by means of a geometrical Monte Carlo model (described in more detail in [Rybicki06]). This model, Fig. 2.10a, was based on the usual "Glauber" approach [Glauber06]. It assumed an unbiased sample of proton-carbon collisions, with protons following straight-line trajectories through the carbon nucleus, and interacting with its nucleons with a constant cross section. The latter cross section was assumed to be equal to the proton-proton inelastic cross section $\sigma_{inel}^{pp} \approx 31.4$ mb as measured by NA49 [Alt06]. A specific aspect of this study was the spatial distribution of target nucleons. Instead of applying the usually assumed Saxon-Woods parametrization [Bartke09], this distribution was obtained from the realistic nuclear charge density profile of the ^{12}C nucleus. This profile is shown in Fig. 2.10b, as coming from electron scattering and partially muonic X-ray data on the basis of two different parametrizations: the Fourier-Bessel [Offermann91] and Sum-of-Gaussians [Sick82] expansions of the charge distribution.

As a result of this study, various relevant quantities were estimated. These included in particular the mean number $<\nu>$ of elementary proton-nucleon collisions in the p+C reaction (about 1.7), and especially the contribution $P(1)$ of *single* proton-nucleon collisions to the total p+C sample (about 60%).
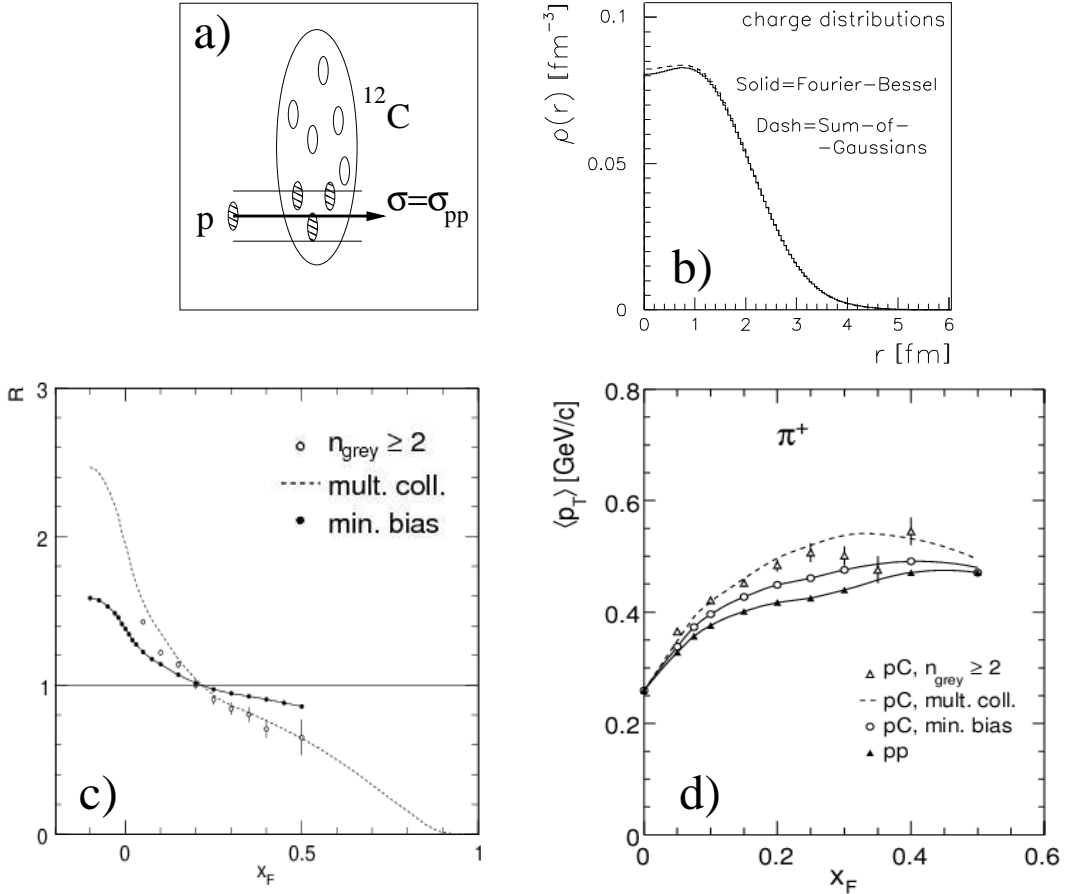
Figure 2.10: Study of p+C reactions. **a)** Schematic sketch of the geometrical model described in the text. **b)** Charge distribution $\rho(r)$, obtained for the ^{12}C nucleus by two different analyses [Offermann91, Sick82]. **c)** x_F-dependence of the ratio R of averaged charged pion production in p+C relative to p+p reactions. The different symbols and curves indicate the ratio $R(min.bias)$, Eq. (2.4), the multiple collision ratio $R(mul.coll.)$, Eq. (2.5), and the ratio obtained with an experimental centrality selection on the number n_{grey} of "grey" protons measured in the p+C event. **d)** The correlation of $<p_T>$ with x_F for positive pions in p+p collisions, minimum bias p+C reactions, the multiple collision component, and the centrality-selected experimental sample of p+C reactions. Panels **(a, b)** are made on the basis of [Rybicki06] while panels **(c, d)** are taken from [Barr07].

The second step of the analysis is shown in Fig. 2.10c where the ratio of the p_T-integrated, averaged charged pion distributions in minimum bias p+C relative to p+p collisions,

$$R(min.\ bias) = \frac{dn/dx_F(p+C)}{dn/dx_F(p+p)} \tag{2.4}$$

is drawn. In the target hemisphere at $x_F = -0.1$, this ratio is 1.6, which is not far from $<\nu> \approx 1.7$ above. This is reminiscent of the scaling with $<\nu>$ which was apparent for baryons in Fig. 2.6a, and was explained by target nucleons suffering single elementary collisions, Section 2.3.1. One may conclude that the situation is roughly similar for the case of pion production.

On the other hand, the production of pions from the *proton projectile* carries the imprint of multiple collisions which the projectile suffers. This results in a specific modification of the pion spectrum at positive x_F, characterized, among others, by a decrease of $R(min.\ bias)$ below unity at high x_F. It is to be noted that a "depletion" of dn/x_F density was present also for high x_F protons, Fig. 2.6b.

As far as studies of the influence of multiple collisions on pion production are concerned,

26

the ratio $R(min.\ bias)$ defined above can be regarded only as an *indirect* observable. This is due to the very sizeable contribution of single proton-nucleon collisions to the minimum bias sample of p+C reactions, see discussion above. An attempt was therefore made to extract the pure *multiple collision content* of the p+C reaction. The key issue here was the knowledge of the single collision fraction $P(1)$, and of the pion distribution in single collisions, here assumed similar to that obtained in elementary p+p reactions. On that basis, the multiple collision ratio

$$R(mult.coll.) = \frac{dn/dx_F(p+C, \nu \geq 2)}{dn/dx_F(p+p)} \tag{2.5}$$

could be extracted. This is also shown in Fig. 2.10c. Compared to minimum bias p+C reactions, a much stronger modification of the pion spectrum is evident. It is to be noted that this approaches the ratio obtained directly for a sub-sample of p+C events selected experimentally by a constraint on centrality (at least two "grey" protons detected by NA49, Section 2.2.2). This consistency confirms both the reliability of extraction of $P(1)$ and $R(mult.coll.)$, as well as the effectiveness of NA49 experimental centrality selection.

The discussion made up to now was focussed on the longitudinal direction. A first look at the *transverse dimension* of positive pion production is given in Fig. 2.10d where the correlation of pion mean transverse momentum $<p_T>$ with x_F is shown for p+p collisions, minimum bias p+C reactions, and the multiple collision component of p+C interactions. A clear systematics is apparent. With increasing content of multiple collisions suffered by the projectile proton, the latter displays an increasing "transverse activity" in pion production, keeping however the rounded "seagull" shape characteristic of this correlation already for p+p collisions[14].

The accumulation of experimental and phenomenological findings discussed above suggests that in spite of the quoted conceptual difficulties, the two-component hypothesis is quite a promising tool for future studies of particle production. Some basic similarity could therefore be drawn between pion production and baryon-related phenomena analysed in Section 2.3.1. The spectrum of baryons (produced particles) would be a superposition of two components issuing from the fragmentation of projectile and target nucleons.
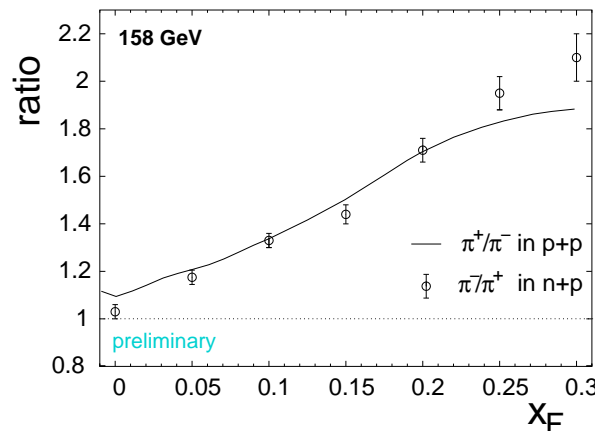
Figure 2.11: p_T-integrated π^+/π^- ratio in the projectile (proton) hemisphere of p+p collisions, compared to the π^-/π^+ ratio in the projectile (neutron) hemisphere of n+p collisions. The p+p data (curve) are re-drawn from Fig. 2.9d while the preliminary n+p data (circles) are re-drawn from [Chvala04].

This brings numerous consequences. Out of these, two are of particular importance for the present work. Firstly, it is of course interesting to consider whether the above reasoning can also

---

[14]The term "seagull" originates from the similarity of the correlation "$<p_T>$ against x_F" discussed in the text to seagull wings, if plotted in the full range of x_F [Fiałkowski83].
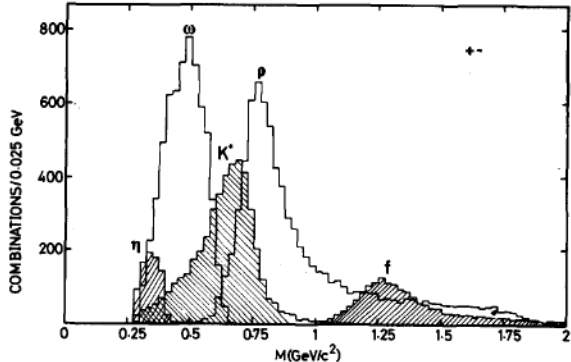
Figure 2.12: Fitted resonance peaks contributing to the background-subtracted $\pi^+\pi^-$ invariant mass spectrum in p+p collisions at $\sqrt{s} = 53$ GeV (the K^* is argued to contribute through kaon misidentification as a pion in the $K^* \to K\pi$ decay). The plot comes from [Jancso77].

be extended to pion production in nucleus-nucleus collisions. Secondly, the connection has to be seen between the two-component picture, the multiple collision phenomena discussed above, and *the valence structure of the incoming hadrons*. This can be illustrated by the comparison of the x_F-dependence of the π^+/π^- ratio in p+p collisions to the π^-/π^+ ratio in n+p reactions, shown in Fig. 2.11. It is known that particle production depends on the incoming hadron quantum numbers [Fiałkowski83]. Specifically, the fragmentation of the proton into pions is characterised by a strong increase of the π^+/π^- ratio with x_F, seen in the Figure. In spite of the preliminary status and low statistics of the NA49 n+p data, it is clear that in the pure neutron fragmentation region at $x_F > 0.1$, the inverse ratio (π^-/π^+) approaches the π^+/π^- ratio seen for proton fragmentation - as it is directly expected from isospin symmetry. On the other hand, the equality of the neutron projectile and proton target components at $x_F = 0$ results in $\pi^-/\pi^+ = 1$, also seen in the Figure.

As far as nuclear collisions (p+A, A+A) are concerned, they are always made of participating *protons* and *neutrons*. The presence of neutrons will result in "isospin effects" [Fischer02] like the inversion of the π^+/π^- ratio shown in Fig. 2.11. Generally, nuclear reactions are not directly comparable to pure p+p interactions but rather to a superposition of p and n fragmentation. This issue will be frequently addressed in the subsequent parts of this paper.

2.3.3 Resonances

The discussion of baryon and pion production made in Sections 2.3.1-2.3.2 was uniquely based on inclusive and semi-inclusive distributions of *final state particles*. This seems in fact quite a poor basis for achieving any kind of assumption-free understanding of the non-perturbative process of the hadronic reaction. Prime importance is therefore to be attributed to any source of model-independent information reaching *beyond the final state*, in particular into the *intermediate stage* of the space-time evolution of the reaction. One of the most evident experimental findings on the above intermediate stage is the issue of resonance production.[15]

It is known that hadronic resonances (i.e., unstable and strongly-decaying excited states) are copiously produced in hadronic reactions. This implies that a very sizeable fraction of final state particles is not produced "directly" but originates as a final product of resonance excitation and decay (*resonance dominance* [Fiałkowski83]).

At least in elementary hadron-hadron interactions, attempts were made to estimate this fraction on an experimental basis. If enumerated in a chronological order, the first analysis to

---

[15]Section 2.3.3 is based on Refs. [Fiałkowski83, Jancso77, Grässler78, Rybicki02, Fischer05, Rybicki09a].
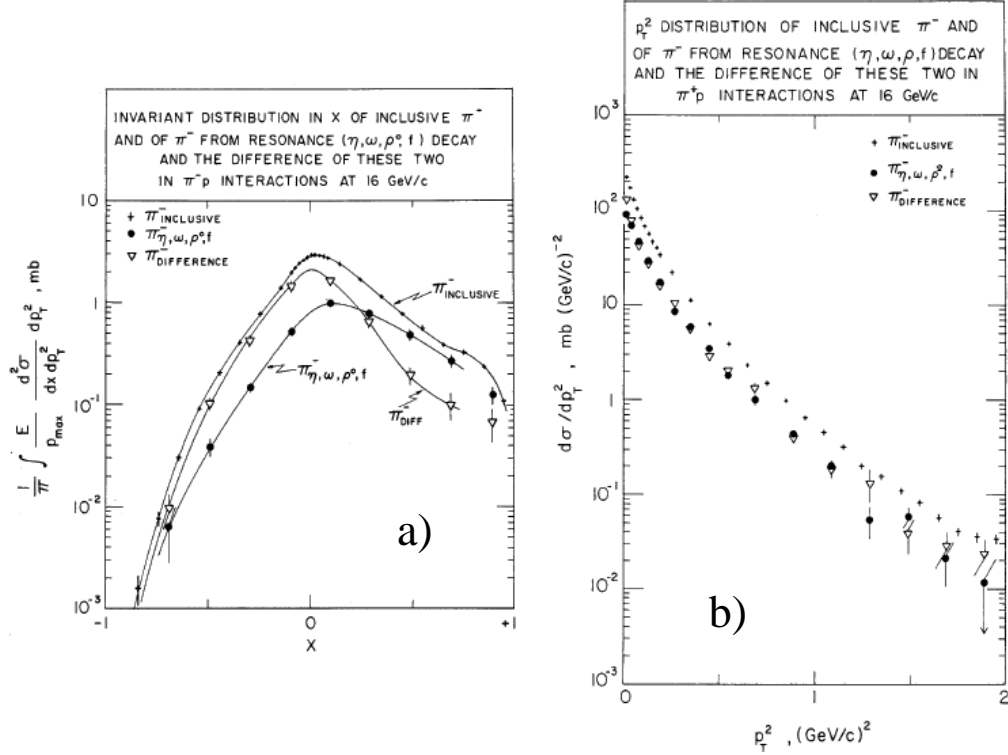
Figure 2.13: Longitudinal and transverse distribution of resonance daughter π^- compared to the inclusive π^- spectrum and to the difference between these two, in $\pi^+ + p$ reactions at 16 GeV/c beam momentum ($\sqrt{s} \approx 5.6$ GeV). The plots come from [Grässler78].

be quoted here came from the Split Field Magnet (SFM) detector at the CERN ISR, and was made for inelastic p+p reactions at $\sqrt{s} = 53$ GeV. Here, Jancso et al. [Jancso77] estimated the number of charged particles originating from vector meson decay, on the basis of a resonance fit to the background-subtracted distribution of invariant mass of $\pi^+ \pi^-$ pairs (Fig. 2.12). The result was 10.3 ± 1.2 secondaries coming from the decays of ρ, ω, and $K^*(890)$; this was compared to the average multiplicity of 10.1 ± 1.5 charged pions and kaons produced per one inelastic event. Account taken of the uncertainties inherent to the study, the authors concluded that more than 60 % (at 95 % confidence level) of charged pions and kaons originated from vector meson decay.

A detailed experimental study was performed by Grässler et al. [Grässler78] for $\pi^+ + p$ reactions at $\sqrt{s} \approx 5.6$ GeV. A data sample of 0.4 million events recorded in a bubble chamber experiment at the CERN PS was used to obtain the rapidity, x_F and p_T^2 distributions of negative pions coming from various resonance decays. This was made by a direct resonance peak determination in the invariant mass spectra associated with the π^- belonging to a given kinematical bin. The authors conclude that about 50 % of final state π^- production results from the decays of η, ω, ρ and f mesons. It is instructive to inspect the *shape* of resonance daughter spectra. Fig. 2.13a shows the x_F distribution of daughter π^- originating from summed η, ω, ρ^0 and f decays ($\pi^-_{\eta,\omega,\rho^0,f}$), compared to the inclusive distribution of produced pions ($\pi^-_{\text{INCLUSIVE}}$), and to the difference between the two distributions ($\pi^-_{\text{DIFFERENCE}}$). An analogous comparison is shown in Fig. 2.13b in the transverse dimension, where the resonance contribution has been supplemented with that of the ρ^- state, see [Grässler78] for more details. As visible in the Figure, resonance daughters do not remain confined to any restricted region of phase space. On the contrary, the shape of the resonance daughters' spectrum exhibits an apparent similarity to that of the inclusive distribution. This is particularly valid for pions in the high x_F region, as well as in the transverse dimension where $\pi^-_{\eta,\omega,\rho,f}$ and $\pi^-_{\text{DIFFERENCE}}$ bring more or less equal fractions
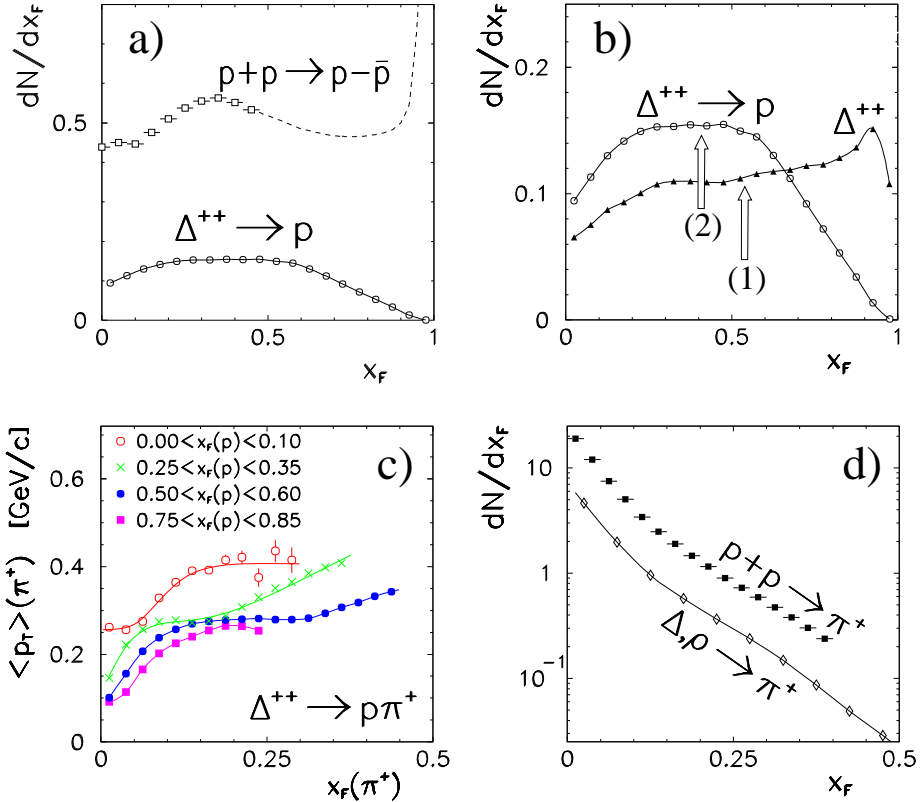
Figure 2.14: **a)** Distribution of protons coming from the decay $\Delta^{++} \to p\pi^+$, compared to the total inclusive net proton spectrum in the projectile hemisphere of the p+p collision. **b)** Distribution of decay daughter protons from panel (a), compared to that of their parent Δ^{++}. Arrows give mean values for the two distributions in the range $0 < x_F < 1$, and illustrate the fraction of momentum loss of the incoming proton taken by the Δ decay (see text). **c)** Positive pion $<p_T>$ vs. x_F dependence, taken with different selections on the Feynman variable of the proton, $x_F(p)$. The proton and the pion come from the decay of the same parent Δ^{++} resonance. **d)** Longitudinal spectrum of π^+ originating from (summed) Δ^{++}, ρ^0, and ρ^+ decays, compared to the inclusive π^+ spectrum in p+p collisions. All the plots come from [Rybicki02].

to the total pion yield at all values of transverse momentum[16].

It should be underlined that both analyses quoted above give only *lower limits* for the resonance contribution to particle production. The authors of [Grässler78] clearly specify that $\pi^-_{\text{DIFFERENCE}}$ cannot be regarded as any pure "direct" (non-resonant) component of pion production, because further resonance contributions must be considered. It is in fact very difficult to exclude the presence of additional yet undetected excited states [Fiałkowski83, Grässler78, Alt06]. As an example, the transition from the dominance of $\pi^-_{\text{DIFFERENCE}}$ over $\pi^-_{\eta,\omega,\rho^0,f}$ at negative x_F into its suppression at positive x_F (Fig. 2.13a) would indicate an important role of baryonic resonances in the proton fragmentation region, in contrast to the pion fragmentation region where excited mesons dominate.

Altogether, the quoted experimental estimates show that resonance-induced effects are evidently very large and indicate the need of similar analyses for other phenomena and at other collision energies. Such an analysis was performed for the role of Δ^{++} and ρ states in baryon stopping and π^+ production in p+p collisions at $\sqrt{s} = 17.3$ GeV [Rybicki02]. This was made by means of a Monte Carlo simulation, based on inclusive spectra of the above resonances as

---

[16]Note: [Grässler78] points that the different components of $\pi^-_{\eta,\omega,\rho,f}$ feed differently into various regions of x_F and p_T. Thus, the total spectrum $\pi^-_{\text{INCLUSIVE}}$ appears in fact as quite a complicated superposition of various effects, and dependent on resonance decay kinematics.

measured by the EHS and SFM experiments in the overall range of $\sqrt{s}$ from 27.5 to 62 GeV [Aguilar-Benitez91, Drijard84]. The simulation took account of such issues as the energy dependence of resonance yields, the mass distribution of the parent resonance and the high-mass damping of the corresponding relativistic Breit-Wigner function [Jackson64], etc.

A selection of results of this study is presented in Fig. 2.14. Panel **(a)** shows the p_T-integrated, longitudinal distribution of protons originating from the decay $\Delta^{++} \to p\pi^+$, compared to the inclusive net proton distribution. With the exception of the diffractive proton peak at high x_F, the two distributions exhibit a clear similarity in shape. The Δ^{++} decay daughters build up a sizeable (20-30%) fraction of the "bump" observed at intermediate x_F in the inclusive spectrum. This fraction will obviously go up as other baryonic resonances will also contribute, to begin with the Δ^+ and Δ^0 states reported by EHS [Aguilar-Benitez91]. The situation seems therefore quite similar to that of produced pions discussed in Fig. 2.13, with baryonic resonances playing a significant role in the baryon stopping processes discussed in Section 2.3.1. As specified in [Rybicki02], whenever present in the p+p event, the $\Delta \to p\pi$ (or $N^* \to p\pi$, $N^* \to p\pi\pi$) decays constitute the *last stage* of the overall process of transport of baryon number from the incoming to the final state proton. Their contribution to this process can be expected to be sizeable. To take the example of the $\Delta^{++} \to p\pi^+$ decay (Fig. 2.14b), it appears responsible for about 25 % of the average loss of longitudinal momentum occurring between the incoming projectile ($x_F = 1$) and the final state proton.

Baryonic resonances appear also responsible for other phenomena. Fig. 2.14c shows the correlation between the $<p_T>$ vs. x_F dependence of the positive pion coming from the Δ^{++} decay, and the Feynman variable $x_F(p)$ of the proton coming from the same parent Δ^{++}. Evidently, an increased stopping (lower x_F) of the daughter proton results in an increased transverse momentum of the daughter pion. A qualitatively similar effect has been observed in an experimental semi-inclusive study of p+p reactions (see [Rybicki02]). This points at the importance of baryonic resonances in building up the internal correlations present in p+p events. Moreover, it is to be reminded that in *nuclear* reactions both baryon stopping and the pion transverse momentum increase with multiple collisions undergone by the projectile (see Figs 2.6b and 2.10d, respectively). Thus, a connection may exist between resonance production discussed here, baryon phenomena analyzed in Section 2.3.1, and pion production in Section 2.3.2.

The last result of this study is presented in Fig. 2.14d where the p_T-integrated longitudinal distribution of positive pions originating from summed Δ^{++} and ρ decays is compared to the total inclusive π^+ spectrum. A remarkable similarity of the two distributions is apparent. Similarly to what was shown for pions at lower energies (Fig. 2.13), and for baryons (Fig. 2.14a), the resonance contribution to the inclusive spectrum is not confined to any particular kinematical region. Instead, it spreads over the whole considered range of phase space.

As argued before, the distribution of resonance daughters in Fig. 2.14d can again not be interpreted as the total resonance contribution to π^+ production in p+p collisions, but only as another *lower limit*. Other excited states present in the inclusive p+p reaction will give additional pions feeding into the total spectrum. In this context, probably the most complete analysis of the contribution of resonances to inclusive pion production was performed by Fischer et al., again for p+p reactions at $\sqrt{s} = 17.3$ GeV [Fischer05]. Technically based on Monte Carlo techniques similar to these used above, the study included negative pions originating from the sum of 13 resonant states: η^0, $\omega^0(782)$, $\rho^0(770)$, $\rho^-(770)$, $f_2^0(1270)$, $\rho_3^0(1690)$, $\rho_3^-(1690)$, $f_4^0(2050)$, $\Delta^0(1232)$, $\Delta^-(1232)$, $N^{*0}(1440)$, $N^{*0}(1520)$, and $N^{*0}(1680)$. The parent cross sections and spectra were deduced from a wide compilation of experimental results, including preliminary data on N^* production [Kreps04]. The analysis took account of the existence of *cascading resonance decays*, like $\rho_3 \to \omega\pi$ or $N^* \to \Delta\pi$. As argued in [Fischer05], these could result in *double counting* of resonance products. To avoid such double counting, only two-body decays were included in the analysis (three-pion decays for the case of η and ω states). Other multi-body
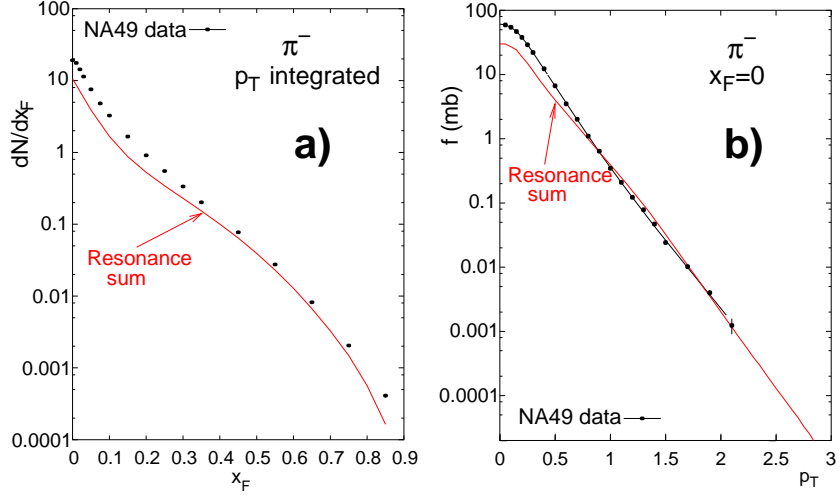
Figure 2.15: **a)** Data points: p_T-integrated density distribution of negative pions produced in inclusive inelastic p+p collisions at $\sqrt{s} = 17.3$ GeV [Alt06], drawn as a function of x_F. Solid curve: distribution of resonance π^- daughters coming from the study [Fischer05] discussed in the text. **b)** Data points: invariant cross section f of π^- measured in p+p collisions [Alt06], drawn as a function of p_T at $x_F = 0$, and compared to the corresponding distribution of resonance daughters. The plots come from [Fischer05].

decays were explicitly *not* included in the study.

Fig. 2.15 shows a selected set of results of the above analysis. A comparison between p_T-integrated longitudinal distributions of inclusive π^- measured by NA49 [Alt06] and of negative pions originating from the summed decays of the 13 excited states enumerated above is presented in panel **(a)**. An analogous comparison of p_T distributions at $x_F = 0$ is displayed in panel **(b)**. As a result of both comparisons, a clear similarity of the shape of the total inclusive and resonance daughter spectra is evident. In that sense, the situation is reminiscent of that shown for $\pi^+ +$p collisions at $\sqrt{s} \approx 5.6$ GeV (Fig. 2.13). The principal difference is that the superior number of considered excited states results in the apparent saturation of the inclusive distribution by resonance daughters at higher values of p_T (panel **b**). This resonance contribution diminishes with decreasing p_T, and also (from c.a. 80 % down to some 50 %) with decreasing x_F. However, it can be argued that the region of lower x_F and lower p_T is where pions from multi-body decays, see above, would additionally contribute to the total inclusive spectrum (note that such pions should have lower momenta in the c.m. system of their parent resonance). This would further increase the already very large resonance contribution to π^- spectra.

The four analyses presented above are all either purely experimental or at least, directly based on experimental information. The similarity apparent between their results, emphasized in the discussion above, seems to crystallize in an overall consistent picture of the role of hadronic resonances in particle production. This picture could be summarized as follows. Intermediate resonant states exert a very strong influence on final state particle production. This influence is not limited to π meson production (where resonant decays appear as the dominant source), but is exerted also on baryons (where they contribute to the baryon stopping process). They also leave their imprint on the internal correlations present in hadronic events (specifically also on correlations between baryon stopping and π meson distributions, Fig. 2.14c). The influence of resonances is not limited to any particular region of phase space (like low x_F, low p_T). On the contrary, in the whole range of x_F and p_T considered in this paper, the measured inclusive particle distributions exhibit a shape similar to that of resonance daughter spectra (Figs 2.13, 2.14a,d, 2.15). This similarity calls for consideration to what extent the remaining final state particles (which are defined as $\pi^-_{\mathrm{DIFFERENCE}}$ in Fig. 2.13 and could be defined analogically in the

other figures) could be attributed to additional resonance decays not yet considered, rather than to "direct" production phenomena. In particular, the role of cascading multi-body decays calls for scrutiny.

At the level of the present discussion, the question of the *origin* of resonances - parton fragmentation, cascading from higher excited states, or any other hypothetical mechanism - must remain open. However, it seems clear from the above that hadronic excitation and decay should always be considered as a potentially important "underlying layer" to particle production phenomena under study. In particular, this also applies to phenomena studied in this paper.

2.3.4 The Spectator System

The discussion made in the precedent Sections was as much based on elementary collisions (p+p, π+p) as on nuclear reactions (p+C, p+Pb, π+Pb, d+Au, Pb+Pb). Phenomena occurring in the nuclear case - like in Figs 2.6 and 2.10 - were implicitly attributed to the fragmentation of participant nucleons, the main difference to elementary reactions residing in the increased thickness of traversed nuclear matter (*multiple collisions* in Section 2.3.1). Such a simple approach seems reasonable on general grounds, and particularly useful in finding similarities between hadron-hadron, hadron-nucleus and nucleus-nucleus collisions [Rybicki04a]. However, it also has clear limitations. The aim of the present Section is to bring out some of these limitations, and to discuss the scientific findings which directly inspired the analysis made in subsequent Chapters.

When seen *a posteriori*, the evolution of physics ideas and phenomenological conclusions described below may appear as very simple and even partially trivial. Nevertheless, it may be instructive under several aspects. Firstly, it shows how the above approach may fail and lead to wrong conclusions in specific cases. Secondly, it gives a practical example of the significance of the methodological postulates **1.**, **2.**, **3.** formulated in Chapter 1, Section 1.1. Thirdly, it shows how the clarification of the above issues results in a more general approach, giving insight into new physics phenomena and pointing at the role of the spectator system in shaping the final state particle distributions. Finally, it specifies the role of the author in defining this problematics which, at least in his closest scientific environment, constituted a complete novelty relative to studies made so far.

Taken in a chronological order, the discussion starts with a preliminary NA49 result on the x_F-dependence of p_T-integrated π^+/π^- ratios, measured in different nuclear reactions at a single beam energy of 158 GeV/nucleon ($\sqrt{s_{NN}} = 17.3$ GeV). These are shown in Fig. 2.16a. This result has been related to "isospin effects" discussed in Section 2.3.2. The x_F-dependence of proton and neutron fragmentation, shown in Fig. 2.11, has been used to predict the x_F-dependence of the π^+/π^- ratio in different systems, composed of a given number of fragmenting protons and neutrons [Chvala04]. The corresponding predictions are shown in Fig. 2.16a as a set of solid curves. For Si+Si reactions, made of 50% protons and 50% neutrons, the prediction corresponds to unity. For Pb+Pb collisions (40% protons and 60% neutrons) it remains below unity due to the prevailance of neutrons which fragment preferably into π^- rather than π^+ (see Fig. 2.11). Preliminary data on Si+Si and central Pb+Pb reactions remain reasonably close to the predicted values, demonstrating the importance of the above-mentioned isospin effects for the interpretation of nuclear reactions.

Fig. 2.16a also includes a set of preliminary data points obtained from an experimental sample of *peripheral* Pb+Pb events. Surprisingly, and unlike in central collisions, in this case the measured π^+/π^- ratios remain significantly below the prediction made for Pb+Pb reactions with 40% protons and 60% neutrons participating. Incidentally, these four data points appeared to fit with another prediction, namely that of a system made of 25% protons and of 75% neutrons (also shown in the Figure). A first interpretation was therefore proposed attributing this effect to the presence of the "neutron halo". It is indeed known that the proton and neutron distributions
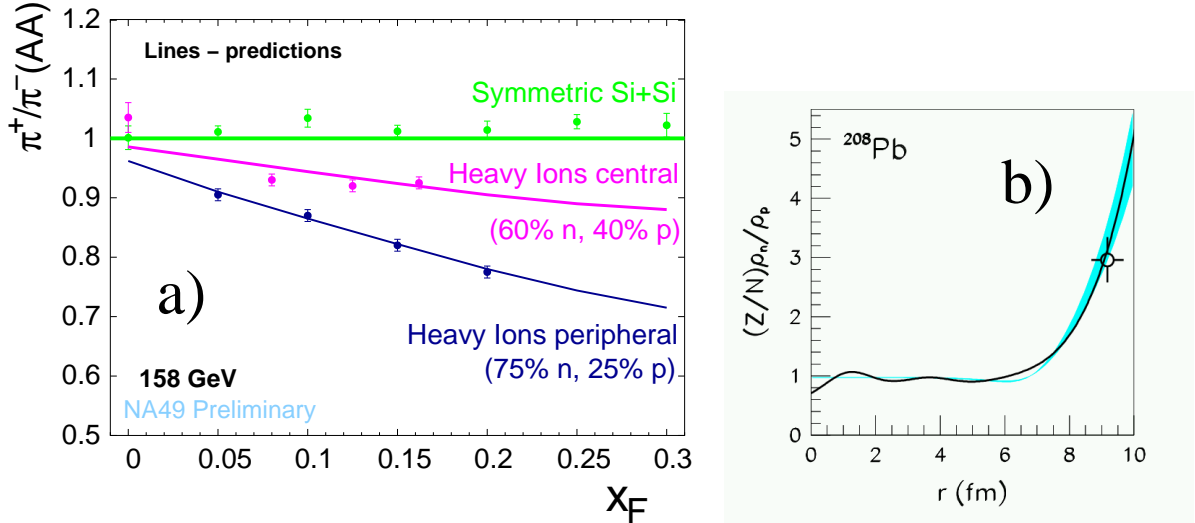
Figure 2.16: **a)** p_T-integrated ratios of produced π^+/π^-, drawn as a function of x_F for Si+Si reactions, central Pb+Pb collisions ("Heavy Ions central"), and peripheral Pb+Pb collisions ("Heavy Ions peripheral"). The data points are compared to the predictions discussed in the text. The plot comes from [Rybicki04b], more details in [Chvala04]. **b)** Normalized ratio of neutron to proton densities $\frac{Z}{N}\frac{\rho_n(r)}{\rho_p(r)}$, drawn as a function of the distance r from the center of the ^{208}Pb nucleus. Compilation of experimental studies on antiprotonic atoms (data point [Trzcińska01a], shaded band [Schmidt03]), and theoretical calculation by the Hartree-Fock-Bogoliubov method (solid line [Mizutori00]). The plot comes from [Pawłowski04].

in the Pb nucleus do not have exactly similar shapes, resulting in the presence of a peripheral region characterised by high values of the neutron/proton ratio (a compilation of experimental and theoretical results is shown in Fig. 2.16b). The idea was therefore that the peripheral Pb+Pb collision would probe this region, resulting in an increase of the neutron/proton ratio in the participant zone relative to the entire Pb nucleus. This in turn would lower the π^+/π^- ratios resulting from participant fragmentation.

The above interpretation was clearly very attractive, among others because it seemed to offer an *independent means for the determination of the distribution of neutrons inside the nucleus*, in high energy nuclear reactions (very different from methods used at lower energies like e.g. these based on antiprotonic atom data [Trzcińska01a, Schmidt03]). This is probably why at first, only the author of the present paper expressed doubts about the correctness of this interpretation. The problem was that the region of high neutron/proton ratio, Fig. 2.16b, corresponded to the far periphery of the Pb nucleus ($r \geq 8$ fm). At the same time the experimental definition of the considered Pb+Pb event sample (from 150 to 300 charged particles observed in the NA49 detector) suggested an appreciable number of participating nucleons, not to be reconciled with very large impact parameters of the collision.

The author suggested to Pawłowski and Szczurek to perform a theoretical study of this problem. The resulting analysis [Pawłowski04] confirmed his doubts, expressed above. The situation is shown in Fig. 2.17. Independently of the model assumed for particle production, the neutron halo had only a very limited influence on produced π^+/π^- ratios. Values as low as seen in the data were attainable only in "extremely peripheral" reactions, characterized by impact parameters of 16 fm or more.

An independent analysis was then performed by the author (later documented in [Rybicki06]). This was made by means of a geometrical Monte Carlo model similar to that described in Section 2.3.2. Nucleons belonging to a given Pb nucleus followed straight-line trajectories
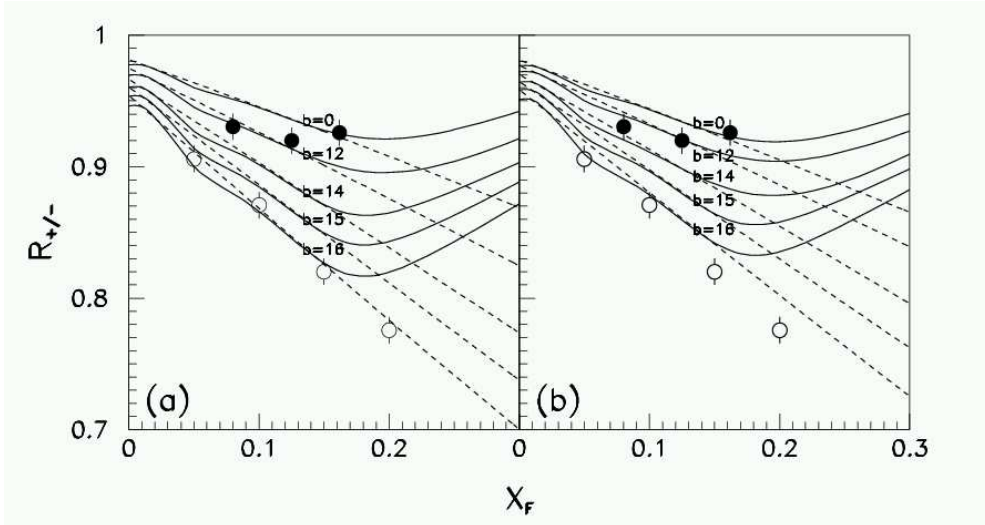
Figure 2.17: Preliminary data points on central and peripheral Pb+Pb collisions from Fig. 2.16a, compared to the results of the study [Pawłowski04]. The theoretically predicted π^+/π^- ratios ($R_{+/-}$) are drawn at various values of the impact parameter b of the Pb+Pb reaction. The different curves correspond to different input assumptions on proton and neutron fragmentation in elementary collisions (solid - obtained from the HIJING model [Gyulassy94], dashed - from a fit to preliminary p+p and n+p data [Rybicki04b]). The two panels correspond to two different particle production models assuming (a) scaling with the number of "binary" nucleon-nucleon collisions, see also Chapter 5, and (b) scaling with the number of wounded nucleons, see also Sections 1.1 and 2.3.2. The plot comes from [Pawłowski04].
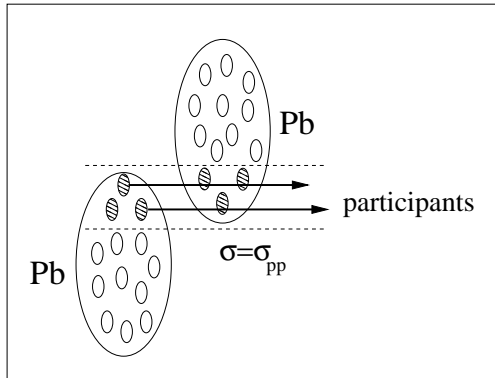
Figure 2.18: Geometrical model of the Pb+Pb reaction described in the text. The participant nucleons are shown as filled ellipses, while the other (spectator) nucleons are indicated by empty ellipses.

through the adverse nucleus, interacting with its nucleons with a constant cross section equal to the proton-proton inelastic cross section (Fig. 2.18). Each nucleon was defined as a *participant* whenever it underwent at least one inelastic interaction[17]. The spatial distributions of protons and neutrons in the Pb nucleus were based on corresponding state-of-the-art proton and neutron density functions [Trzcińska01, Mizutori00]. The basic conclusions from this analysis were similar to [Pawłowski04]. As apparent in Fig. 2.19a, the participant neutron/proton ratio reached the expected values of $\frac{75\%}{25\%} = 3$ only at very high impact parameters of the Pb+Pb collision,

---

[17]Note: this means that the term "participant" defined in the text is strictly equivalent to "wounded nucleon" defined in [Białas76], see also Section 1.1. The same equivalence will apply to all the NA49 centrality studies and electromagnetic Monte Carlo analyses performed in the subsequent parts of this paper.
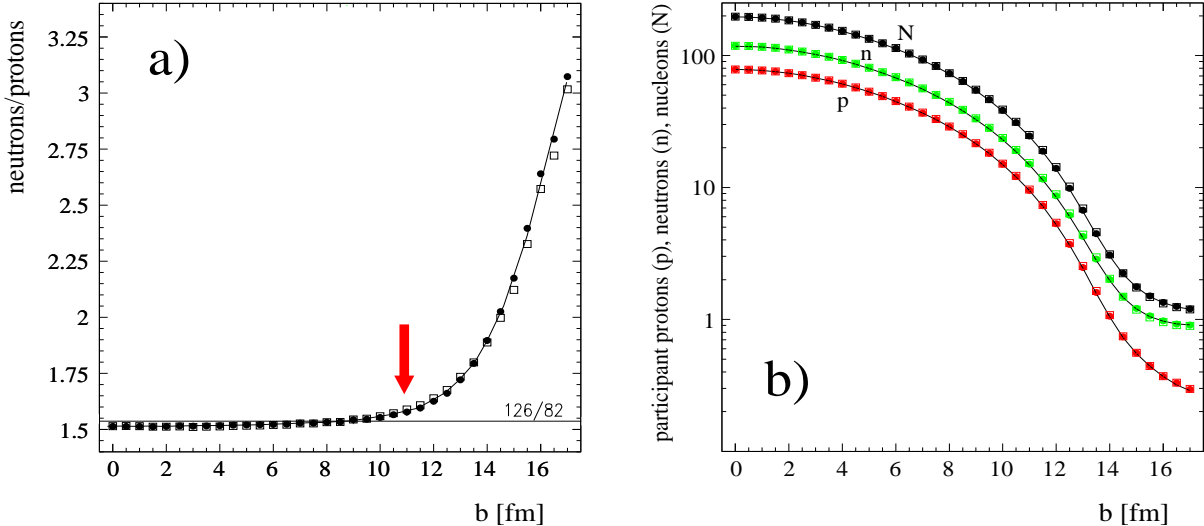
Figure 2.19: **(a)** Neutron-over-proton ratio and **(b)**, number of projectile protons, neutrons, and summed nucleons in the participant zone of the Pb+Pb reaction, drawn as a function of the impact parameter b. The calculation was made for two sets of nuclear proton and neutron density profiles (● [Trzcińska01], □ [Mizutori00]). The solid horizontal line in panel **(a)** represents the average neutron-to-proton ratio in the ^{208}Pb nucleus. The vertical arrow indicates the average impact parameter estimated for the experimental sample of peripheral Pb+Pb events discussed in the text. The results come from [Rybicki06].

$b > 16$ fm. This in turn meant a very small number of participating nucleons, see Fig. 2.19b, which seemed impossible to reconcile with the observed multiplicity of 150-300 charged particles. Indeed, a subsequent analysis (described in detail in Section 3.2) estimated the average impact parameter in this experimental sample to be about 11 fm. This imposed constraints on the participant neutron/proton ratio, which should remain close to the same ratio in the entire Pb nucleus (60% neutrons over 40% protons), see Fig. 2.19a. The conclusion had therefore to be made that the hypothesis of the neutron halo as source of the effect seen in Fig. 2.16 was in evident contradiction with the nucleon density functions obtained in [Trzcińska01] and [Mizutori00]. Numerous attempts have then been made to reach the agreement with the experimental data by bringing various modifications to the above-mentioned density functions, but all these attempts failed. This brought the final conclusion that the neutron halo hypothesis could not be further defended, and had to be completely abandoned.

Only at that point did it become apparent to the author that the reasoning underlying the neutron halo hypothesis contained one basic flaw: phenomena occurring in the projectile fragmentation region of peripheral Pb+Pb reactions were *not* to be understood as induced solely by the fragmentation of participant nucleons. This was triggered by a trivial constatation on the four data points from Fig. 2.16a, which were located at four values of x_F: 0.05, 0.1, 0.15, and 0.2. In particular, let us note that the value $x_F = 0.15 \approx \frac{m_\pi}{m_N}$ corresponds, for longitudinally moving pions, to velocities equal to these of beam (spectator) nucleons:

$$x_F \approx \frac{p_\pi}{p_s} = \frac{m_\pi \beta_\pi \gamma_\pi}{m_N \beta_s \gamma_s} \tag{2.6}$$

where β is the velocity defined in units of the speed of light, $\gamma = (1 - \beta^2)^{-1/2}$, and the subscripts π, N and s stand for pion, nucleon, and spectator, respectively. Such pions could spend a sizeable time in the vicinity of the *massive spectator system* emerging from the collision (Fig. 1.1). Therefore they could interact with spectator nucleons. As a result, *such an interaction could influence the π^+/π^- ratios observed in the final state of the reaction.*

While not very precise, the above conjecture was sufficient to suggest an experimental

36
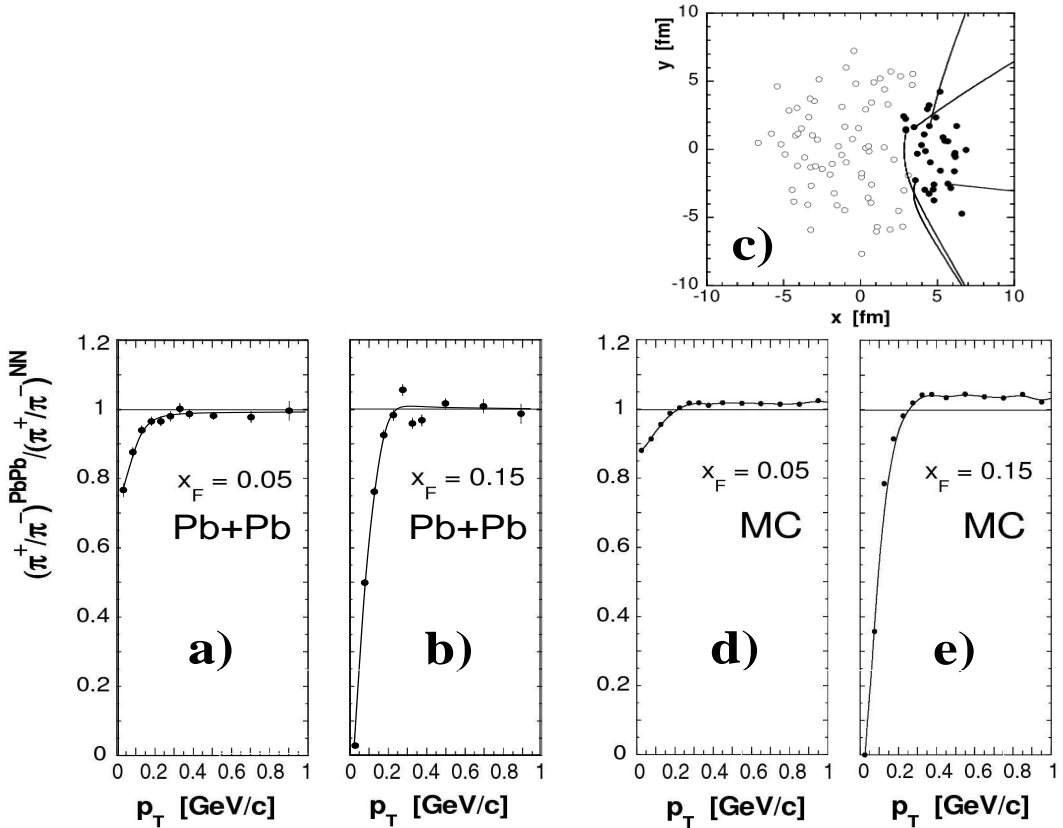
Figure 2.20: **Panels (a) and (b)**: experimental data on the π^+/π^- ratio in peripheral Pb+Pb collisions at $\sqrt{s_{NN}} = 17.3$ GeV, normalized to the same quantity predicted for a superposition of nucleon-nucleon (NN) interactions, and drawn as a function of p_T at $x_F = 0.05$ and $x_F = 0.15$. **Panel (c)**: Monte Carlo simulation of the electromagnetic effect induced by the projectile spectator system, visualized in the transverse xy plane of the peripheral Pb+Pb reaction. Pions are emitted from participating projectile nucleons (closed circles) and their trajectories (solid lines) are modified by the electromagnetic field of projectile spectator charges (open circles). The Figure is made for positive pions with $0.1 < x_F < 0.2$ and $p_T < 0.1$ GeV/c. Note that only the projectile participants and spectators are shown. **Panels (d) and (e)**: results of the Monte Carlo simulation described above, taken from [Rybicki07a].

scrutiny of the p_T-dependence of the observed effect, in addition to the x_F-dependence studied so far. The results of this scrutiny are shown in Fig. 2.20, panels **(a)** and **(b)**. The plotted quantity is the π^+/π^- ratio in the peripheral sample of Pb+Pb collisions, normalized to the same ratio predicted for a superposition of nucleon-nucleon (NN) interactions[18]. As apparent from the Figure, the observed depletion of π^+/π^- ratios reveals a surprising structure in the transverse direction. At $x_F = 0.15$, the ratio remains close to unity above $p_T = 0.3$ GeV/c, but then rapidly falls down with decreasing p_T, approaching zero at lowest transverse momenta. A similar but less pronounced behaviour is also apparent at $x_F = 0.05$.

It rapidly became clear to the author that the result seen in Fig. 2.20 was extremely difficult to explain by any effect of a purely hadronic origin (i.e., caused exclusively by the strong interaction). Indeed, one could expect that for an initial state made of 40% protons and 60% neutrons as in the Pb+Pb collision under study (see discussion above), the final state π^+/π^- ratio would not fall below $\sim \frac{2}{3}$ if the interaction obeyed isospin symmetry. It became thus clear that the experimental evidence pointed towards an interaction explicitly breaking isospin invariance, like

---

[18]That is, for a mixture of 40% fragmenting protons and 60% neutrons as in the entire Pb nucleus, similarly to Fig. 2.16a.

the *electromagnetic force*. Intuitively, a good candidate for the source of this force was the highly charged spectator system. The presence of the positive spectator charge would result in the repulsion of positive and attraction of negative pions, and therefore in a decrease of the final state π^+/π^- ratio.

For a quantitative verification of the above hypothesis, a Monte Carlo model was devised by the author[19]. Based on the geometrical model of the Pb+Pb collision shown above in Fig. 2.18, a realistic space distribution of spectator charges was obtained. A very simple particle production scenario was assumed: pions were emitted from participating nucleons, following kinematical distributions in x_F and p_T as they resulted from nucleon-nucleon collisions. Each pion was then traced through the electromagnetic field of the spectator protons by means of a relativistic equation of motion. This situation is illustrated in Fig. 2.20, panel **(c)** for positive pions with $0.1 < x_F < 0.2$ and $p_T < 0.1$ GeV/c. The results of this simulation are shown in panels **(d)** and **(e)**. Evidently the basic features of the effect seen in the experimental data (panels **a** and **b**) are reproduced by the Monte Carlo, both in terms of p_T- and also of x_F-dependence.

Thus indeed, *the spectator-induced electromagnetic interaction appears responsible for the observed phenomena.* This implies that at least in non-central heavy ion collisions, the projectile fragmentation region constitutes the playground for a potentially complex *interplay of strong and electromagnetic interactions*, involving the presence of spectators[20]. As such, the emission of secondary particles in this region, their final state spectra, etc., cannot be regarded solely as a consequence of participant nucleon fragmentation. Also, they trivially cannot be treated as resulting from a pure superposition of phenomena occurring in the projectile hemisphere of nucleon-nucleon or nucleon-nucleus reactions. This evidently does not preclude the presence of similarities in the mechanism of particle production in elementary and heavy ion collisions, but the search for these similarities must take account of the presence of the spectator system.

Two remarks can be added here:

- In view of the large distortion induced by the above electromagnetic interaction in final state π^+ and π^- spectra (Fig. 2.20), it may be instructive to note that the initial spectator c.m.s. electrostatic potentials induced on the pion are relatively small, of the order of about 20 MeV [Rybicki07]. For comparison, pion energies in the collision c.m.s. reach many GeV (about 1.3 GeV at $x_F = 0.15$, for $\sqrt{s_{NN}} = 17.3$ GeV).

- The influence of the spectator system on the projectile fragmentation region of nuclear reactions does not need to remain limited to electromagnetic interactions. On the contrary, various hadronic or nuclear effects can be considered. The presence of such effects in peripheral Pb+Pb reactions will be discussed in Chapter 5.

It is interesting to consider the evolution of physics ideas and interpretations in the introductory study of peripheral Pb+Pb reactions described in this Section. This leads from a hypothetical neutron halo effect on participant fragmentation to an electromagnetic distortion imposed by spectator protons. This evolution demonstrates, on a purely practical example, the importance of completeness of experimental information (two-dimensional instead of one-dimensional phase space coverage) as well as that of properly versatile information input (including e.g. nuclear density functions from antiprotonic atom data) for the correct understanding of soft hadronic physics phenomena. This matches the methodological postulates **1.** and **2.** proposed in Chapter 1. The issues related to the postulate **3.** (deeper insight into the mechanism of particle production in view of the electromagnetic effect discussed above) will be touched in Chapter 4.

Finally, it should be underlined that the short introductory analysis of the p_T-dependence of π^+/π^- ratios described above constituted a *starting point* for more elaborated studies presented

---

[19]Work done with help from D. Varga, CERN (presently ELTE Budapest).

[20]It should be noted that generally, electromagnetic phenomena in nuclear collisions have already been studied in the past. The subject of these existing studies will be addressed in Chapter 4.
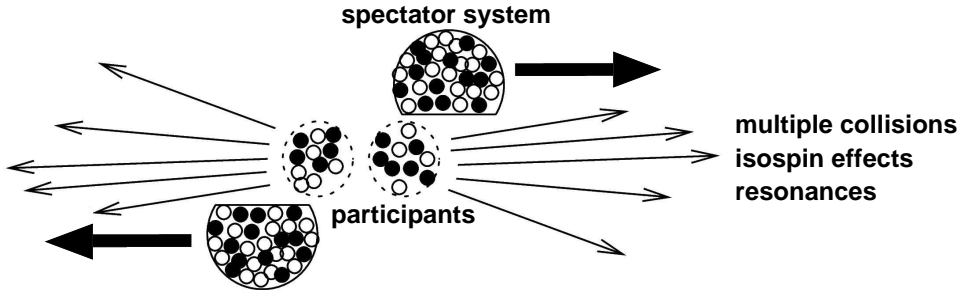
Figure 2.21: Schematic drawing of particle production in the peripheral Pb+Pb reaction, together with an enumeration of the basic issues discussed in Sections 2.3.1-2.3.4 (particles produced in the participant zone are marked by thin arrows).

in subsequent parts of this paper. On one hand, it directly triggered a systematic experimental study of double differential pion spectra in a very much extended range of x_F (from 0.0 to 0.4) and p_T (from 0 to 2 GeV/c). The details of this study will be presented in Chapter 3. On the other hand, it inspired an in-depth phenomenological analysis of the implications of the spectator-induced electromagnetic effect; this will be presented in Chapter 4.

2.3.5   Synthesis

Rather then remaining an enumeration of loosely connected items, the experimental and phenomenological findings discussed in Sections 2.3.1-2.3.4 will now be brought together. This will be made with the aim of providing a list of basic issues which are to be considered in the analysis of peripheral Pb+Pb collisions performed in the subsequent Chapters.

The basic starting point for the present discussion is the geometry of the nuclear reaction which, as it is known [Bartke09], largely defines the bulk of particle production. For the peripheral Pb+Pb reaction, the situation is drawn in Fig. 2.21. The two main elements of the reaction are the participant zone and the spectator system(s).

1. *The participant zone.* Generally, the participant zone consists of protons and neutrons, a large part of which will undergo multiple nucleon-nucleon collisions rather than just one single elementary interaction. On the basis of the discussion made in the precedent Sections, the following is to be said:

   - *Multiple collisions.* Various experimental findings, in particular in proton-nucleus interactions in Sections 2.3.1 and 2.3.2, show that multiple collisions[21] undergone by the projectile nucleon influence particle production. This is particularly valid for the shape of longitudinal and transverse particle spectra which will be modified relative to elementary nucleon-nucleon interactions (see Figs 2.6, 2.10). On that basis, it can expected that similar modifications will be present for particle production from the participant zone of the Pb+Pb reaction. Therefore, in view of the presence of such modifications, a comparison between Pb+Pb and proton-nucleus interactions may be particularly useful for the understanding of the underlying dynamics. A behaviour similar in Pb+Pb and proton-nucleus reactions will suggest similar mechanisms acting in the two reactions; a different behaviour may suggest the presence of qualitatively new phenomena (like e.g. QGP formation) in heavy ion reactions.
   The *two-component picture* of particle production elaborated in the above-mentioned Sections may provide a valuable help in the comparative studies postulated above,

---

[21]Or more generally: the increased depth of nuclear matter traversed by the projectile relative to the elementary nucleon-nucleon interaction.

because it gives a chance for a better understanding of the fate of a single nucleon undergoing multiple collisions through the nucleus in proton-nucleus reactions. This can be subsequently compared to phenomena occurring in Pb+Pb collisions.

- *Isospin effects.* Apart from multiple collisions, an additional factor to influence particle production in Pb+Pb interactions will be the presence of participant neutrons in addition to participant protons. Following the observations made in Sections 2.3.2 and 2.3.4, it is straight-forward to expect that various observables, like e.g. π^+/π^- ratios, will be (trivially) different from these measured in proton-proton interactions. The size of this effect will be governed by the neutron-over-proton ratio in the participant zone, which can be established on the basis of existing knowledge (Fig. 2.19).

- *Resonances.* Several studies, all of them following from experimental information rather than from model-dependent assumptions, indicate that final state particle distributions in elementary hadron-hadron interactions are dominated by products of decays of intermediate resonant states (Section 2.3.3). As such, also in nuclear reactions resonance decays should be considered as a potentially important mechanism directly underlying final state particle production[22].

2. *The spectator system.* Quite contrary to its name, the "spectator" system appears to play an *active* role in the peripheral Pb+Pb reaction. This role is not limited to the emission of nuclear fragments. In fact the presence of spectator nucleons exerts its influence on phenomena occurring in the region of phase space which, in proton-proton or proton-nucleus reactions, would exclusively be attributed to the fragmentation of the projectile proton (like, e.g., $x_F > 0.1$ for pions). This implies that any comparison of the fate of the nucleon(s) undergoing multiple collisions in proton-nucleus and peripheral nucleus-nucleus reactions will need to disentangle participant fragmentation from spectator-induced phenomena. Generally, the influence of spectators in the fragmentation region may be twofold:

   - As discussed in Section 2.3.4, the *electromagnetic interaction* induced by the spectator charge modifies the momentum vectors of produced pions, and changes their final state distributions. As it will be demonstrated in Chapter 4, this influence may spread over the complete region of high x_F.

   - On top of electromagnetic interactions, the spectator system can contribute to *particle emission* in the projectile fragmentation region. It is to be considered whether apart from pion momentum vector modification, *additional* pions could be produced as a result of the presence of the spectator system.

One more remark should be made on this *interplay between hadronic and electromagnetic phenomena* in the projectile fragmentation region, which, as follows from the above, characterizes the non-central nucleus-nucleus reaction. On the contrary to the non-perturbative strong interaction, the electromagnetic force is subject to precise, quantitative theoretical calculations. On the other hand, as clearly apparent from Fig. 2.21, it depends on the (x, y, z) position of the produced particle relative to the spectator charges, as well as on the evolution of this position in time. Thus, it seems logically clear that the modification of charged pion spectra by the electromagnetic interaction should provide some new information on the particle production process, which would go beyond the final state distribution. Can it serve as a probe of the space-time evolution of this process? This question constitutes the last point of the present discussion, and the starting point for the analysis made in the subsequent Chapters.

---

[22]While particle production from resonance decays is considered in various Monte Carlo models of nuclear collisions, no studies exactly similar to these quoted above are known to the author for nucleus-nucleus reactions.

Chapter 3

Analysis of Pb+Pb Reactions

Starting from the present Chapter, we will focus in more detail on the phenomenon of pion production in peripheral Pb+Pb collisions at the c.m.s. energy of $\sqrt{s_{NN}} = 17.3$ GeV. A new experimental dataset, collected by the NA49 fixed target detector at the corresponding beam energy of 158 GeV/nucleon, will be introduced. This will be done with the aim to show how the phenomenological knowledge gathered in the precedent studies, Chapter 2, can now be enriched by means of a precise, double differential measurement of particle production in a non-central heavy ion collision. Main attention will be devoted to the question of modification of the production mechanism induced by the transition from the elementary to the heavy ion environment, and to a closer scrutiny of the electromagnetic effects briefly introduced in Section 2.3.4.

The discussion starts with a description of the most important experimental aspects of this study of peripheral Pb+Pb collisions. This is made in this Chapter. Apart from the description *per se*, its aim is to give to the reader, on a practical example, an idea on the inherent complexity of multiparticle production measurements in modern high energy hadronic and heavy ion physics experiments.

The complete set-up of the NA49 experiment was already presented in Section 2.2.2, Fig. 2.2 which will also constitute the basis of the present discussion. For the sake of clarity, this is supplemented in Fig. 3.1 with a top view of a Pb+Pb event as seen by the NA49 Time Projection Chamber tracking system, put together with a re-drawing of the beam definition in Pb+Pb data taking. A more detailed description of the beam and detector set-up can be found in [Afanasiev99]. Apart from this latter reference, the somewhat simplified discussion made below is also partially based on [Alt06, Alt08] and, to a smaller extent, on [Alt07, Laszlo07, Szymański06].

3.1 Beam, Target and Interaction Trigger

The beam. The beam line (BEAM in Fig. 3.1a) transported a fraction of the SPS heavy ion beam through a set of two Čerenkov counters (S1,S2') and three Beam Position Detectors (BPD-1/2/3). This provided precise timing reference, charge and position measurement of the incoming beam particles [Afanasiev99]. Anti-coincidence with a ring-shaped scintillator counter (V0) reduced the background from "upstream" interactions.

The target (T in Fig. 3.1a) was made of a 200 μm lead foil. It's thickness was 224 mg/cm^2, corresponding to 1 % interaction length.

The trigger. The Pb+Pb events were selected by an interaction trigger of the "minimum bias" type provided by anti-coincidence with a Helium Gas-Čerenkov counter placed directly behind
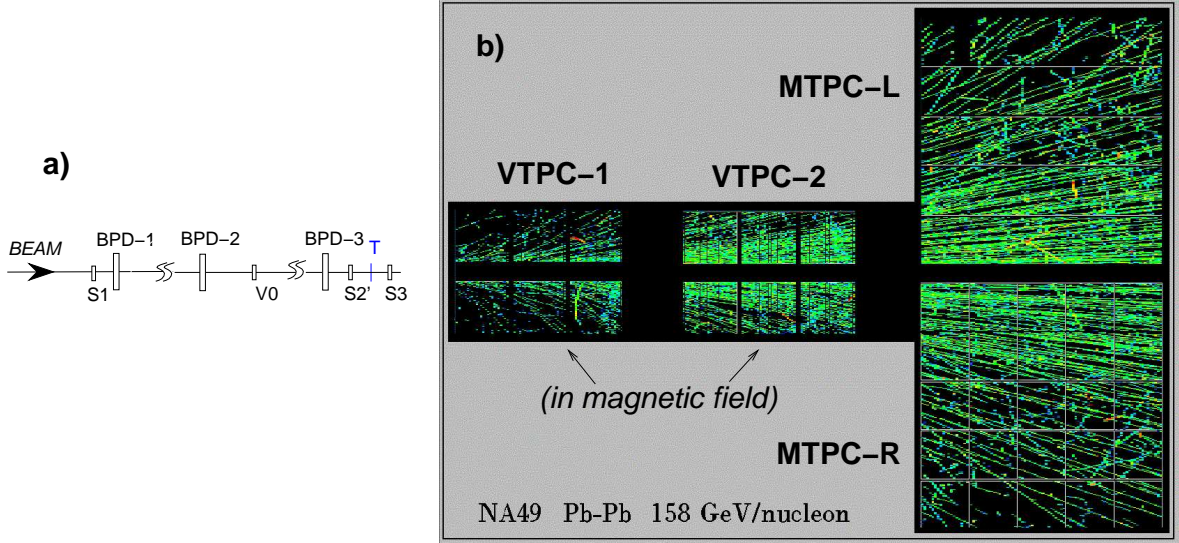
Figure 3.1: **a)** NA49 beam definition for Pb+Pb data taking (not to scale). **b)** Top view of a central Pb+Pb event as detected by the NA49 TPC system (note that only a 7 mm thick slice around the beam plane is shown in order to allow for a visual resolution of the tracks). Both plots are re-drawn on the basis of [Afanasiev99].

the target (S3 in Fig. 3.1a). The trigger condition required a reduction of the Čerenkov signal. As the latter signal was proportional to the square of the charge, this ensured that the Pb beam had indeed *interacted* with a minimal constraint on the type of interaction [Alt08].

The triggered events were then registered by the NA49 Data Acquisition system. The principal part of the detector being the TPC tracking system, a total number of up to about 1500 charged particle tracks were recorded in most central Pb+Pb events. An example of such a situation is shown in Fig. 3.1b.

3.2   Off-line Data Analysis

Tracking and Event Reconstruction. In terms of NA49 data reconstruction and analysis, a *track* was defined by the total ensemble of three-dimensional electron clusters ("points") that the charged particle left in the effective gas volume of the TPC system [Alt06]. As apparent from Fig. 3.1b, each track included one, two or three segments corresponding to VTPC-1, VTPC-2 and one of the MTPC's. The procedure for track and event reconstruction was made of several steps, including a cluster-finding code, algorithms for track segment reconstruction and segment merging, a fit of the primary event vertex (the interaction point reconstructed as the origin of the outgoing tracks), and a final path of fitting of particle momentum on the basis of the track bending in the magnetic field present in the two VTPC's.

Selection of Peripheral Collisions. The peripheral Pb+Pb data sample was selected by means of an off-line cut on the multiplicity of charged particle tracks registered by the TPC system. The overall tracking acceptance was about 80 % of all charged particles produced in the collision. The minimum bias multiplicity distribution is shown in Fig. 3.2a. The multiplicity bin used in this analysis contained events with 150 to 300 charged tracks[1].

---

[1]This is to be compared to up to 1500 tracks in most central Pb+Pb interactions (Section 3.1), and to about
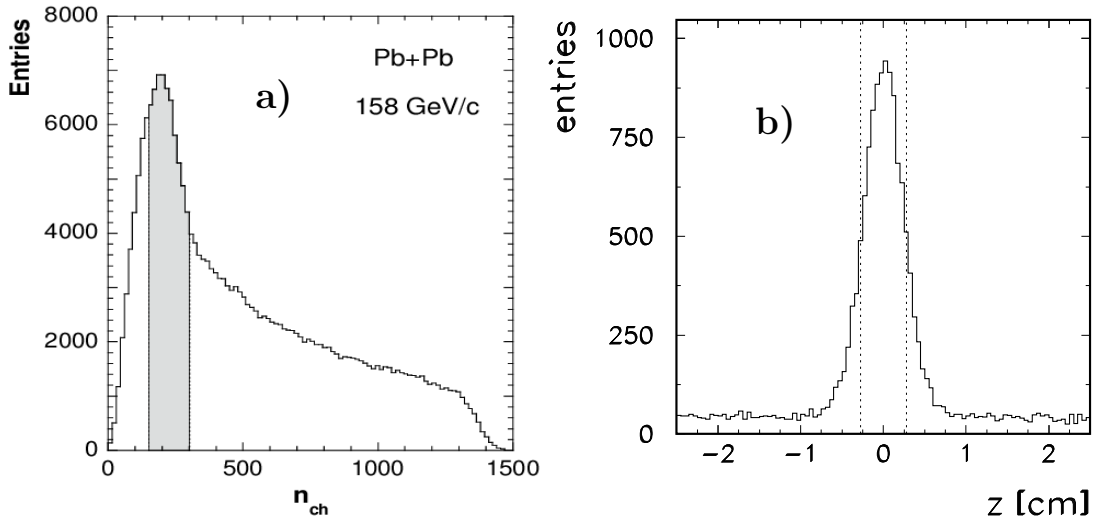
Figure 3.2: **a)** Charged particle multiplicity distribution from minimum bias Pb+Pb data. The multiplicity window used for the present analysis is indicated by the shaded area. **b)** Distribution of the longitudinal position of the reconstructed interaction point. The figure is made for events with a multiplicity of 200 to 250 charged tracks seen in the TPC system.

Centrality. The determination of event geometry, or centrality, of a heavy ion reaction presents an untrivial problem. The latter feature of the reaction is not experimentally measurable and has to be inferred indirectly. Also, existing works [Back06, Alt08] indicate that the uncertainties inherent to the various applied methods tend to largely increase when going from central to peripheral reactions.

The relatively simple approach applied in the present study was to relate the cut on charged multiplicity (see above) to the results of a recent NA49 analysis [Anticic09]. The latter analysis was based on the measurement of projectile spectator energy made by the NA49 zero-degree calorimeter, and on the determination of the corresponding number N_{part} of participant (or "wounded") nucleons by means of the Venus 4.12 generator [Werner03], including various detector effects (calorimeter resolution, interaction trigger condition, etc). An eye-ball fit to these results gave an average number $<N_{part}>$ of about 54 participant nucleons for the present multiplicity cut. The connection between $<N_{part}>$ and the mean impact parameter of the reaction $<b>$ or the mean number of elementary collisions $<\nu>$ was determined by means of the geometrical model of the Pb+Pb reaction described in Section 2.3.4. A summary of the resulting centrality parameters is shown in Table 3.1.

$<b>$	$<N_{part}>$	$<\nu>$
10.9 ± 0.5 fm	54 ± 11	2.4 ± 0.2

Table 3.1: Mean impact parameter $<b>$, mean number of participant nucleons $<N_{part}>$, and mean number of collisions per participant nucleon $<\nu>$, for the peripheral Pb+Pb reactions of this study.

In order to keep track of inherent model dependencies and systematic uncertainties, a comparison was made to an independent set of results obtained by the PHOBOS experiment for Au+Au collisions at $\sqrt{s_{NN}} = 19.6$ GeV [Back06]. Here, the centrality was defined directly on the basis of the measurement of charged particle multiplicity supplemented with Monte Carlo

---

6 tracks seen in a typical p+p event.

model calculations. This comparison, put together with a set of additional Monte Carlo studies made by means of the geometrical model mentioned above, suggested the size of error bars to be attributed to the obtained centrality parameters. These are also listed in Table 3.1. The uncertainties on $<b>$ and $<\nu>$ do not bring any serious obstacle to the discussions made in this paper. However, some importance should be brought to the sizeable uncertainty on $<N_{part}>$, which can be regarded as a consequence of the "peripherality" of the reaction.

Background Rejection. The NA49 target setup, Fig. 3.1a, was not contained in a vacuum pipe. This implied that a number of non-target interactions could satisfy the interaction trigger condition, Section 3.1, and enter the selected Pb+Pb data sample. The situation is illustrated in Fig. 3.2b which shows the longitudinal position z of the reconstructed interaction point, obtained for events with 200 to 250 charged tracks. Under the target peak which is made of physical Pb+Pb collisions, a flat background is visible which corresponds to beam-gas events. In order to reduce the contamination from these events, a cut on z was applied as shown in the Figure: only events in the central part of the target peak were accepted for further analysis. The peripheral sample was split in sub-bins in multiplicity for this operation, and the cut was adjusted separately in each sub-bin in order to take account of the broadening of the peak with decreasing event multiplicity. The above selection reduced the overall beam-gas background in the peripheral sample to about 5 %; this was additionally corrected for, as discussed in Section 3.3. The size of the peripheral Pb+Pb dataset after this final selection was about 28,000 events. This relatively moderate statistics[2] constituted a clear limiting factor for the present study, see also Chapter 6.

Pion Phase Space Binning and Azimuthal Acceptance. The subsequent analysis was performed in separate, rectangular bins of pion x_F and p_T: $[x_F \pm \Delta x_F, p_T \pm \Delta p_T]$, with x_F ranging from 0 to 0.4 and p_T from 0.025 to 1.9 GeV/c. The bin size increased with both x_F and p_T, due to the corresponding decrease of produced pion density (see Section 3.5.1, Fig. 3.5). As the azimuthal acceptance of the TPC system varied with x_F and p_T of the particle (see Fig. 2.3a and b), an individual wedge in azimuthal angle was adjusted for each bin, separately for positive and negative particles. This insured full geometrical acceptance and reasonable length for tracks falling in this wedge. Only such tracks were accepted for further analysis[3].

Particle Identification. The extraction of identified π^+ and π^- yields was based on the measurement of ionization energy loss by charged particles in the TPC gas [Afanasiev99]. For each track in the data sample, this quantity was determined by calculating a "truncated mean" of 50 % smallest charge deposits from all electron clusters belonging to the track. This was done separately for VTPC and MTPC track segments, due to the gas difference between the two chamber types: Ne and Ar, respectively. On this basis, a "global" truncated mean energy loss per unit length (dE/dx) was evaluated for the whole track.

All tracks of a given charge were sorted into the bins in x_F and p_T defined above, assuming the pion mass in the transformation from laboratory momentum to the collision c.m.s. This gave one dE/dx distribution in each bin, shown in Fig. 3.3. In order to extract the number of charged pions in the bin, this distribution was fitted with the sum of ionization energy loss functions for different contributing particles. These functions, also shown in the Figure, were determined by a Monte Carlo method on the basis of detailed information obtained from experiment [Alt06]. The fit was individually performed and carefully optimized in each bin in order to correct for

---

[2]For a limited number of analyzed $[x_F, p_T]$ bins, mostly with low statistics, a different selection was applied resulting in a better statistical significance but higher background contamination. This contamination was also corrected for, using the same method as discussed in Section 3.3.

[3]Note: this introduced no bias in the measurement, thanks to its azimuthal symmetry (Section 2.1).
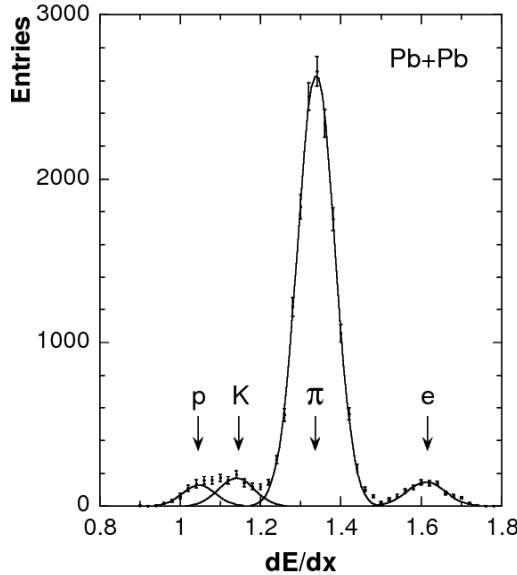
Figure 3.3: Data points: distribution of energy loss dE/dx for positive particles in peripheral Pb+Pb interactions, measured at $x_F = 0.05$ and $p_T = 0.1$ GeV/c. Solid lines: corresponding fitted response functions for protons (p), kaons (K), pions (π), and positrons (e).

possible imperfections in the description of detector response[4].

3.3 Evaluation of Double Differential Densities and Corrections

The process of data analysis described in Section 3.2 allows us to define the experimental quantity

$$d_{\text{measured}}(x_F, p_T, \Delta p^3) = E(x_F, p_T, \Delta p^3) \cdot \frac{1}{N_{\text{ev}}} \cdot \frac{\Delta n(x_F, p_T, \Delta p^3)}{\Delta p^3} \qquad (3.1)$$

where Δp^3 is the finite phase space element defined by the experimental bin width, N_{ev} is the number of events originating from the vicinity of the target, and Δn is the number of identified pions measured in the bin Δp^3. The quantity d_{measured} serves as a basic measure of the invariant density $d = E\frac{d^3n}{dp^3}$ defined in Section 2.1. However, several corrections need to be applied in order to make d_{measured} approach d. These will be described below.

Beam-gas Background. Due to the remnant contamination of the experimental sample by beam-gas events (Section 3.2), the quantity d_{measured} was in fact a weighted average from both Pb+Pb and beam-gas interactions. The pure Pb+Pb component was extracted by removing the beam-gas component in each $[x_F, p_T]$ bin. The latter was obtained by extending the cut on the position z of the reconstructed interaction point, Fig. 3.2b, and extrapolation of the corresponding value of d_{measured} to a pure beam-gas event sample. The size of this correction, i.e., the typical change of d_{measured} after background removal, depended on x_F and p_T. It remained below 4% for the cut shown in Fig. 3.2b.

Absorption in the Detector Material. Due to interactions in the material of the detector, a small fraction of pions were lost from the analyzed sample. The correction for this effect was

---

[4]This simplified summary given above does not enter such details as, e.g., calibration issues (see Section 1.3), or the "reflection technique" used in the limited region of pion $x_F \approx 0$, low p_T. For further reference on these subjects, see [Afanasiev99, Rybicki02] and [Alt06], respectively.
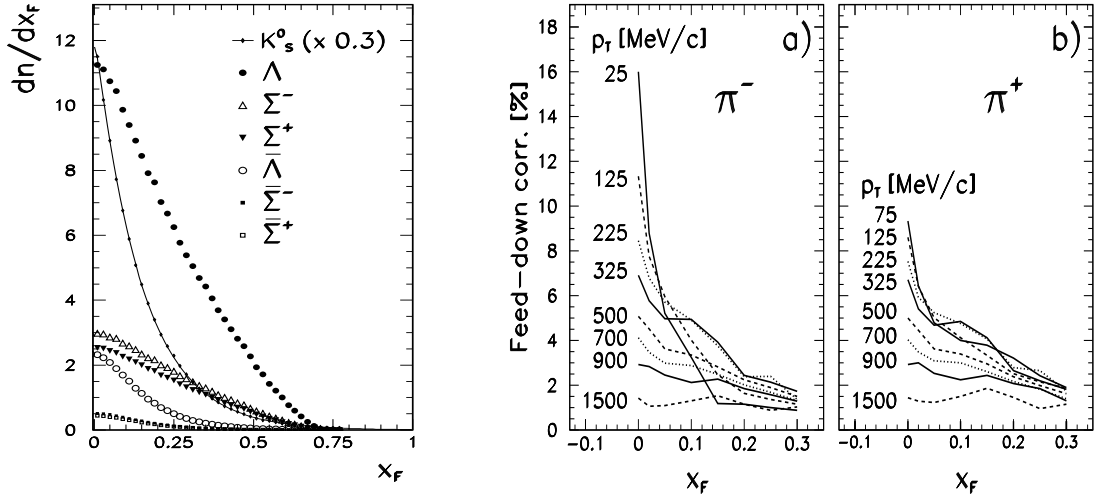
Figure 3.4: **Left panel**: p_T-integrated dn/dx_F distribution of all the parent particles contributing to the weak decay feed-down correction. **Right panels**: feed-down correction for π^- and π^+.

identical to that used in the study of p+p reactions [Alt06], where it was determined on the basis of a GEANT [Geant5013] simulation of the NA49 detector supplemented by eye-scan studies. The correction remained below 2.5 % for the present analysis.

Pion Decay. A small fraction of produced pions could be lost from the analyzed sample due to weak decays $\pi \rightarrow \mu + \nu_\mu$. While this effect was small for NA49 experimental conditions, a correction was devised on the basis of Monte Carlo simulations, eye-scans and short track studies. It was essentially identical to that used in [Alt06] and reached a maximum value of 0.36 % at $x_F = 0$ and $p_T = 0$.

Feed-down to Pions from Weak Decays of Strange Particles. The high abundance of strange particles produced in Pb+Pb collisions [Afanasiev02, Dainese06] resulted in a sizeable amount of daughter pions originating from weak decays. These made up a significant, strongly varying contribution to measured double differential pion densities. The present analysis included a complete weak decay feed-down subtraction from all the relevant sources, namely the decays $K_s^0 \rightarrow \pi^+\pi^-$, $\Lambda \rightarrow p\pi^-$, $\bar{\Lambda} \rightarrow \bar{p}\pi^+$, $\Sigma^+ \rightarrow n\pi^+$, $\bar{\Sigma}^- \rightarrow \bar{n}\pi^-$, $\Sigma^- \rightarrow n\pi^-$, and $\bar{\Sigma}^+ \rightarrow \bar{n}\pi^+$. The correction followed a three-step procedure. First, the double differential distributions of all parent particles were evaluated. They served as an input to obtain yields of corresponding daughter pions in the $[x_F, p_T]$ bins of the experiment. These yields were then folded with the reconstruction efficiency determined from a GEANT simulation of the detector (see [Alt06] for more details).

The main difficulty consisted in a precise, model-independent evaluation of double differential x_F and p_T distributions of parent particles. For the present analysis, *the K_s^0 distribution* was extracted from averaged charged kaon (K^+, K^-) spectra. These spectra were directly measured in a large number of $[x_F, p_T]$ bins using the same particle identification technique as described in Section 3.2. *The Λ and $\bar{\Lambda}$ distributions* were evaluated on the basis of existing NA49 measurements [Blume07]. At high values of x_F the experiment had no acceptance for the Λ; here the shape of the Λ spectrum was constrained on the basis of p+p reactions [Alt06], assuming that from p+p to Pb+Pb collisions it followed a baryon stopping trend similar to that observed for protons, Section 2.3.1. Finally, the total yields of Σ *baryons and their anti-particles* were deduced assuming that the total yield ratios Σ^+/Λ, Σ^-/Λ, $\bar{\Sigma}^+/\bar{\Lambda}$ and $\bar{\Sigma}^-/\bar{\Lambda}$ did not change from

p+p [Alt06] to Pb+Pb reactions, up to straight-forward isospin effects accounting for the mixed proton/neutron content of the Pb nucleus (see discussion in Sections 2.3.2, 2.3.4). Additionally, the *shapes* of the Σ^+ and Σ^- distributions were established by assuming that their evolution from p+p to Pb+Pb reactions was similar to that of the Λ above; the shapes of the $\bar{\Sigma}^+$ and $\bar{\Sigma}^-$ distributions were assumed to be similar to that of the $\bar{\Lambda}$.

Fig. 3.4 (left panel) shows the p_T-integrated density distributions of parent particles as a function of x_F. The resulting correction to the pion yields is drawn in Fig. 3.4 (right panels) as a function of x_F for different bins in p_T. As visible in the Figure, the correction reaches large values which can go well above 10 % for negative pions at low x_F and low p_T. It also has a complex overall structure resulting from the inherent interplay of physical, kinematic and detector issues. As such, it is clearly apparent from the above that the knowledge of weak decays is of great importance in double differential production measurements.

Binning Correction. As the double differential pion yields were extracted in finite bins in $[x_F, p_T]$, Section 3.2, the measured yield was the integral of pion density over the bin. The correction for finite bin width followed the procedure developed in earlier studies, where the deviation of the real density at the bin center from the measured value was determined using the local second derivative of the density distribution [Alt07, Alt06]. This derivative was directly evaluated from the experimental data. The resulting correction to the pion yields was usually at the level of 0-6 %.

An exception was the region $x_F = 0.15$ and 0.2, at the lowest value of transverse momentum, $p_T = 0.025$ GeV/c. Here, very rapid variations of pion density were induced by electromagnetic effects, Section 2.3.4, and therefore large deviations between the real and integrated density were to be expected. For better control of the inherent systematics, the binning correction in this region was directly determined by reducing the bin size; it reached a maximal value of 70% down (12% up) for positive (negative) pions at $x_F = 0.15$.

Track reconstruction efficiency	1 %
Beam-gas background	2 %
Detector absorption	
Pion decay $\pi \rightarrow \mu + \nu_\mu$	0.5 %
Feed-down	1-3.5 %
Binning	0.5 %
Total (upper limit)	7.5 %
Total (quadratic sum)	4.2 %

Table 3.2: Summary of typical systematic errors.

3.4 Systematic Errors

An estimate of typical systematic errors induced by the applied corrections, as well as other known error sources, is given in Table 3.2. This Table also gives an estimate of the typical total systematic uncertainty as an upper limit of 7.5 % from linear addition of the error sources, and 4.2 % from quadratic summation. This latter low value is to be regarded with caution[5]. It should also be remembered that the quoted values are *typical* and larger deviations in specific regions of phase space are possible. This applies in particular to the narrow region where the binning correction is large, see above. The systematic error of this correction may reach sizeable

---

[5]The problem of systematic error determination and propagation in hadronic cross section studies is addressed in more detail in [Alt06].

values in this region, without however introducing any bias of real importance for the analysis presented in this paper.

3.5 Results

This Section includes the experimental results of the analysis presented above. This is supplemented with a short discussion of the most basic features of charged pion production in peripheral Pb+Pb collisions which will serve as a basis for the next Chapters.

3.5.1 Double Differential Pion Densities

A general overview of the dependence of π^+ and π^- invariant density on pion x_F and p_T is presented in Fig. 3.5. Transverse momentum distributions at fixed values of x_F are shown in panel **(a)** while x_F spectra at fixed p_T are shown in panels **(b)** and **(c)**. It should be remembered that the x_F distributions in Pb+Pb reactions are by definition symmetric around $x_F = 0$. In order to clearly bring out the different trends visible in the data, some of the distributions have been multiplied by arbitrary factors as specified in the Figure caption. Several basic features of these distributions are noteworthy:

- An overall excess of negative over positive pion production can be observed, panel **(a)**. While it remains moderate in the region $p_T > 0.3$ GeV/c where the π^+ and π^- densities observe a similar x_F- and p_T-dependence, this excess continuously grows with increasing x_F. As it will be demonstrated in Chapter 4, a connection can be drawn between this excess and the isospin content of the Pb nucleus, characterized by a sizeable surplus of neutrons over protons (see also Sections 2.3.2, 2.3.4).

- A number of general similarities can be noticed between the shape of pion x_F and p_T distributions in Pb+Pb collisions and in elementary p+p interactions. This is particularly valid for the rapid decrease of pion density with transverse momentum (panel **a**, see Fig. 2.15b for comparison). Another example is the evolution of the x_F-dependence of the pion yield, which starts from a steep decrease at lower values of p_T, followed by a flattening at higher transverse momenta (panels **b**, **c**, see Fig. 2.8a,b for comparison). Such a behaviour corresponds to a broadening of the p_T distribution when passing from the central production zone at $x_F = 0$ into the fragmentation region at large x_F (visible also in panel **a**).

- Finally, large variations of invariant density with x_F and p_T are present in the region of low transverse momentum, $p_T < 0.3$ GeV/c. Here, the spectator-induced electromagnetic effect introduced in Section 2.3.4 results in a strong charge asymmetry, reaching its maximum at $x_F = 0.15$ and $p_T \approx 0$ as shown in panel **(a)**. This charge asymmetry can be inspected in more detail in panels **(b)** and **(c)**, where the x_F-dependence of π^+ density displays a sharp drop at low transverse momentum, while a local accumulation of density is simultaneously present for π^-.

3.5.2 Integrated Spectra

Information complementary to that shown in Fig. 3.5 can be obtained by integration of the measured double differential distributions over transverse momentum. In analogy to the procedures applied in preceding analyses [Alt06, Alt07, Anticic10, Anticic10a], a dense numerical interpolation of the experimental data points serves this purpose (this interpolation is presented
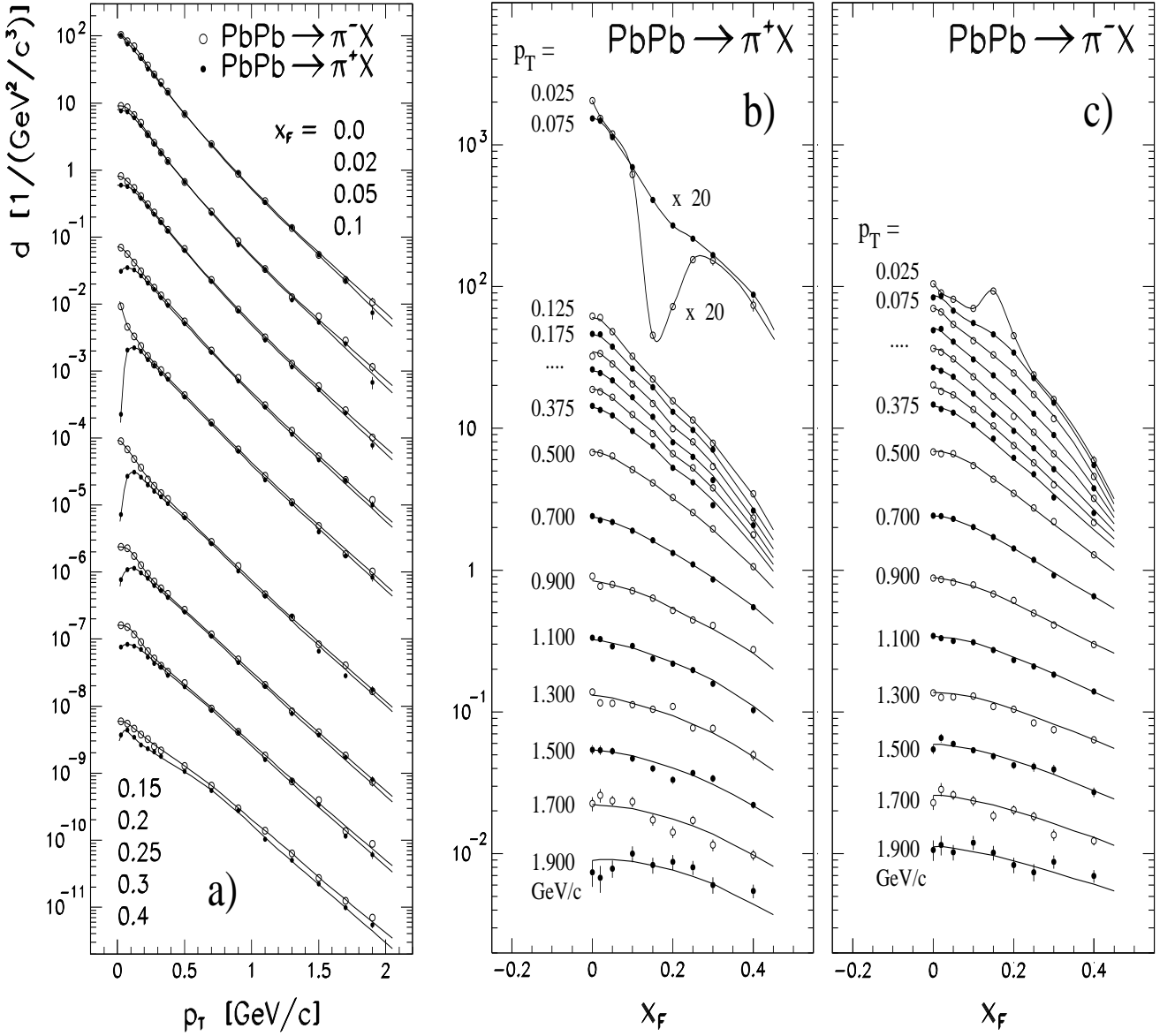
Figure 3.5: Invariant density $d = E\frac{d^3n}{dp^3}$ of charged pions produced in the projectile hemisphere of peripheral Pb+Pb collisions at $\sqrt{s_{NN}} = 17.3$ GeV, drawn as a function of p_T and x_F.

a) Density of negative (circles) and positive (full dots) pions, drawn as a function of transverse momentum at fixed values of x_F, listed in the Figure from the top to the bottom distribution. Note: in order to allow for a better visual resolution, the subsequent distributions are multiplied by 1, 0.1, 0.01, 10^{-3}, 10^{-4}, $2 \cdot 10^{-6}$, 10^{-7}, 10^{-8}, and 10^{-9}; the solid curves correspond to a numerical interpolation of the data points, described in the text.

b) Density of positive pions, drawn as a function of x_F at fixed values of p_T. Note: the distributions corresponding to the two lowest values of p_T are multiplied by a common factor of 20. The three curves marked with the multidot ("....") correspond to $p_T = 0.225$, 0.275, and 0.325 GeV/c, respectively.

c) Density of negative pions drawn as a function of x_F as in panel (b). All the distributions are drawn in absolute scale; the multidot corresponds to $p_T = 0.125$, 0.175, 0.225, 0.275, and 0.325 GeV/c, respectively.

49
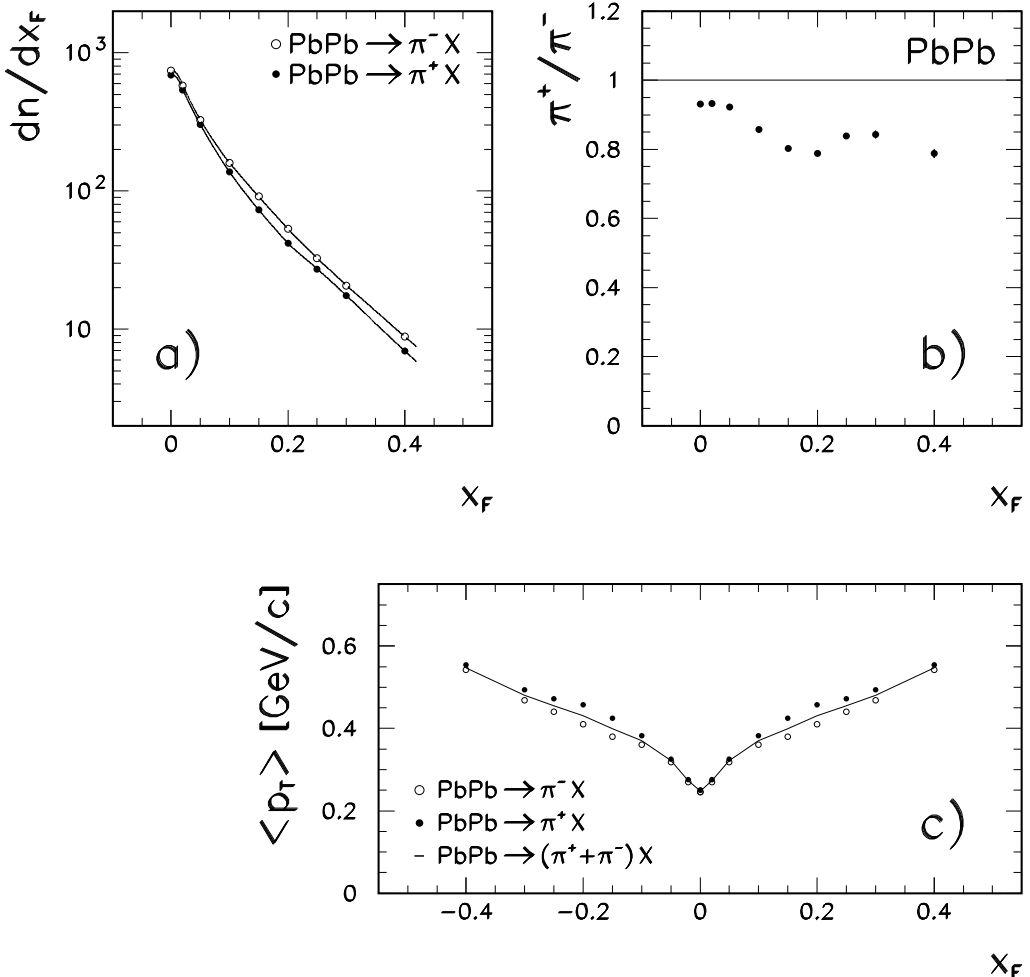
Figure 3.6: **a)** Longitudinal density of negative and positive pions produced in the projectile hemisphere of peripheral Pb+Pb collisions, drawn as a function of x_F. **b)** x_F-dependence of the p_T-integrated π^+/π^- ratio in the projectile hemisphere of peripheral Pb+Pb collisions. **c)** Mean transverse momentum of positive, negative, and summed charged pions produced in peripheral Pb+Pb collisions, drawn as a function of x_F. Note: the evaluated statistical errors are (nearly always) below the symbol size. The plot in panel (c) is drawn in a different range of x_F than the other panels in order to emphasize its similarity to the "seagull" shape [Fiałkowski83] discussed in the text; values at $x_F < 0$ are obtained by reflection.

as a set of smooth curves in Fig. 3.5a). As a result, the x_F-dependence of several quantities is shown in Fig. 3.6.

Panel **(a)** shows the spectra of longitudinal pion density, dn/dx_F, drawn for positive and negative pions. Analogically to what was said in the preceding Section, the shape of these two distributions is altogether similar to that in p+p collisions (see, e.g., Fig. 2.15a), with however a marked excess of π^- over π^+ production. The integration of these distributions over x_F gives the average total multiplicities of charged pions in this sample of peripheral Pb+Pb interactions. These amount to 95.7 positive and 107.5 negative pions produced per one Pb+Pb event. Relative to p+p reactions [Alt06], this gives an enhancement of summed charged pion production $(\pi^+ + \pi^-)$ by a factor of about 38. This is to be compared with the corresponding increase in the number of participant nucleons by a factor of 27±5.5, as can be deduced from Table 3.1. Thus, the peripheral Pb+Pb data indicate a "growth of pion production per participant nucleon", as was also the case for central Pb+Pb reactions [Afanasiev02]. However, the presence of sizeable uncertainties suggests caution in drawing too strict quantitative conclusions about

the magnitude of this effect.

The p_T-integrated ratio of π^+ over π^- production shown in panel **(b)** displays an interesting systematics. While the four data points at $x_F = 0.05$, 0.1, 0.15, and 0.2 are within 3% consistent with the preliminary data discussed in Fig. 2.16a, the broader x_F-coverage of the present measurement reveals a picture which is in fact very different from that suggested by the latter Figure. Instead of a continuous fall with x_F, the π^+/π^- ratio exhibits a shallow minimum centered at $x_F = 0.15 - 0.2$, that is, at the values of x_F which correspond to largest manifestations of the spectator-induced electromagnetic effect, see Fig 3.5.

Finally, the x_F-dependence of the average transverse momentum $<p_T>$ of positive, negative, and summed charged pions is presented in panel **(c)**. Several features of the data are noteworthy. Firstly, mean transverse momenta of pions produced in peripheral Pb+Pb reactions display a clear increase with increasing $|x_F|$. This is similar, although not identical, to the rounded "seagull" shape characteristic of this correlation in p+p and proton+nucleus interactions (see Fig. 2.10b for comparison). Secondly, a *split* is present between the values of $<p_T>$ obtained for positive and negative pions: positive pions reach larger mean transverse momenta. This is qualitatively opposite to what happens in p+p reactions [Alt06] and in the projectile hemisphere of p+C collisions [Alt07]. The position of this split seems to be correlated with the presence of the shallow minimum in the π^+/π^- ratio, panel **(b)**. Both appear in a similar region of x_F, $0.1 \leq x_F \leq 0.3$, and the maximum difference between the two values of $<p_T>$ corresponds to the lowest value of the π^+/π^- ratio. It can naturally be expected that the spectator-induced electromagnetic interaction mentioned above will contribute to this phenomenon by increasing (decreasing) the transverse momentum of final state positive (negative) pions. However, more quantitative studies are necessary for a full clarification of this subject as the presence of other (hadronic) effects is also to be considered.

Chapter 4

Electromagnetic Effects on Charged Pion Spectra

The preceding Chapter contained only a very brief description of the basic features of new data on peripheral Pb+Pb reactions obtained by the NA49 experiment. The following part of this paper aims at a somewhat more in-depth study of various phenomena characterizing pion production in these reactions, analyzed in the context of the specific findings summarized in Chapter 2. This analysis will be divided into two Chapters, devoted to electromagnetic and hadronic phenomena. It is needless to say that such a division is somewhat arbitrary as in fact, effects induced by the strong and the electromagnetic force are mixed in the reaction and may easily interplay in non-trivial ways. With due caution however, such a division seems necessary to the author, be it only for the clarity of the discussion where these two sides of the analysis appear as complementary.

The present Chapter will be devoted to electromagnetic phenomena induced by the charge of spectator protons on spectra of charged pions produced in Pb+Pb collisions. The principal aim here will be the study of their possible implications in view of obtaining novel, independent information on the mechanism of the nuclear reaction in the non-perturbative sector of QCD.

This study can be regarded as an extension of the short, introductory analysis described in Section 2.3.4. It will include both new experimental information and new theoretical (phenomenological) results. While largely based on two main sources, [Rybicki07] and [Rybicki09], and partially summarizing their content, it will aim at presenting a picture altogether more complete than formulated in any of the two quoted references. Also, it will contain additional new information, not published before.

With the exception of a few cases which will be indicated in the text, the present phenomenological analysis is based on the ideas of the author, and the new results presented here (that is, not directly derivable from the precedent Chapters nor from publications other than the above) constitute mainly the result of his own work. However, the very important role of Antoni Szczurek at all levels of the presented Monte Carlo study up to the publication of results is to be gratefully recognized[1].

4.1 The General Context

The present description will remain limited only to a specific class of electromagnetic phenomena occurring in nuclear collisions, namely to the modification of kinematic distributions of produced particles by the net electric charge present in the collision. As already explained in Chapter 2, the presence of this net charge causes the repulsion (attraction) of positive (negative) produced

---

[1]The complete contribution of the author to the work presented in this paper is summarized in Chapter 1.
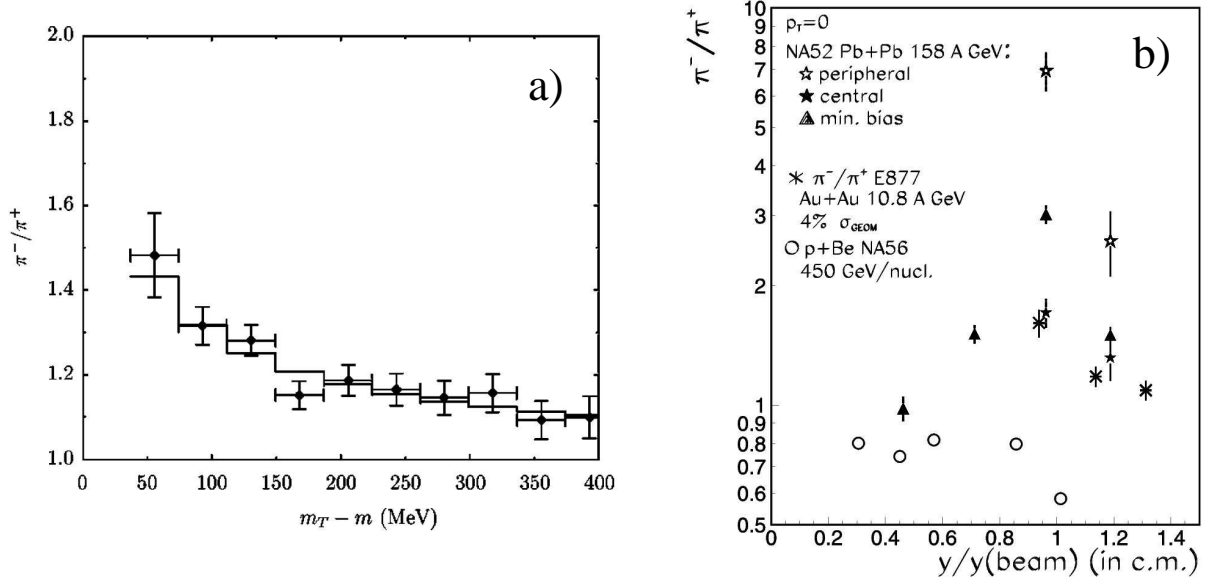
Figure 4.1: **a)** Data points: ratio of negative over positive pions produced in the vicinity of mid-rapidity in Au+Au collisions at 11.6 GeV/nucleon, drawn as function of $(m_T - m)$ of the pion. Histogram: theoretical model calculation assuming a spherically symmetric central fireball, with a radius of 10 fm at pion freeze-out. The plot comes from [Ayala99] while the data points come from [Ahle98]. **b)** Ratio of π^- over π^+ produced near $p_T = 0$, drawn as a function of the rapidity of the pion normalized to the beam rapidity in the c.m.s. Experimental data from the NA52 experiment (peripheral, central and minimum bias Pb+Pb reactions at 158 GeV/nucleon [Ambrosini99]) are shown together with data on central Au+Au reactions at 10.8 GeV/nucleon [Lacasse96], as well as data on p+Be collisions at 450 GeV/nucleon from NA56 [Ambrosini99a]. The plot comes from [Ambrosini99].

particles, and consequently changes their energy and momentum vectors. As a typical result, a charge asymmetry may appear in the final state of the reaction, like e.g. the depletion of the π^+/π^- ratio discussed in Section 2.3.4. In the following a few examples of studies of such effects will be enumerated and in their context, the importance of the new experimental and phenomenological information provided by the present paper will be shortly discussed. Apart from [Rybicki07], the description made here will be partially based on [Bartke09].

It is not surprising that various types of such electromagnetic (or "Coulomb") effects were known since a long time in nuclear collisions. In early (1952) experiments with cosmic rays, large π^+/π^- asymmetries were observed for produced slow pions [Yagoda52]. In the kinetic energy spectrum of particles produced in reactions of 9 GeV protons with emulsion nuclei, a charge asymmetry was also found [Friedländer62]. At the energies of the Bevalac, it was found that the Coulomb field causes very large effects at forward angles, that is, at projectile velocity [Beneson79, Sullivan82]. A more recent result was reported in studies of p+Au and He+Au collisions at several GeV/nucleon, where the non-relativistic approach to the Coulomb field brought information on the evolution of the process of nuclear fragmentation [Karnaukhov06].

Another charge asymmetry was reported at the AGS, in central heavy ion (Au+Au) collisions at 11.6 GeV/nucleon [Ahle98]. Fig. 4.1a shows the dependence of the π^-/π^+ ratio on the pion transverse mass, for pions emitted in the neighbourhood of mid-rapidity[2]. Evidently a sizeable enhancement of π^-/π^+ is present; this is equivalent to a depletion of π^+/π^-, see Fig. 2.20 for comparison. The quoted reference suggests the Coulomb interaction as responsible for a

---

[2]Note: *mid-rapidity*, which refers to the laboratory c.m.s., corresponds to $y = 0$, or $x_F = 0$, in the collision c.m.s.

major part of this effect. However, in *central* collisions, the direct responsible would not be the spectator charge, but the net charge of the system created in the collision: the "central fireball" [Bartke09], "co-moving media" [Ahle98], or simply "participant zone" following the terminology used in the present paper, Fig. 2.21. A similar effect was observed in central Pb+Pb collisions at the beam energy of 158 GeV/nucleon, by the NA44 experiment at the SPS [Xu96].

On the other hand, less information is available on the electromagnetic influence of *spectator protons* on charged particle spectra at the SPS. Only one experimental result is known to the author. This is a measurement of forward pion production in Pb+Pb collisions at 158 GeV/nucleon, performed by the NA52 experiment [Ambrosini99], and shown in Fig. 4.1b. This measurement is made at different centralities of the collision, but unfortunately remains restricted to a narrow acceptance range (forward angles i.e. $p_T \approx 0$). In fact it is limited to as little as two data points near beam rapidity for the case of peripheral and central Pb+Pb collisions, while four data points are available for the total minimum bias sample. No information on transverse momentum dependence is available. Nevertheless, the Figure clearly suggests the presence of a large peak in the π^-/π^+ ratio, decreasing with increasing centrality as it is to be expected from the decreasing number of spectator nucleons. For peripheral reactions $\pi^-/\pi^+ \approx 7$ is attained nearest to beam rapidity. For central Pb+Pb collisions, the NA52 result is compared to that from the E877 experiment at the AGS [Lacasse96] on central Au+Au reactions at 10.8 GeV/nucleon beam energy[3]. An overall agreement is obtained. On the other hand, no peak is present in the projectile fragmentation region of p+Be reactions at 450 GeV beam energy [Ambrosini99a], where no spectator system is present.

Parallel to the experimental works, a sizeable theoretical effort took place, aiming at a description and interpretation of the electromagnetic effects induced by the nuclear charge on final state spectra of charged pions (as well as other charged particles). Several examples can be quoted [Libbrecht79, Cugnon81, Gyulassy81, Bonasera87, Li95, Barz98, Ayala97, Osada96, Ayala99 and others]. Notwithstanding various specific problems considered therein (classical equations of motion vs. quantal effects, relativistic retardation, modelling of the pion emission source and various contributing processes, evolution of the participant zone and of the spectator systems, etc), a basic element apparent in these works is the general hope that account taken of the good theoretical knowledge of the electromagnetic force and of its long-range character, the electromagnetic distortion of charged particle spectra could provide new information on the space-time evolution (geometry) of the nuclear collision. As such, various models were built to reproduce the experimental data and at the same time, constrain their intrinsic parameters characterizing the space-time evolution of the reaction. An example is given in Fig. 4.1a where the AGS data are described by the histogram corresponding to a central fireball, expending radially up to a "freeze-out" radius of 10 fm where pions stop to interact via the strong force [Ayala99]. Thus, it is hoped that such measurements would prove complementary to the information provided by hadronic interferometry (see e.g. discussion in [Cugnon81, Bartke09]).

In the author's opinion, the discussion made above defines very well the role of the study presented in this Chapter, as well as at least some of its essential technical aspects. This can be summarized as follows:

- The principal observable of this study will be the double differential π^+/π^- density ratio, introduced in Section 2.1;

- The selection of peripheral Pb+Pb reactions will reduce the contribution of the electromagnetic effect induced by the *participant* charge, and at the same time enhance that of

---

[3]For completeness, one can add that contrary to [Ambrosini99], the measurement at the AGS [Lacasse96] is not limited to $p_T \approx 0$. With a dense set of data points, it covers a two-dimensional region 2.8-4.5 in lab rapidity (beam rapidity being 3.14), and maximally 0-0.8 GeV/c^2 in $(m_T - m)$. This brings some degree of similarity to the NA49 measurement discussed below.

the *spectator* charge, apparently less known at SPS energies;

- Focussing on the spectator charge automatically moves the interest of this analysis into the projectile fragmentation region at sizeable pion x_F (e.g., comparable to spectator velocity). This gives a chance of fully exploiting the extended coverage of the present measurement, including the whole region from mid-rapidity up to $x_F = 0.4$ which is well above beam rapidity at low p_T;

- The two-dimensional character of the present measurement will give a chance of following the dependence of the electromagnetic distortion as a function of transverse momentum of the pion, a possibility not available in [Ambrosini99]. Thus, the NA49 measurement will by far overmatch that from Fig. 4.1b in terms of both phase space coverage and granularity;

- The presence of p+p data from the same experiment [Alt06], measured at the same beam energy of 158 GeV/nucleon and characterized by a similar (in fact, more extended) phase space coverage and a similar granularity in x_F and p_T, will provide a direct "reference" to an elementary process where no spectator system is present. This will give a chance of an at least partial disentanglement of spectator-induced effects from other phenomena;

- Finally, this will be supplemented with a phenomenological Monte Carlo analysis which will identify the basic features of the spectator-induced electromagnetic effect, and, most of all, study its implications in view of the hopes of using it as a source of new insight into the space-time evolution of the reaction, as expressed above.

Notwithstanding all these advantages, it must be kept in mind that the present analysis is still, essentially, rather an introductory study. In particular, it is based on a very simplified phenomenological approach, and aimed only at responding most basic questions on the subject. Extensions of this study both on the experimental and theoretical sides are clear to define, as it will become apparent in the course of this Chapter.

4.2 Dependence of π^+/π^- Ratios on x_F and p_T

This analysis starts with a general inspection of double differential π^+/π^- ratios in the final state of the peripheral Pb+Pb interaction. These are shown in Fig. 4.2, drawn as functions of x_F at fixed values of transverse momentum.

The peripheral Pb+Pb data points are compared to the π^+/π^- ratios in nucleon-nucleon collisions at the same energy, $\sqrt{s_{NN}} = 17.3$ GeV. It should be noted that by "nucleon-nucleon" a mixture of 40% colliding protons and 60% colliding neutrons is meant. This proportion matches the isospin content of the Pb nucleus, and should therefore properly describe the isospin effects resulting from the mixture of proton and neutron fragmentation into pions, see also Sections 2.3.2 and 2.3.4. As the relation between neutron fragmentation and proton fragmentation can be deduced from isospin symmetry ($n \to \pi^+ = p \to \pi^-$, etc)[4], the π^+/π^- ratios resulting from this mixture of incoming protons and neutrons can be directly derived from NA49 p+p data [Alt06]. What comes out is shown as a set of solid curves in Fig. 4.2. The excess of neutrons over protons results in a moderate, smooth decrease of the π^+/π^- ratio with x_F. This can be regarded as a reflection of the corresponding increase of this ratio in p+p reactions, presented in Fig. 2.9d.

From the comparison, the following picture emerges.

---

[4]Note: it is worthwhile to remind that this relation between proton and neutron fragmentation into π^+ and π^- was verified experimentally for p_T-integrated π^+/π^- ratios (Section 2.3.2, Fig. 2.11). A more detailed description of these issues, including analytical formulae, can be found in [Chvala04].
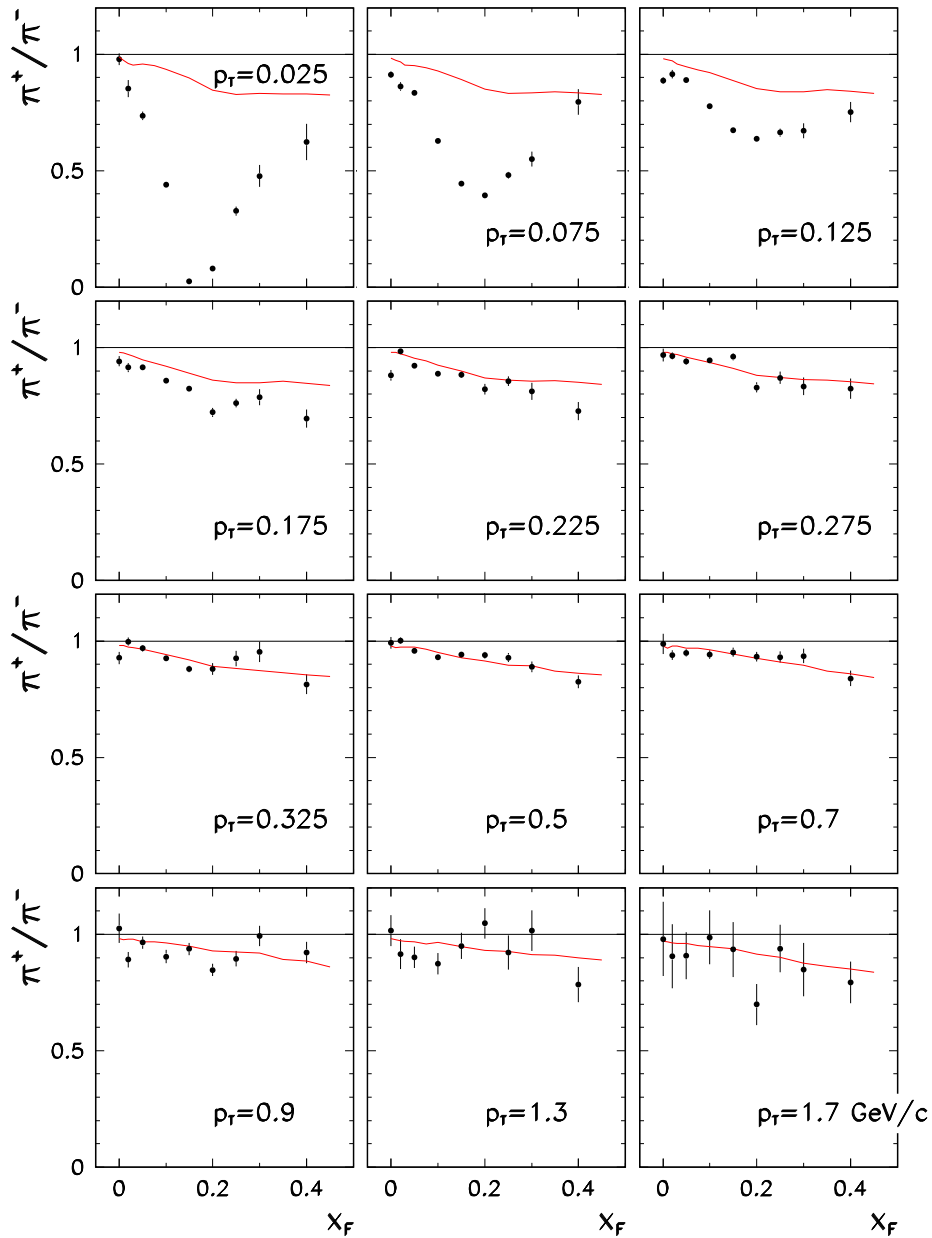
Figure 4.2: Data points: ratio of positive over negative pions produced in the projectile hemisphere of peripheral Pb+Pb collisions at $\sqrt{s_{NN}} = 17.3$ GeV, drawn as a function of x_F at fixed values of p_T. Solid curves: the same ratio for nucleon-nucleon collisions, as described in the text. The plot comes from [Rybicki09].

- At higher transverse momenta (above $p_T \approx 0.25$ GeV/c) a fair overall agreement between π^+/π^- ratios in Pb+Pb and nucleon-nucleon collisions can be claimed within experimental errors[5].

- At lower transverse momenta, an increasingly violent charge asymmetry (drop of π^+/π^- ratio) can be observed in Pb+Pb collisions when approaching $p_T = 0$. The drastically low

---

[5]Note: the fact that π^+/π^- *ratios* in Pb+Pb reactions are similar to nucleon-nucleon interactions does not imply that there is no difference in the corresponding pion density *spectra*. Such differences are in fact clearly present in the experimental data and will be discussed in Chapter 5.
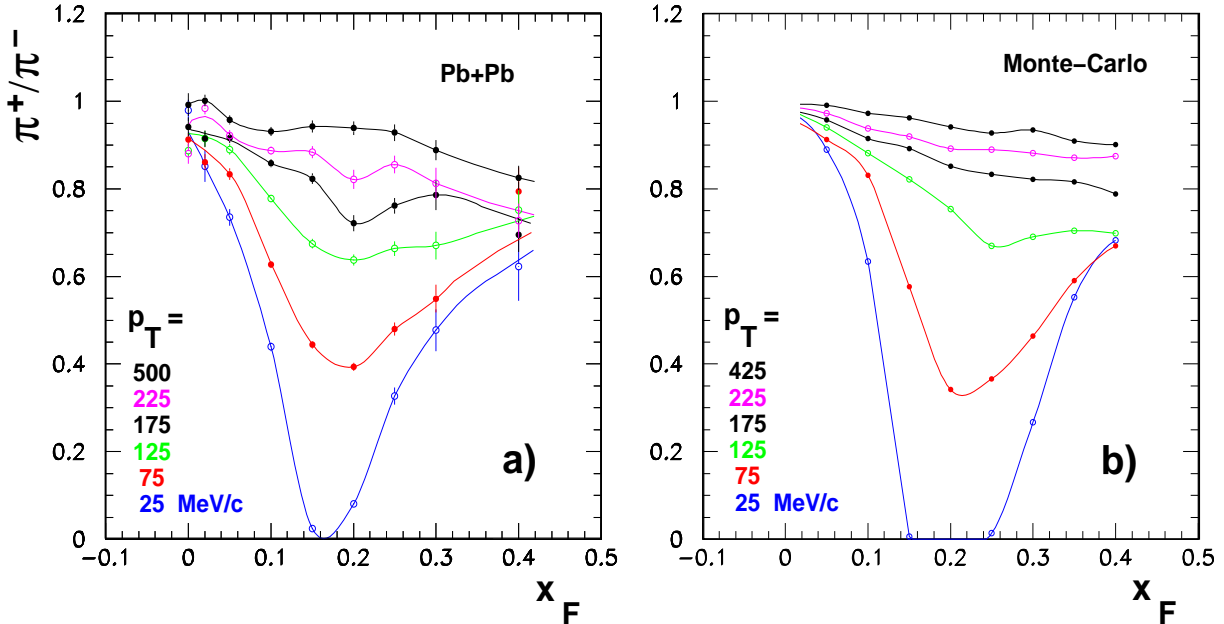
Figure 4.3: **a)** π^+/π^- ratios in the projectile hemisphere of peripheral Pb+Pb collisions at $\sqrt{s_{NN}} = 17.3$ GeV, drawn as a function of x_F at several selected values of p_T (listed from top to bottom curve). **b)** π^+/π^- ratios obtained by the Monte Carlo simulation described in Section 4.4.1. Both panels are redrawn from [Rybicki09].

> minimum value of the π^+/π^- ratio reached for low-p_T pions moving at spectator velocity ($x_F = 0.15$) can be regarded as a "signature" of the spectator-induced electromagnetic repulsion (attraction) of positive (negative) pions, see also discussion in Section 2.3.4.

- Once lower and higher transverse momenta are taken together, the x_F-dependences of π^+/π^- ratios in Pb+Pb reactions suggest an overall superposition of two components: a sharp drop at low p_T, which seems to appear on top of a fairly p_T-independent, smooth decrease with x_F (tentatively described by the solid curves).

- This situation can be tentatively claimed as an example of the *interplay* between hadronic and electromagnetic phenomena in the peripheral Pb+Pb reaction. The hadronic component in pion production would reflect in the smooth decrease of π^+/π^- ratios with x_F. At least in a large part, it could be directly identified by the same ratios in elementary nucleon-nucleon collisions (solid curves). This would then be distorted be the electromagnetic influence of the spectator system[6], strongly dependent on p_T.

4.3 The Electromagnetic Distortion

Once this basic interplay between hadronic and electromagnetic effects is, to first order at least, understood from the experimental data on π^+/π^- ratios above, the analysis may focus on the electromagnetic distortion. A summary plot is shown in Fig. 4.3a which puts together a selection of p_T bins from Fig. 4.2, up to a maximal value of $p_T = 0.5$ GeV/c. Clearly the NA49 data are precise enough to image the full two-dimensional structure of this effect. This consists of a steep valley in the (x_F, p_T) plane, with the π^+/π^- ratio rapidly decreasing when approaching the minimum localised in the vicinity of the spectator velocity, $x_F = 0.15$ for pions moving

---

[6]Some influence of the participant charge is also to be considered, as discussed in Section 4.5.

longitudinally. This minimum corresponds to the depopulation of this region of phase space by Coulomb repulsion of positive pions, and accumulation by attraction of negative pions (see also Figs 3.5b and c, respectively). As a result, the π^+/π^- ratio comes close to zero.

The structure visible in Fig. 4.3a can be regarded as an (inverted) reflection of the preceding measurements shown in Fig. 4.1b. The present measurement gives a much more complete picture of this spectator-induced phenomenon in terms of granular coverage of phase space, although on the other hand it remains limited to a single (peripheral) configuration of collision geometry.

In principle, some of the basic features of the effect seen in Fig. 4.3a can be understood from very simple considerations. For instance, the impressive depopulation of the region $x_F = 0.15$, low p_T from positive pions can be attributed to the fact that a sample (pion) charge in the spectator c.m.s. acquires an additional, non-zero kinetic energy from the Coulomb potential of the spectator system. It is however clear that any more detailed understanding of the whole phenomenon and of its implications requires phenomenological Monte Carlo studies. Such an approach will be followed in the next Section.

4.4   Monte Carlo Studies

This Section summarizes a phenomenological analysis of the spectator-induced electromagnetic effect in peripheral Pb+Pb collisions at top SPS energy, $\sqrt{s_{NN}} = 17.3$ GeV. The main part of this analysis was published in [Rybicki07] (partially also in [Szczurek07]) before the experimental data from Chapter 3 were available in their present form. As such, this analysis was mainly aimed at a principle understanding of basic features and implications of the electromagnetic effect, rather than at a fully quantitative description of the data. A comparison between the results of this study and the presently existing experimental information is nevertheless instructive. It gives an idea on the extent to which the interplay between particle production and final state electromagnetic interactions can be understood by means of an extremely simplified phenomenological apparatus; this simplicity facilitates interpretation.

4.4.1   The Model

The present description summarizes only the most important aspects of the model used in this study[7]. A maximally simplified approach has been applied as shown in Fig. 4.4. A peripheral Pb+Pb reaction can be imagined to consist of three steps [Rybicki07]:

1. the collision takes place at a given impact parameter b. The two highly charged spectator systems follow their initial path;

2. the participating system evolves until it finally gives birth to final state pions. The evolution of the pion emission region in space and time is *a priori* unknown;

3. charged pion trajectories are modified by the electromagnetic interaction with the spectator charge; the spectator systems undergo a complicated nuclear fragmentation process.

These three steps were modelled in a simplified way, described below:

1. *Collision geometry.* The model assumed a peripheral Pb+Pb reaction involving 60 participating nucleons, which corresponded to an impact parameter b equal to 10.61 fm. The two spectator systems were modelled as two homogeneous, uniform spheres in their respective rest frames. Their density was the standard nuclear density $\rho = 0.17/\text{fm}^3$ and the total charge of each spectator system was $Q = 70$ elementary units. In the collision c.m.s. frame

---

[7]A more detailed description can be found in [Rybicki07].
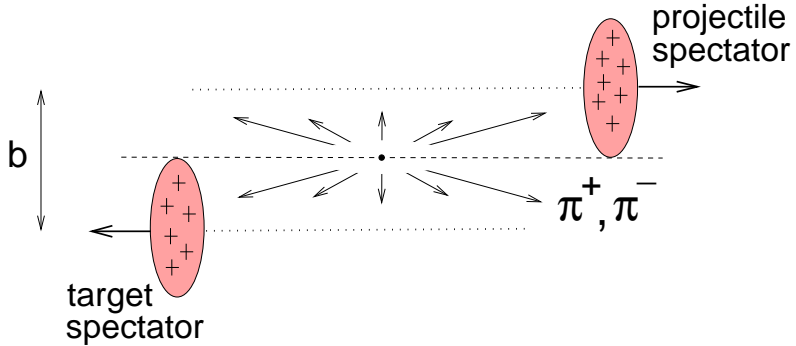
Figure 4.4: Simplified model of the peripheral Pb+Pb collision at $\sqrt{s_{NN}} = 17.3$ GeV. The hypothetical pion emission region is reduced to a single point in position space (see text). The plot comes from [Rybicki07].

the two spheres became charged disks as illustrated in Fig. 4.4.

All the numerical parameters listed above were determined from a geometrical Monte Carlo simulation based on realistic nuclear profiles [Trzcińska01, Mizutori00] and on the elementary nucleon-nucleon cross section equal to 31.4 mb [Alt06], similarly to the model described in Section 2.3.4. The spectator charge Q was also obtained from this simulation as in principle, it could be modified by neutron halo effects. The simplification of spectator systems into spherical shape was adjusted to agree with the results of the simulation. In particular, this required an additional sideways displacement of the spheres centers' by 0.76 fm in order to match the center of gravity of the spectator systems.

2. *Pion emission.* The pion emission zone was reduced to a single point in space: the original interaction point. The emission time t_E was a free parameter of the model and various values of t_E were considered. For the case of the peripheral Pb+Pb reaction analyzed in this study, the initial double differential (x_F, p_T) distribution of the emitted pions was assumed to remain similar to that in underlying nucleon-nucleon collisions. It was deduced from experimental p+p data [Alt06], account taken of the mixed isospin content of the Pb nucleus, see Section 4.2 above. The model assumed full azimuthal symmetry of the emission.

3. *Charged pion propagation into the final state.* With their initial momentum vector defined above (point 2.), the emitted charged pions were numerically traced in the electromagnetic field induced by the spectator charges; this took place until their distance from the original interaction point and from each of the two spectator systems exceeded 10,000 fm. Classical relativistic equations of motion, implicitly taking account of retardation effects, served this purpose (see [Rybicki07] for more details). The model neglected the fragmentation of the spectator systems. The additional influence of the participant charge, strong final state interactions, etc, were also not considered.

4.4.2 Comparison between Data and Model

A direct comparison between the experimental data and the Monte Carlo model simulation described above was presented in Fig. 4.3. The simulation shown in panel **(b)** was performed assuming a "mixed" set of initial conditions[8]: for 50 % of the generated peripheral Pb+Pb

---

[8]Note: it should be remembered that the term *initial conditions* used in the text is to be understood as "initial conditions for the spectator-induced electromagnetic interaction" rather than "initial conditions for the Pb+Pb collision".

events, the pion emission time was assumed equal to $t_E = 0.5$ fm/c, while the remaining 50 % were generated assuming $t_E = 1$ fm/c.

As for practical reasons, the simulation was limited in the considered range of transverse momenta, Fig. 4.3b stops at $p_T = 425$ MeV/c. It is nevertheless clear that with the specific set of initial conditions defined above, the simulation properly describes the main characteristics of the experimental data. This may seem quite surprising account taken of the extreme simplicity of the model, Section 4.4.1. It gives some confidence in the conclusions drawn on its basis, see below.

Apart from similarities, more detailed differences between the data and Monte Carlo can also be seen from Fig. 4.3. These will be discussed in Section 4.5.

4.4.3 Dependence on Initial Conditions

After a first comparison between the Monte Carlo and the experimental data, a discussion of implications of the electromagnetic effect will follow. The analysis of these was performed using the same Monte Carlo model as discussed in Section 4.4.1, however with further simplifications aimed at an easier interpretation of the results of the simulation.

These simplifications concerned the undistorted, initial spectra of pions emitted from the collision (item 2. in Section 4.4.1). While these spectra were all the time postulated to be similar to nucleon-nucleon collisions, the difference between π^+ and π^- distributions was neglected - they were simply assumed to be equal. Both distributions were parametrized[9] by the same smooth, analytical function in (x_F, p_T), adjusted to the average pion ($\frac{\pi^+ + \pi^-}{2}$) data from p+p reactions [Alt06]. This meant that the hadronic isospin effects resulting from the mixture of proton and neutron fragmentation, Section 4.2, were explicitly removed from the final state π^+/π^- ratio: *any deviation of this ratio from unity was exclusively resulting from the spectator-induced electromagnetic interaction.* In addition, applying a smooth shape for the pion distribution eliminated some local resonance structures present in the original p+p data (see Section 2.3.3 for comparison). These were judged as an undesirable complication for the present analysis.

The first result of this study is presented in Fig. 4.5a, which shows the final state π^+/π^- ratios drawn as a function of x_F; these are computed for the simplest situation where the initial pion emission time t_E is equal to zero ("immediate pion creation" [Rybicki07]). As the Figure extends over the whole available range of x_F, $-1 < x_F < 1$, it displays a symmetric structure, where the electromagnetic field from the two spectator systems produces a characteristic, complex pattern of deviations of π^+/π^- ratios from unity. The first element of this pattern is the steep two-dimensional valley seen in the NA49 data, Fig. 4.3. The second element is the continuous rise of the π^+/π^- ratio at higher absolute values of x_F. This rise is apparent for all the considered transverse momenta. At fixed values of x_F, the ratio slowly diminishes with increasing p_T.

The principal problem discussed in this Section is the *sensitivity of the spectator-induced electromagnetic effect to initial conditions imposed on pion emission.* This problem is analyzed in Fig. 4.5 (panels **a-e**). In the Figure, the π^+/π^- distortion pattern computed assuming the initial pion emission time t_E equal to zero is compared to these obtained with $t_E = 0.5, 1, 1.5$, and 2 fm/c. Indeed, clear differences are apparent for different values of t_E. With increasing emission time, a broadening of the two valleys at $x_F \approx \pm 0.15$ is visible, together with a decrease of the π^+/π^- ratio at higher $|x_F|$. A complementary view is presented in Fig. 4.6. Here, the π^+/π^- distortion patterns resulting from different values of t_E are directly compared at fixed transverse momenta. It becomes clear from this comparison that a change of 0.5 fm/c in the pion emission time is already sufficient to produce a visible modification in the π^+/π^- ratio. In the region of low transverse momentum ($p_T < 200$ MeV/c), a displacement of the two valleys

---

[9]For a more detailed description of this parametrization, see [Rybicki07].
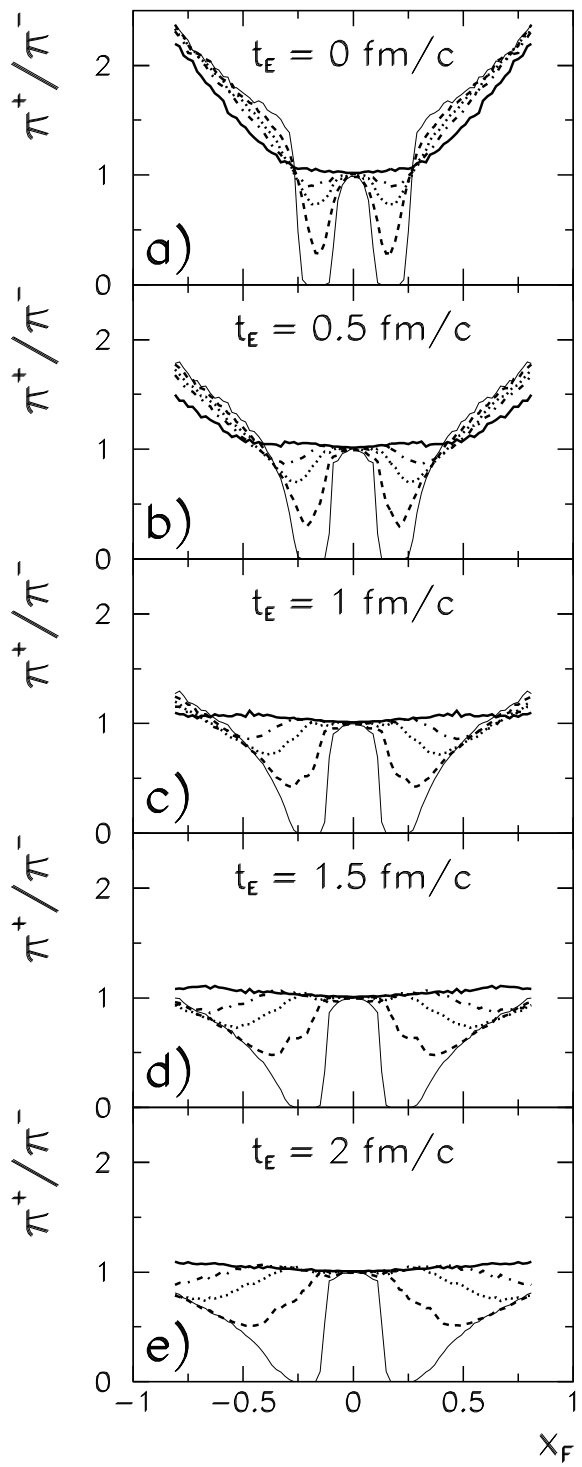
Figure 4.5: Ratio of density of produced π^+ over produced π^- in the final state of the peripheral Pb+Pb reaction at $\sqrt{s_{NN}} = 17.3$ GeV, obtained for five values of the pion emission time t_E. In all the panels, the π^+/π^- ratio is drawn as a function of x_F at $p_T = 25$ MeV/c (thin solid), 75 MeV/c (dash), 125 MeV/c (dot), 175 MeV/c (dash-dot), and 325 MeV/c (thick solid). The small cusps on the curves correspond to the statistical fluctuations in the Monte Carlo described in the text. At negative x_F reflected curves are drawn. The plot comes from [Rybicki07].
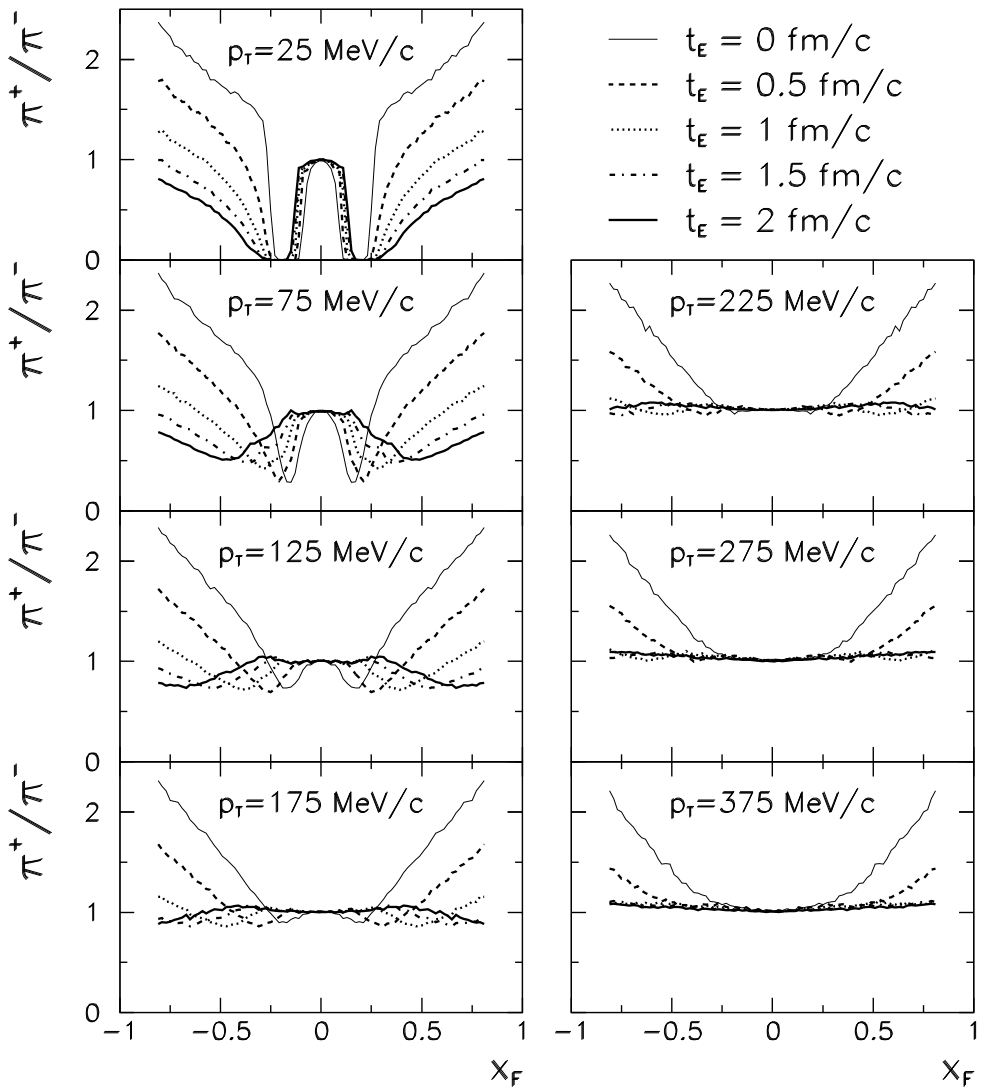
Figure 4.6: Final state π^+/π^- ratio for the peripheral Pb+Pb reaction, shown at fixed values of p_T as a function of x_F. The five considered values of the pion emission time t_E are differentiated by means of different line types. At negative x_F reflected curves are drawn. The plot comes from [Rybicki07].

towards higher absolute values of x_F becomes apparent, on top of their broadening with t_E. On the other hand, at higher p_T, the π^+/π^- ratio seems to stabilize for $t_E > 1$ fm/c.

Altogether, the Monte Carlo studies presented in this Section clearly show the sensitivity of the π^+/π^- ratio to the pion emission time t_E. Thus, they indicate that the electromagnetic effect induced by spectators on π^+ and π^- spectra depends on the initial conditions imposed on the process of pion emission. It should be remarked that within the simplified model used for the present analysis, the different values of the emission time t_E are directly equivalent to different distances between the pion formation site and the two spectator systems (see Fig. 4.4). Thus, it can be concluded that the spectator-induced electromagnetic distortion discussed above carries information on the evolution of the non-perturbative process of particle production in space and in time. This important issue will be further addressed in subsequent parts of this Chapter.
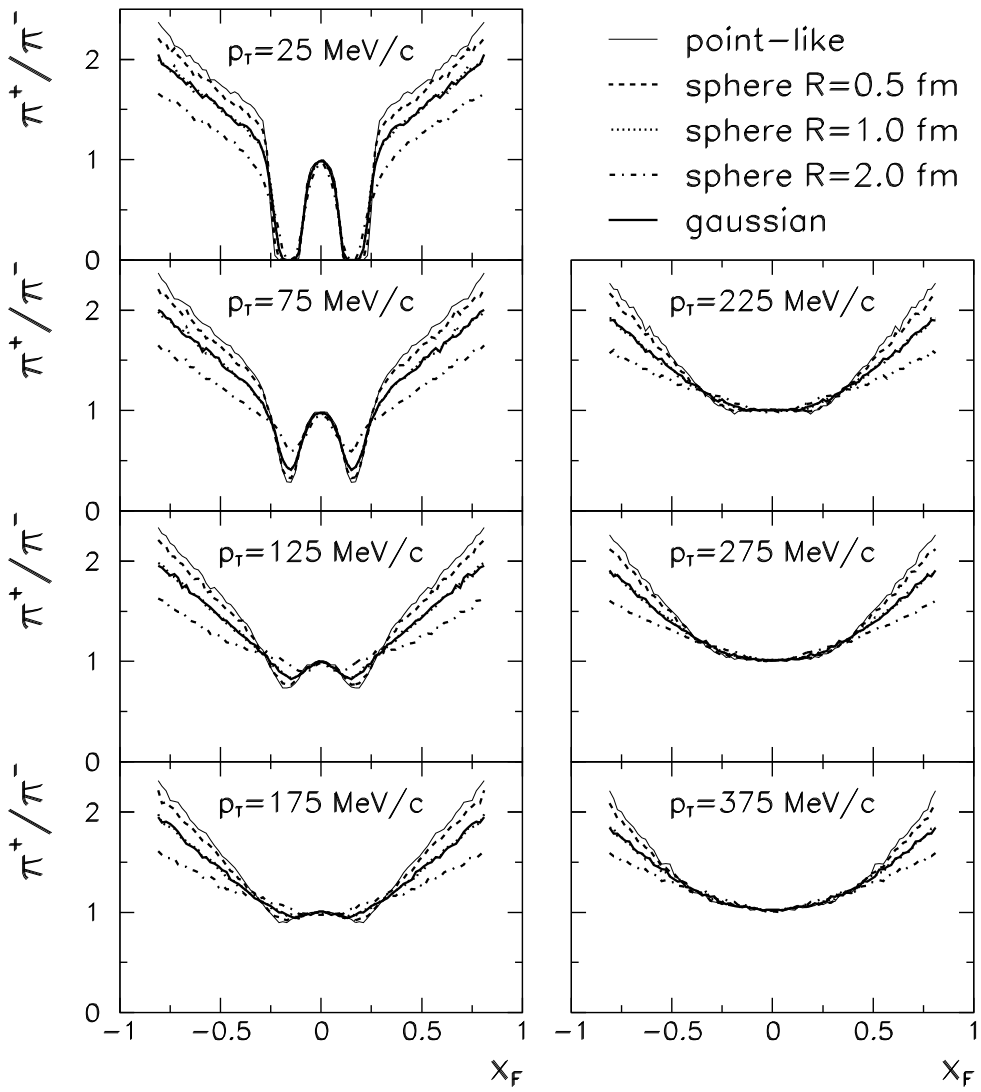
Figure 4.7: Dependence of the final state π^+/π^- ratio on the size and shape of the initial pion emission zone. The π^+/π^- ratio is drawn as a function of x_F for different values of pion transverse momentum. The simulation was made assuming t_E equal to zero. The result obtained for the point-like source is the same as in Fig. 4.6; the Gaussian distribution has been adjusted to match the average size of the sphere with $R = 1$ fm (see text). At negative x_F reflected curves are drawn. The plot comes from [Rybicki07].

4.4.4 Extended Sources

Up to now, for simplicity, all the Monte Carlo simulations discussed above assumed the emission of pions to take place from a unique point in position space - the original interaction point (see Section 4.4.1 and Fig. 4.4). This very strong simplification was, of course, by no means realistic. On the contrary, even simplest, intuitive pictures of the heavy ion collision will consider, for the pion emission region, some kind of extended area where the formation of pions will occur over a finite volume of space (and finite period of time). Therefore the concept of "pion source" is used to deal with this problem (see, e.g. [Libbrecht79]), and numerous different descriptions of the source were tried in the past.

In the context of the above, it is important to know how the results of the precedent studies will change once a finite pion emission region is assumed instead of a point-like source. An
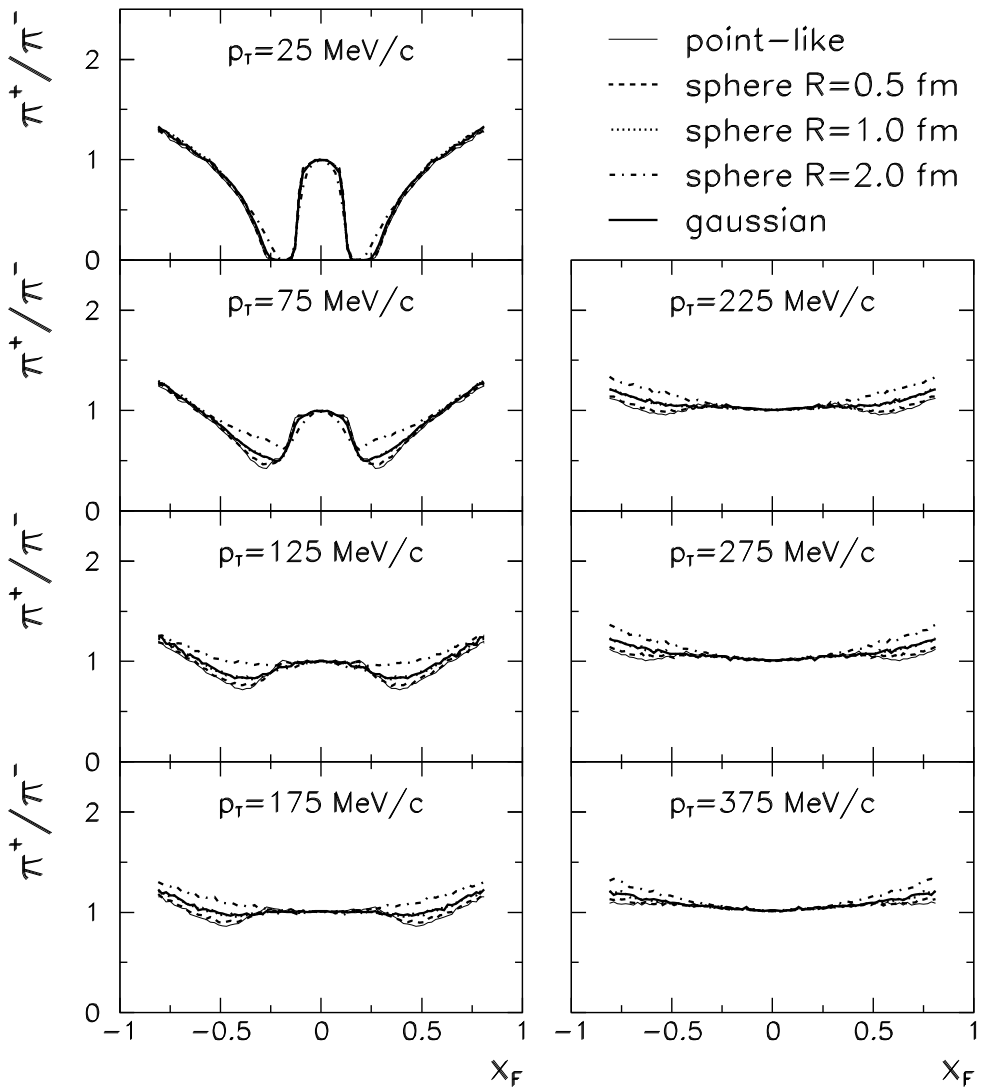
Figure 4.8: Dependence of the π^+/π^- ratio in the final state of the peripheral Pb+Pb reaction on the size and shape of the initial pion emission zone. The simulation assumed $t_E = 1$ fm/c.

introductory study was therefore performed to explore this problem. This will be described in this Section.

In this introductory study, two simple shapes were considered for the pion emission source. These were a uniform sphere and a three-dimensional Gaussian density distribution. The latter was cut off at three standard deviations in order to prevent too long tails. For both shapes, the source center was set at the original interaction point from Fig. 4.4. For the sphere radius R, several values were considered: $R = 0, 0.5, 1,$ and 2 fm. A single value of the standard deviation σ was considered for the Gaussian source. This was adjusted to 0.486 fm, which gave the same average radius as that of the sphere with $R = 1$ fm. This facilitated the comparison of results obtained for the two shapes. For simplicity, the simulation assumed a unique value of the pion emission time t_E, and neglected the possible dynamical correlations between the pion momentum and its formation time and position.

In a first example, the influence of the source size and shape on final state π^+/π^- ratios is shown in Fig. 4.7. The π^+/π^- ratios are drawn as a function of x_F for different fixed transverse

momenta; this simulation is made assuming the emission time $t_E = 0$. As visible in the Figure, the electromagnetic distortion pattern induced by the spectator charge depends on the source size: the distortion decreases with increasing sphere radius R. This is especially visible for $|x_F| > 0.3$, namely, outside of the two characteristic valleys. One should remark that on the other hand, there is no difference visible between the results obtained for the uniform sphere and for the Gaussian distribution, if only the average size of the source is identical. One has to conclude that the shape of the source has, at best, a marginal influence relative to the dominant effect of the source size.

This situation changes when the pion emission source' center "moves behind" the spectator system. This is illustrated by another simulation, this time made assuming $t_E = 1$ fm/c, shown in Fig. 4.8. For such a configuration where the extended source (or at least, the bulk of its volume) is contained between the two Lorentz-contracted spectator systems[10], the dependence on the source size is evidently strongly reduced relative to $t_E = 0$. This is particularly apparent at low transverse momenta where the spectator-induced electromagnetic distortion corresponding to a point-like source is kept almost intact for all the extended sources considered. One could therefore conclude that for such configurations as the one discussed here, this distortion keeps better track of the first-order space-time characteristics of the pion formation zone (that is, of the emission time which defines its average longitudinal position with respect to the two spectator systems). There is less dependence on the source extension. Again, at least in the highly simplified approach discussed here, no indication of the dependence on the detailed source shape (spherical or Gaussian) is seen.

4.5 Discussion

This Section constitutes an attempt at a general synthesis of the different experimental and phenomenological findings described in Sections 4.2-4.4.

The situation can be summarized as follows:

- New experimental information has been obtained on the electromagnetic distortion of final state π^+/π^- ratios in peripheral Pb+Pb collisions at $\sqrt{s_{NN}} = 17.3$ GeV. This information is more detailed than the existing measurements (Fig. 4.1) and covers the region from $x_F = 0$ to $x_F = 0.4$ in a wide range of p_T (Figs 4.2, 4.3).

- The basic features of the observed distortion are fairly described by a very simple relativistic model (Fig. 4.3). This model (Fig. 4.4) postulates pion emission from a single point-like source. It takes account of the modification of π^+/π^- ratios induced by the mixed isospin content of the Pb nucleus (Fig. 4.2) but practically neglects all the other hadronic phenomena in the reaction. The fair agreement between data and model is obtained if the pion emission time t_E is assumed to be 0.5 fm/c and 1 fm/c, each for 50 % of the simulated events.

- The determination of t_E is not arbitrary in the sense that the electromagnetic distortion depends on the initial conditions imposed on pion emission (Fig. 4.5). In particular, the region $|x_F| > 0.3$ displays a clear sensitivity of the π^+/π^- ratio to t_E.

- A first study of the influence of the source extension seems to imply that for the initial conditions mentioned above (like $t_E = 1$ fm/c, shown in Fig. 4.8), this influence would

---

[10]Note that in the simple model used here, $t_E = 1$ fm/c corresponds to a situation where, at the moment of pion emission, each of the two spectator systems moved by ~ 1 fm from the point of closest approach (see also Fig. 4.4). This means that the longitudinal extension of a sphere with, e.g., $R = 1$ fm does not exceed that defined by the centers of the two strongly Lorentz-contracted spectator discs.

be quite limited, especially in a situation where the source would not extend beyond the longitudinal position of the spectator system at the moment of pion emission.

At the beginning of the discussion, it should be stressed that the term "fair agreement between data and model" should be taken with some caution. In particular, it makes no sense to claim that the picture of pion emission from a point-like source, postulated in the model, has any direct correspondence to physical reality. As such, the parameter t_E could rather be interpreted as the (average) longitudinal displacement of the pion formation site relative to the corresponding spectator system, see also Fig. 4.4. For instance, the two values of t_E quoted above would closely correspond to $0.5 - 1$ fm in position space for the SPS kinematics. At least for fast pions (e.g., at $x_F \approx 0.4$) which are more sensitive to the initial conditions of the electromagnetic effect[11], this would suggest a source placed behind, i.e. moving slower than the actual spectator system. This would be the case for e.g., indirect production of fast pions from baryonic resonances like Δ or N^*, similarly to what was demonstrated for p+p collisions in Section 2.3.3, Fig. 2.14.

Drawing too strictly quantitative conclusions on the basis of the adjusted values of t_E is, of course, made difficult by the extreme simplicity of the model. Here a few hadronic (or nuclear) effects explicitly not included in the simulation should be enumerated as some of them bring valuable items to the present discussion.

Nuclear fragmentation. The first effect to be addressed is the fragmentation of the spectator system. The latter is known to break up into single nucleons as well as other, heavier fragments. Versatile information on this process was gathered in the past; a comprehensive summary, including in particular angular and isotopic spectra, can be found in [Bartke09], examples of other studies including kinematical distributions in e.g. [Barrette92, Deines-Jones00]. As reported by NA49 [Appelshäuser98], for peripheral Pb+Pb collisions at 158 GeV/nucleon most of the spectator forward-going energy is carried by fragments rather than single nucleons.

As noticed already in 1952 [Yagoda52], the nuclear fragmentation process may decrease the effect of the Coulomb distortion, for instance for pions with low kinetic energies in the spectator c.m.s. This corresponds to $x_F \approx 0.15$, low p_T for the present analysis. The influence of spectator expansion on the shape of the "Coulomb hole" at spectator rapidity, $p_T = 0$ was explicitly demonstrated in a phenomenological analysis of nuclear collisions at lower energies [Cugnon81], where an expansion velocity of $0.16c$ was postulated for the spectator system.

For the case of high energy peripheral Pb+Pb reactions discussed here, a reflection of this process seems apparent from the comparison of data and model made in Fig. 4.3. At low pion transverse momentum, the model predicts a finite region in x_F completely depopulated from positive pions ($\pi^+/\pi^- = 0$), while a significantly less violent structure is seen in the experimental data. This disagreement can in fact be regarded as an indication that the characteristic valley seen in the data and model is indeed sensitive to spectator fragmentation. As such, on top of the information on the space-time scenario of the pion production process, Section 4.4.3, the spectator-induced electromagnetic effect may be used to gain knowledge on the evolution of the spectator system in times characteristic to pion propagation in its vicinity.

Coming back to the region of $x_F \approx 0.4$ discussed above, pions in this region of phase space have, in the spectator c.m.s., sizeably larger velocities than in the "Coulomb hole". To give an example, at $p_T = 0$ this velocity is $\beta \approx 0.76$ for pions at $x_F = 0.4$, to be compared with $\beta = 0.29$ for pions at $x_F = 0.2$. As such, pions at $x_F = 0.4$ will spend a shorter time in the vicinity of the spectator system, which may somewhat decrease the influence of spectator fragmentation. Assuming, however, pion emission taking place from *behind* the spectator system as said above,

---

[11]Realistically, the longitudinal position of the pion formation zone relative to that of the spectator system can depend on the x_F and p_T of the pion. For this reason, the conclusions made above are limited to fast pions which are sensitive to t_E; see also discussion made below.

this time will nevertheless remain non-negligible. Some influence of this effect is therefore to be expected, presumably resulting in a decrease of the distortion (increase of π^+/π^- ratio) in this region of x_F. This would indicate that higher values of t_E would be required in order to come into an agreement with the data.

__Other effects.__ The fragmentation of the spectator system is not the only effect to be accounted for in an attempt at a precise description of the experimental data. Another issue is the participant charge discussed in Section 4.1 which, even for this peripheral sample of Pb+Pb collisions, may exert some influence on the π^+/π^- ratio. However, the final state phase space localisation of the net participant charge would be mostly given by the final state pion and proton spectra (Figs 3.6 and 2.6, respectively). As such, most of it would remain at velocities below these corresponding to pion $|x_F| = 0.15$, for instance near $x_F = 0$ as it was shown in Fig. 4.1a.

Various further issues, absent from the present study due to the extreme simplicity of the model, could be quoted. The space-time evolution of pion production does not have to be the same for positive and negative pions, which would in principle require the introduction of two different values for the parameter t_E; it should be noted however that all the corresponding differences will be diminished by the approximate isospin symmetry of the Pb nucleus. Emitted pions could possibly undergo a hadronic final state interaction with the spectator system which could, in turn, contribute to final state pion production through various hadronic/nuclear processes (see also the discussion made in the next Chapter).

While the above list of possible additional effects could still be elongated, the discussion made above seems sufficient to formulate several conclusions. It seems quite clear that the experimental data presented in this Chapter, put together with the apparent sensitivity of the electromagnetic effect to various elements of the reaction, give a chance of investigating the space-time evolution of the underlying non-perturbative processes. In view of the simplicity of this analysis, it is difficult to state whether the obtained information could be fully model-independent (that is, extracted without assuming any arbitrary scenario of the space-time evolution of the reaction). This does not seem impossible if a phenomenological Monte Carlo apparatus more detailed than the one presented here, including e.g. a compilation of existing knowledge on the nuclear fragmentation process, of experimental information on charged particle distributions, etc, is properly developed. In this context, it is quite reassuring that the present highly simplified approach gives a reasonable agreement with the data; this suggests that it properly describes the dominant underlying elements of the whole phenomenon. On the basis of this simplified analysis, a picture emerges where the emission of high x_F pions would take place from a source placed behind the corresponding spectator system. This is reminiscent of pion production from resonances in p+p collisions but more detailed studies, including other possible scenarios, are necessary.

The last item in the present discussion is, of course, the possibility of improving the existing models of the nuclear reaction, including in particular the "microscopic" Monte Carlo generators. It seems clear that the (x_F, p_T) shape of the spectator-induced electromagnetic distortion provides a useful, quantitative constraint on the space-time evolution of particle production (and, possibly, on its relation to nuclear fragmentation). This should provide a way for testing the microscopic model predictions and thus, improving the description that a given model provides for various detailed aspects of particle production. As it comes from the present analysis, this "discriminative power" can be expected to concern in particular the fragmentation region at reasonably high x_F. This would make it complementary to studies of Coulomb effects induced by the participant charge, Section 4.1.

4.6 Charged Kaons

The last study to be presented in this Chapter concerned the dependence of the spectator-induced electromagnetic effect on the mass of the produced charged particle. Here the kaon mass was selected as apart from pions, kaons are the lightest charged mesons easily accessible to experiments of the type of NA49. Also, they provide information on phenomena considered very important in heavy ion physics, namely the issues of strangeness production and strangeness enhancement in heavy ion collisions [Rafelski82, Koch86].

The present, introductory analysis aimed at the understanding of the basic, kinematical aspects of the spectator-induced electromagnetic effect for kaons. A detailed description of the interplay of the electromagnetic force with hadronic and nuclear phenomena characteristic to kaon production in Pb+Pb collisions (like the strangeness enhancement quoted above) was left for a subsequent analysis. As such, this study was made by means of the same Monte Carlo simulation as discussed in Section 4.4.3, with the mass of the sample particle modified from pion to kaon. This implied assuming identical initial, undistorted spectra for emitted K^+ and K^-. Such a simplified approach offered the convenience of an easy identification of the influence of the electromagnetic force by (any) deviations of the final state K^+/K^- ratio from unity. However, it should be remembered that in reality, the ratio K^+/K^- is always greater than unity due to associate production of K^+ with hyperons; this will have to be taken into account in future more detailed studies[12].

The principal result of the present introductory analysis is shown in Fig. 4.9. This shows the x_F-dependence of the double differential K^+/K^- ratios in the final state, drawn at several fixed values of kaon transverse momentum. The different panels of the Figure correspond to different values of the kaon emission time t_E defined identically as in Section 4.4.1. The influence of the spectator-induced electromagnetic interaction manifests itself by the presence of two large and deep valleys in the K^+/K^- ratio, followed, for lower values of t_E and very high $|x_F|$, by a steep increase of this ratio above unity.

If compared to the analogical plot made for pions (Fig. 4.5), the two valleys present in the K^+/K^- ratios are shifted towards much higher absolute values of x_F. This is due to the higher value of x_F corresponding to spectator velocity ($x_F = \frac{m_K}{m_N} \approx 0.53$ for longitudinally moving kaons, relative to $x_F = 0.15$ for pions). The increase of final state particle mass results also in a sizeable broadening of the two valleys, as much in x_F as in p_T. Finally, the electromagnetic distortion of charged kaon spectra exhibits a dependence on initial conditions, imposed on kaon emission by means of the parameter t_E. A similarity can be noticed between this behaviour and that of π^+/π^- ratios, Fig. 4.5. However, the region of highest sensitivity to t_E is "compressed" from $|x_F| > 0.3$ for pions into a significantly narrower range at very high $|x_F|$ for kaons.

A few remarks should be made here. Following the discussion made in Section 4.5, it can be expected that the shape of the large valleys visible in Fig. 4.9 will be sensitive to the effect of fragmentation of the spectator system. This would imply another possibility of studying this phenomenon, this time on time scales characteristic to kaon propagation in its vicinity. The dependence of K^+/K^- ratios on initial conditions mentioned above could also in principle be exploited to obtain independent information on the space-time evolution of strangeness production. However, on one hand, a more detailed study (including a more realistic description of the initial K^+/K^- ratios) would be required. On the other hand, the information obtained from such a study would remain limited to kaon production in the deep fragmentation region at high $|x_F|$.

---

[12]A more detailed analysis, which will include a more realistic description of initial kaon spectra and K^+/K^- ratios in view of the hadronic phenomena discussed in the text above, is in progress.
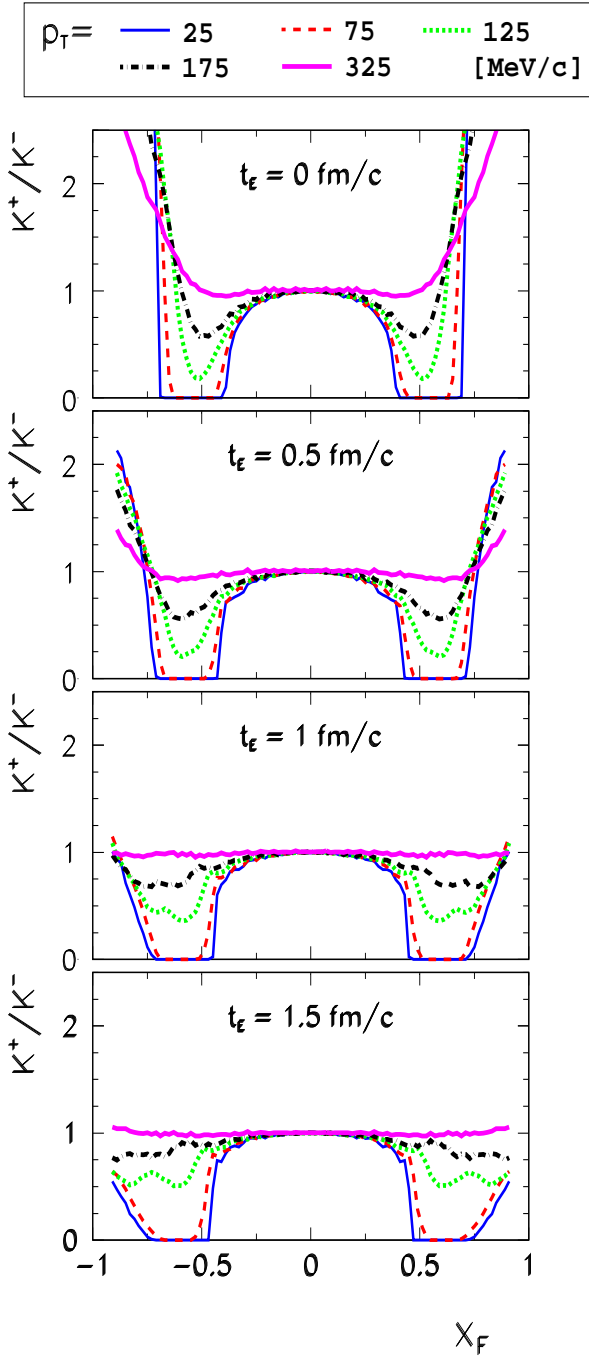
Figure 4.9: The electromagnetic distortion induced by the spectator charge on K^+/K^- ratios in the final state of the peripheral Pb+Pb collision, resulting from the study described in the text. The K^+/K^- ratios are drawn as a function of x_F for fixed values of p_T equal to 25 MeV/c (thin solid), 75 MeV/c (dash), 125 MeV/c (dot), 175 MeV/c (dash-dot), and 325 MeV/c (thick solid). The four panels correspond to four values of the assumed kaon emission time t_E. The plot is directly redrawn from [Rybicki09].

4.7 Summary and Outlook

The new data on pion production obtained by the NA49 experiment at the SPS allow for a detailed inspection of π^+/π^- ratios measured in the final state of peripheral Pb+Pb collisions at $\sqrt{s_{NN}} = 17.3$ GeV. This inspection brings a clear, highly granular picture of the electromagnetic

distortion induced on pion spectra by the charge present in the collision. In particular, the presence of the highly charged spectator system results in a characteristic, rapidly changing pattern in the x_F- and p_T- dependence of π^+/π^- ratios.

The main features of this experimentally observed electromagnetic distortion are fairly reproduced by a simple, one-parameter model of pion emission and propagation in the electromagnetic field of the two spectator systems. Monte Carlo calculations performed on the basis of the same model show that the final state π^+/π^- ratios distorted by the spectator charge are sensitive to the initial conditions imposed on pion emission, in terms of pion emission time or position of the pion formation site relative to that of the spectator system. As such, it can be concluded that the observed electromagnetic distortion can provide new information on the space-time evolution of the non-perturbative pion production process.

The same model gives an estimate on the influence of the finite size of the pion source on the electromagnetic distortion. Furthermore, a more detailed comparison between the model and the experimental data, combined with information gathered from past studies [Yagoda52, Cugnon81], suggests that the electromagnetic effect is also sensitive to the fragmentation of the spectator system. This means that the experimental measurement of π^+/π^- ratios discussed above could additionally provide information about this process on time scales characteristic to pion propagation in its vicinity.

A first study of the spectator-induced electromagnetic distortion of final state K^+/K^- ratios was also performed. This shows a qualitative similarity to the effect shown for pions. However, the bulk of the distortion and in particular the region of main sensitivity to initial conditions are both moved in the direction of much higher $|x_F|$.

As it was specified at the beginning of the present Chapter, this study should be considered rather as an "introduction to the subject" than as a complete analysis. In this context, several extensions can be proposed. Some of these are enumerated below.

1. The construction of a more involved phenomenological apparatus, containing at least some from the additional phenomena discussed in Section 4.5 (spectator fragmentation, participant charge, etc) would be indicated. It can be hoped that with the number of free parameters kept at a strict minimum and constrained by experimental knowledge on various elements of the reaction, more quantitative information on the space-time evolution of the reaction could be obtained.

2. Both in terms of phenomenology and of experimental measurements, the centrality dependence of the full (x_F, p_T)-pattern of the electromagnetic distortion should be investigated. This would give the important opportunity to follow the interplay of the influence of the spectator and participant charge and therefore put additional constraints on the space-time scenario of the collision.

3. As it comes out from this analysis, the region of high x_F is interesting in view of its sensitivity to the assumed initial conditions of pion (or kaon) emission. It is therefore clear that experimental information on charged particle ratios in the region of x_F higher than $x_F = 0.4$ would be highly valuable, in particular also for kaons.

Altogether, this introductory analysis of the influence of the spectator-induced electromagnetic interaction on final state particle spectra suggests quite a promising area of experimental and phenomenological studies. In spite of several difficulties, partially mentioned in the discussions above, it seems that the whole phenomenon offers a chance for obtaining independent information on the space-time evolution of particle production in the fragmentation region of nucleus-nucleus collisions. This would make it as much complementary to analyses based on the participant charge in the central region, as to completely different studies summarized in Chapter 2.

Chapter 5

Other Effects in Peripheral Pb+Pb Collisions

The aim of the present Chapter is to complete the discussion of strong and electromagnetic effects, made in this paper, with additional information on various phenomena occurring in peripheral Pb+Pb collisions at $\sqrt{s_{NN}}$ = 17.3 GeV. In the context of analyses discussed in the preceding Chapters, this will demonstrate how the electromagnetic phenomena in Pb+Pb reactions are, at the same time, accompanied by a modification of particle spectra resulting from the transition from the elementary (nucleon-nucleon) to the nuclear (heavy ion) system. This behaviour can then be discussed in the context of earlier studies, summarized in Chapter 2.

Unlike the analysis made in the precedent Chapter, and based on π^+/π^- ratios, the present study will be concentrated on summed charged pion ($\pi^+ + \pi^-$) production, without differentiation on positive/negative pion charge. This will eliminate the isospin effects induced by the mixed proton/neutron content of the Pb nucleus (see Sections 2.3.2, 2.3.4, 4.2), and reduce the influence of electromagnetic effects on the presented phenomena.

It should be underlined that the study presented here is not an idea of the author. The present analysis follows strictly the approach proposed in an earlier work, based on a preliminary set of NA49 data on pion production in peripheral Pb+Pb and p+Pb reactions [Fischer07]. This is also valid for most of the data discussion and interpretation. Relative to the quoted reference, the principal difference in the present analysis is the use of fully processed Pb+Pb results presented in Chapter 3, and of published data on p+C collisions [Alt07]. Some specific items have also been added on the data presentation and discussion level.

5.1   Spectra of Pions in Elementary and Nuclear Reactions

While the precedent Chapter contained a relatively detailed analysis of electromagnetic effects in peripheral Pb+Pb collisions, the problem of similarities and differences between the actual shape of produced pion spectra in elementary and heavy ion reactions obtained, up to now, relatively less attention. A concise discussion made in Section 3.5 pointed at **1)** a general resemblance in the shape of double differential pion density distributions in x_F and p_T in Pb+Pb and p+p interactions, **2)** an overall similarity of corresponding p_T-integrated longitudinal pion spectra, and **3)** the increase of pion $<p_T>$ with increasing $|x_F|$ in Pb+Pb collisions, partially similar to the "sea-gull effect" observed in p+p reactions.

However, it is clear that the double differential data discussed in this paper allow for a more in-depth discussion. As such, the input to the present analysis are the double differential pion transverse momentum distributions at fixed x_F, measured in inclusive inelastic p+p and p+C reactions, as well as in peripheral Pb+Pb collisions at $\sqrt{s_{NN}} = 17.3$ GeV. The data on peripheral
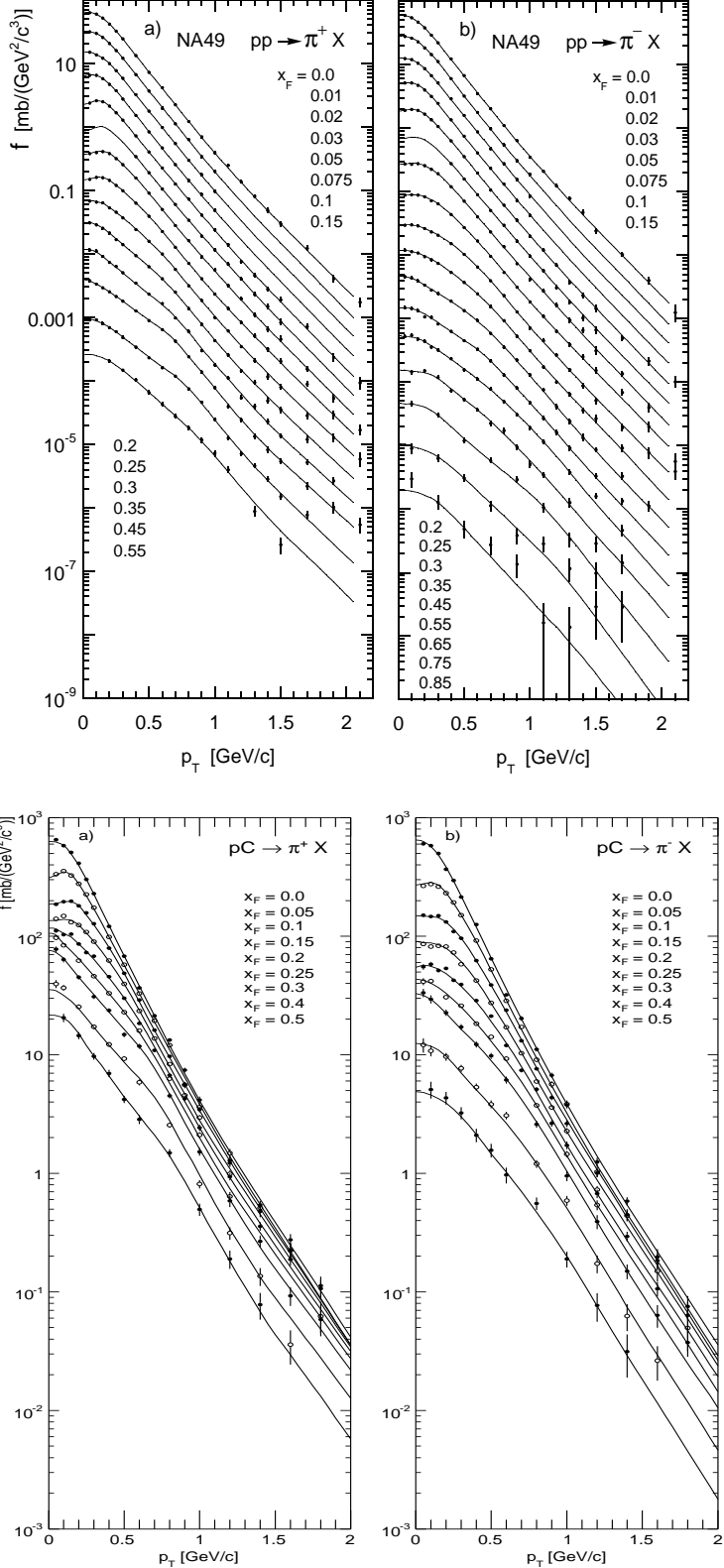
Figure 5.1: **Top panels:** invariant cross section drawn as a function of p_T at fixed values of x_F for π^+ (left) and π^- (right) produced in p+p collisions at $\sqrt{s} = 17.3$ GeV. In order to allow for a better separation, the data points and lines for π^+ are successively multiplied by 0.5, while these for π^- are successively multiplied by 0.5 up to $x_F = 0.35$ and by 0.75 for $x_F \geq 0.45$. Both panels are taken from [Alt06].
**Bottom panels:** invariant cross section as a function of p_T at fixed x_F for π^+ (left) and π^- (right) produced in p+C reactions at $\sqrt{s_{NN}} = 17.3$ GeV. Both panels are taken from [Alt07].

72

Pb+Pb collisions were shown in Fig. 3.5a. The other reactions are illustrated in Fig. 5.1. A few features of these three datasets are noteworthy:

- for all the three reactions, the measured datasets on π^+ and π^- production cover a wide region in x_F and p_T;

- the datasets on p+p [Alt06] and p+C [Alt07] reactions are both characterized by a coverage in x_F which is superior to that on Pb+Pb reactions;

- the dataset on p+C reactions has somewhat lower coverage in p_T with larger statistical error bars;

- while the measurements are not always made at exactly the same values of x_F and p_T for the three reactions, the overall dense coverage in phase space, and the presence of precise interpolations for all the three sets of data points, allows for a direct point-by-point comparison on the double differential level. The above-mentioned interpolations (see Section 3.5.2, [Alt06, Alt07]) are indicated by solid curves in Figs 3.5a and 5.1.

On the basis of the p_T-distributions introduced above, double differential pion production ratios were constructed:

$$R_{PbPb/pp} = \frac{d_{PbPb \to \pi^\pm X}}{d_{pp \to \pi^\pm X}} \tag{5.1}$$

where $d_{PbPb \to \pi^\pm X}$ and $d_{pp \to \pi^\pm X}$ are the summed invariant densities of charged pions in Pb+Pb and p+p reactions, respectively:

$$d_{PbPb \to \pi^\pm X} = \left(E \frac{d^3 n}{dp^3} \right)_{PbPb \to \pi^+ X} + \left(E \frac{d^3 n}{dp^3} \right)_{PbPb \to \pi^- X} \tag{5.2}$$

$$d_{pp \to \pi^\pm X} = \left(E \frac{d^3 n}{dp^3} \right)_{pp \to \pi^+ X} + \left(E \frac{d^3 n}{dp^3} \right)_{pp \to \pi^- X} \tag{5.3}$$

It should be emphasized that the ratios $R_{PbPb/pp}$ defined above constitute a convenient tool for comparison of the shape of pion spectra in x_F and p_T in different reactions, and particularly for identifying deviations from conformity. As an example, an *identical* shape of these spectra in Pb+Pb and p+p reactions would correspond to a constant value of $R_{PbPb/pp}$ as a function of x_F and p_T.

An overview of the p_T- and x_F-dependence of $R_{PbPb/pp}$ is presented in Fig. 5.2. Panel **(a)** shows their dependence on p_T, where a clear systematics is present at all considered values of x_F. Starting from $p_T = 0$, the ratio rapidly decreases, down to a well defined minimum localised in an intermediate region of transverse momentum which can be defined here as $\sim$200-600 MeV/c. After passing this minimum, another trend starts which is a continuous increase of $R_{PbPb/pp}$ with p_T. The quantitative size as well as relative importance of the two trends changes with x_F. As such, the x_F-dependence of the minimum as well as that of the low-p_T and higher-p_T parts of the pion distribution have to be discussed separately.

- As apparent in Fig. 5.2b, the minimum exhibits a reasonably flat x_F-dependence; a slight increase towards higher values of x_F is suggested by the data. The typical values of the minimum (30-31 at $x_F \approx 0$) are not far from the number of participant pairs of 27±5.5, estimated for the present sample of peripheral Pb+Pb collisions in Section 3.2.

- The behaviour of the minimum is in sharp contrast with the x_F-dependence of $R_{PbPb/pp}$ at low transverse momentum; an example at $p_T = 0.025$ GeV/c is shown in Fig. 5.2b. Here,
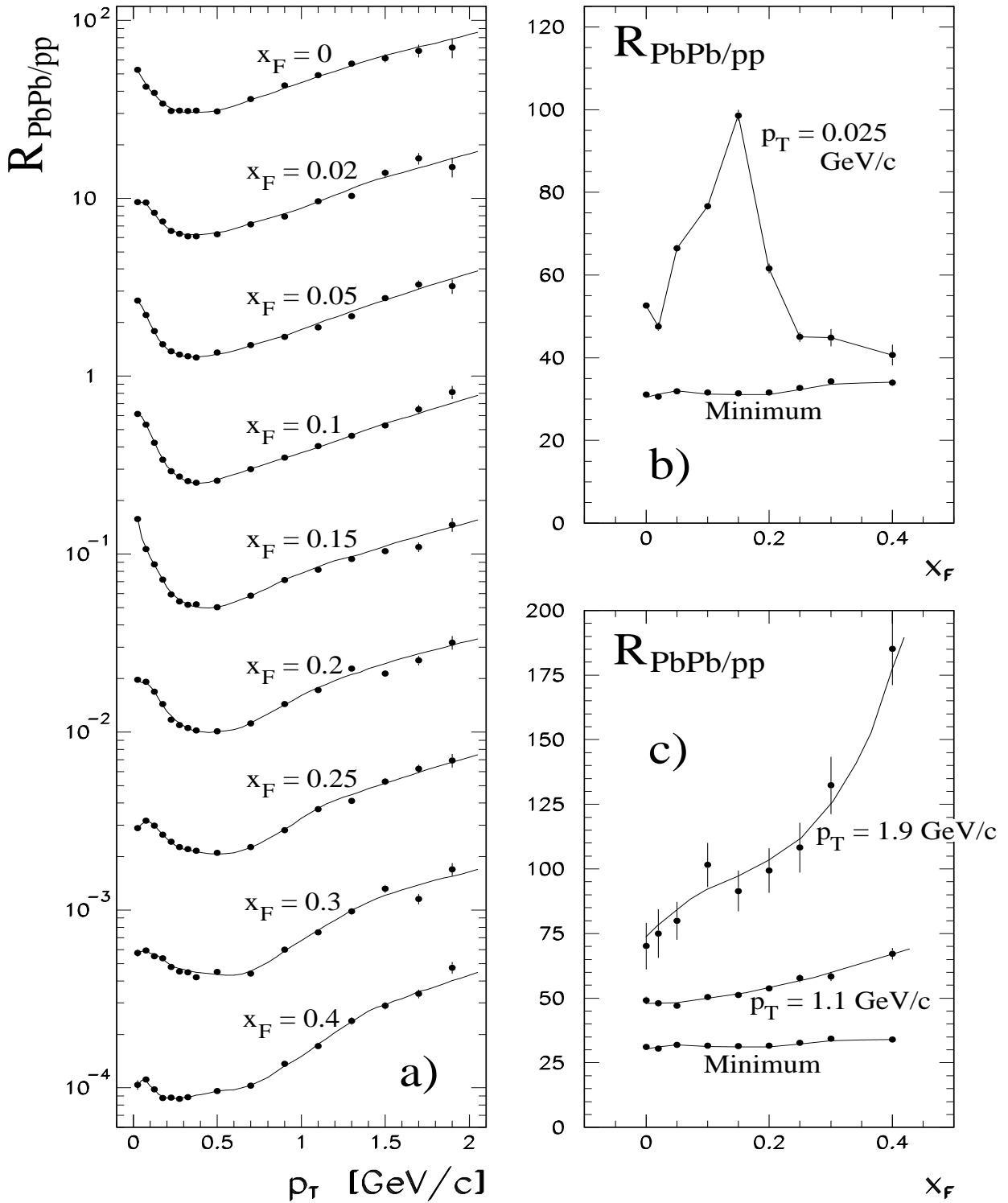
Figure 5.2: Ratio of densities of summed charged pions produced in peripheral Pb+Pb reactions over p+p collisions, **a)** drawn as a function of p_T at fixed values of x_F, **b)** and **c)** drawn as a function of x_F at selected values of p_T, and compared to the minimal value of the same ratio.

Note: the data points and curves in panel **(a)** are subsequently divided by a factor of five to allow for a better visual separation. All the solid curves drawn correspond to the interpolation of the data points as described in the text, with the exception of the x_F-dependence at $p_T = 0.025$ and 1.9 GeV/c where the line connecting points and the curve drawn serve merely to guide the eye.

the enhancement of pion production relative to p+p collisions is always larger than in the minimum. It reaches an apparently sharp maximum at $x_F \approx 0.15$, exceeding the value of the minimum by a factor of three.

- Finally, the x_F-dependence of the ratio at higher transverse momenta is illustrated in Fig. 5.2c for two values of p_T. As apparent from the Figure, pion production at $x_F = 0$ observes a sizeable enhancement in the region of higher p_T if taken relative to the minimum (see also Fig. 5.2a). However, this effect still rapidly increases when moving into the projectile fragmentation region at higher values of x_F. As a result, very large values of $R_{PbPb/pp}$ are attained at highest considered x_F and p_T.

As it can be seen from the description above, the transition from the elementary to the peripheral heavy ion collision results not only in a very large increase of the total multiplicity of produced pions (see Section 3.5.2), but also in a series of modifications of the shape of corresponding distributions. In principle, the main aim of this Chapter was to state and describe this experimental fact, which is apparent as much in the central region near $x_F = 0$ as in the projectile fragmentation region at higher x_F. It seems however worthwhile to present also some comments and enumerate some of the hypotheses aiming at an explanation of the experimentally observed phenomena. This will be made below, again with a distinction between the region of the minimum, the low-p_T and the higher-p_T parts of the spectrum.

5.2 The Minimum at Intermediate Transverse Momenta

The total enhancement of $(\pi^+ + \pi^-)$ production in the present sample of peripheral Pb+Pb collisions is a factor of ~ 38 relative to p+p reactions. It can therefore be seen from Fig. 5.2b that most of this enhancement is already contained in the minimum, where the obtained values vary between 30.5 and 34 depending on x_F. As such, it can be tentatively said that the minimum is representative for *the bulk of pion production*, with the low-p_T and higher-p_T effects being "small additions", characteristic to specific regions of phase space.

In this context, it is interesting to compare what is presented in Fig. 5.2b to what was shown for proton-nucleus reactions in Fig. 2.10c. The pion production ratio in p+C over p+p collisions shown in the latter Figure displayed a smooth, continuous decrease with increasing x_F, starting at 1.6 at $x_F = -0.1$ and going below unity above $x_F = 0.2$. In Section 2.3.2 this was connected with the pile-up of target nucleons suffering single elementary collisions while participating in the p+C reaction, and also with multiple collisions suffered by the proton projectile.

No such trend is visible in Pb+Pb reactions. This is, of course, natural that no asymmetric target nucleon pile-up takes place in a symmetric Pb+Pb reaction, where the projectile and target are equal by definition. However, also above $x_F = 0.2$, the Pb+Pb data give no sign of depletion of pion density which was visible for p+C interactions.

This depletion of density in the far projectile fragmentation region of proton-nucleus interactions has been known since a long time and its interest was pointed out in, e.g., [Fiałkowski83]. According to [Busza88], it would be a manifestation of energy conservation. It can therefore be expected that the apparently different behaviour of Pb+Pb collisions in this respect will bring new insight into the detailed mechanism of energy transfer in projectile fragmentation, in asymmetric as well as symmetric nuclear reactions.

5.3 The Region of Low p_T

The position of the peak in the $R_{PbPb/pp}$ ratio at $x_F \approx 0.15$, shown in Fig. 5.2b, corresponds to low-p_T pions moving at the same velocity as the beam nucleons, see Section 2.3.4 for comparison.

This gives some analogy to the electromagnetic effect induced by the spectator system, discussed in the preceding parts of this paper.

Following the interpretation proposed in [Fischer07, Chvala05], the observed excess of pion production at low transverse momenta would again come from the spectator system. As it is discussed therein, an argument in favour of this hypothesis would come from a comparison between Pb+Pb and proton-nucleus interactions.

An example of such a comparison is given in Fig. 5.3, which shows the p_T-dependence of double differential ratios of pion densities in p+C relative to p+p reactions:

$$R_{pC/pp} = \frac{d_{pC \to \pi^\pm X}}{d_{pp \to \pi^\pm X}} \tag{5.4}$$

Here, $d_{pC \to \pi^\pm X}$ is the summed invariant density of charged pions, analogically to Eqs (5.2), (5.3):

$$d_{pC \to \pi^\pm X} = \left(E\frac{d^3 n}{dp^3} \right)_{pC \to \pi^+ X} + \left(E\frac{d^3 n}{dp^3} \right)_{pC \to \pi^- X} \tag{5.5}$$

As it can be seen from the comparison between Figs 5.2a and 5.3, if no spectator system is present in the projectile hemisphere of the reaction (Fig. 5.3), the p_T-dependence of pion production ratios remains similar to Pb+Pb reactions in the region of higher transverse momenta, but lacks the large, x_F-dependent structure of pion enhancement at low p_T, which was visible in Fig. 5.2a. This suggests that the presence of the spectator system is indeed necessary to explain the behaviour of the Pb+Pb data in the region of low transverse momenta.

As a possible dynamical origin for this effect, the quoted references propose the low-mass excitation of some among the spectator nucleons. Other mechanisms can also be considered, especially towards the central region near $x_F = 0$ where the Pb+Pb data also show some enhancement at low p_T, see Fig. 5.2a. From the above considerations, the most important conclusion would be that in a non-central Pb+Pb reaction, not all the produced pions would originate from the participant zone, but some would come from the spectator system. A first idea on the potential importance of this effect for the present sample of peripheral Pb+Pb collisions can be obtained by integrating the total excess of low-p_T pions present above the minimum in Fig. 5.2a. This gives about 12 % of the total pion yield[1]. It can therefore be expected that this issue may have some impact on the understanding of particle production in Pb+Pb collisions, in particular of its dependence on centrality[2].

5.4 The Region of Higher p$_T$

The effect of modification of transverse momentum spectra in nuclear collisions relative to elementary interactions has been known since a long time. In 1975, it was reported in proton-nucleus reactions where a sizeable enhancement of particle production was observed at high values of p_T [Cronin75, Antreasyan79]. This phenomenon, known as "Cronin effect", was at the time measured in the vicinity[3] of $x_F = 0$, and found to increase with nucleus size. The interest in the Cronin effect has been more recently renewed [Accardi02] due to the experimental finding

---

[1]More detailed methods for estimating this contribution were also proposed [Fischer07].

[2]In the context of the precedent Chapter, it is natural to ask whether the low-p_T effect discussed here could have an electromagnetic origin. Indeed the sum $(\pi^+ + \pi^-)$ is not fully invariant against the electromagnetic distortion of π^+ and π^- spectra, see also [Ambrosini99]. In principle, this could influence the $R_{PbPb/pp}$ ratio from Eq. (5.1) in the region of phase space where the latter electromagnetic distortion is present. However, the Monte Carlo analyses made up to now by the author bring no support to this hypothesis.

[3]In fact the experimental conditions corresponded to x_F values between -0.05 and +0.15, see [Barr07].
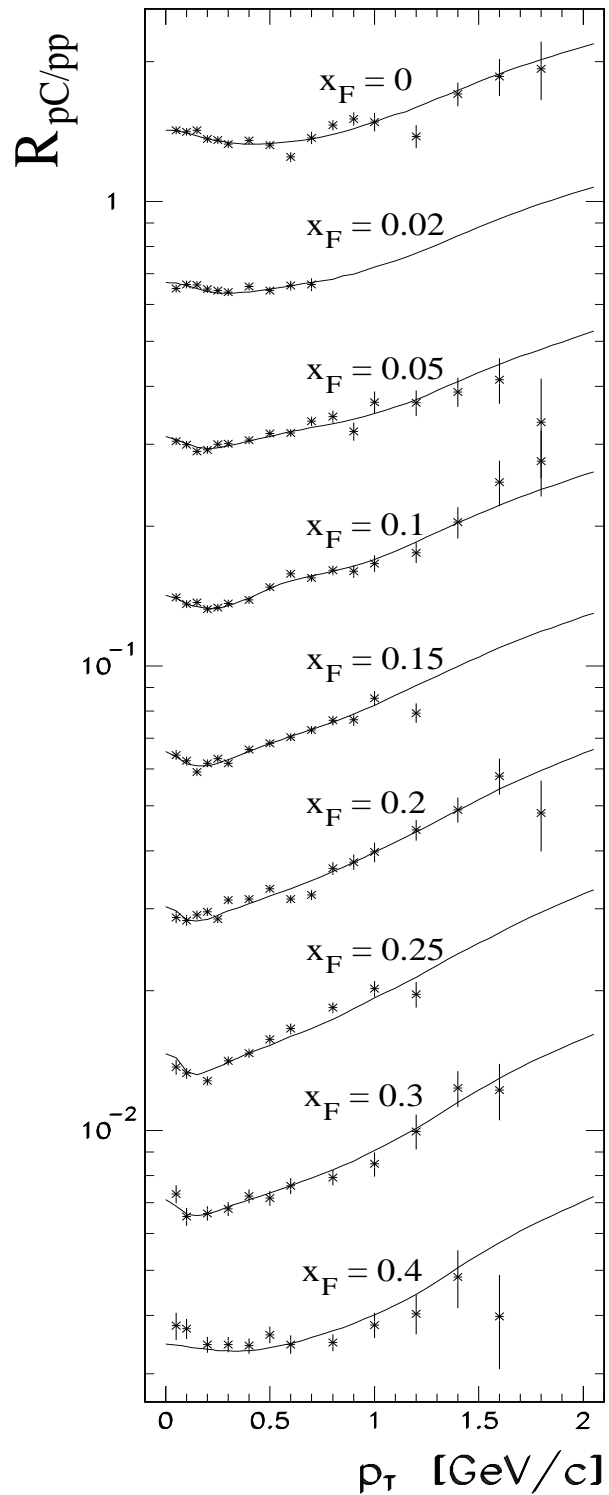
Figure 5.3: Ratio of densities of summed charged pions produced in p+C reactions, over charged pions produced in p+p collisions. The ratios are drawn as a function of p_T at fixed values of x_F. Note: the data points and curves are subsequently divided by a factor of two to allow for a better visual separation. All the solid curves correspond to the ratio of interpolations of double differential charged pion spectra obtained for p+C and p+p collisions, see [Alt07] and [Alt06], respectively.
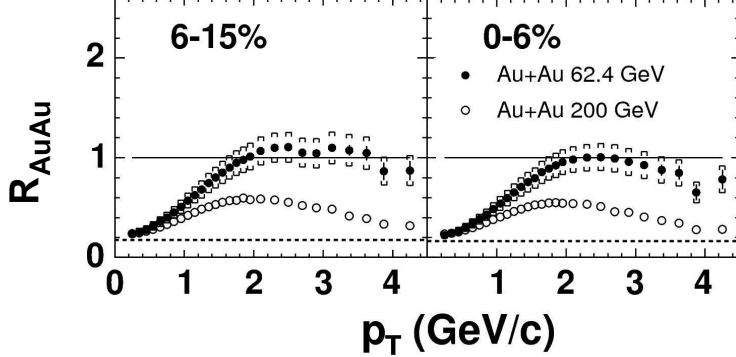
Figure 5.4: Nuclear modification factors in Au+Au collisions at $\sqrt{s_{NN}} = 62.4$ GeV (closed symbols) and $\sqrt{s_{NN}} = 200$ GeV (open symbols), drawn as a function of p_T. The plot is made for summed charged hadrons ($h^+ + h^-$) produced near mid-rapidity ($x_F \approx 0$), for the two most central collision bins as obtained by the PHOBOS experiment. The centrality of the two samples is defined by the percentage of total cross-section indicated in the plot. The solid line corresponds to scaling with N_{coll} (see text) while the dashed line to scaling with the number of participant pairs ($N_{part}/2$). Both panels are taken from [Trzupek06].

made by RHIC experiments, of the depletion of the "nuclear modification factor" in Au+Au collisions,

$$R_{AuAu} = \frac{1}{<N_{coll}>} \frac{d^2 n_{AuAu}/dp_T d\eta}{d^2 n_{NN}/dp_T d\eta} \qquad (5.6)$$

below unity. In the above equation, $<N_{coll}>$ is the average total number of "binary" nucleon-nucleon collisions in the Au+Au event, while $d^2 n_{AuAu}/dp_T d\eta$ and $d^2 n_{NN}/dp_T d\eta$ are the densities of particles produced in Au+Au and elementary nucleon-nucleon reactions (in practice, p+p or p+$\bar{p}$ interactions). Following the expectation that particle production at high transverse momenta corresponded to "hard" (perturbative) parton scattering processes, a "normal superposition" of elementary collisions was assumed to scale with N_{coll}, yielding by construction $R_{AuAu} = 1$. As such, the depletion of R_{AuAu} for high-p_T particles, Fig. 5.4, was interpreted as resulting from the formation of a strongly coupled nuclear medium, a *strongly coupled Quark-Gluon Plasma* [Trzupek06, Bnl05, Accardi02].

The above issues build a very rich phenomenology which remains far beyond the scope of the present paper, centered on "soft" rather than "hard" processes. A detailed discussion has to await a separate publication. However, the experimental data presented in Fig. 5.2 call for at least a few basic remarks. These will be made below.

Similarly to the preceding Sections, the discussion below will be based on the purely experimental and model-independent ratios $R_{PbPb/pp}$ and $R_{pC/pp}$ defined in Eqs. (5.1) and (5.4), respectively. For the purpose of an easier comparison between Figs 5.2 and 5.4, it can in principle be said that the "nuclear modification factor" for the present peripheral Pb+Pb sample would correspond to $\frac{R_{PbPb/pp}}{<N_{coll}>}$, where $<N_{coll}>\approx 64\pm18$ (estimated similarly to the other centrality parameters, Section 3.2). It should however be underlined that the latter "nuclear modification factor", constructed as a measure of scaling with N_{coll}, has no direct applicability in any region of phase space where non-perturbative effects dominate.

1. If viewed relative to the existing experimental data gathered on the nuclear modification of p_T spectra, the information contained in Fig. 5.2 is only partially complementary. Being limited to the region $0 \leq p_T \leq 2$ GeV/c, the latter Figure displays only the "softer part" of the transverse momentum distribution. In particular, the region of decrease of R_{AuAu} with increasing p_T, Fig. 5.4, remains beyond the p_T range available for the present analysis of

peripheral Pb+Pb reactions. On the other hand, this analysis has the important advantage of exploring the "longitudinal dimension" of the effect measured mostly[4] in the vicinity of $x_F = 0$.

2. The scrutiny of this "longitudinal dimension" (x_F-dependence), made by means of Fig. 5.2, panels **(a)** and **(c)**, reveals a characteristic pattern. The enhancement of pion production at higher p_T in the central region ($x_F = 0$, Fig. 5.2a) resembles what was shown in Fig. 5.4, but occupies no special position relative to the projectile fragmentation region where this effect is in fact much larger (and largely exceeds N_{coll}-scaling at high x_F, which is similar to the original "Cronin effect" in the region of p_T above 2-3 GeV/c [Antreasyan79, Blume07a]). Such a smooth transition between the projectile fragmentation and the central region was characteristic of the *two-component picture* hypothesis discussed in Section 2.3.2, where particle production in the central region was the effective result of the overlay of projectile and target fragmentation, see Fig. 2.9e (also Figs 2.7b and 2.5).

3. The above situation is quite similar to that resulting from a very detailed study of p+C reactions, where the two-component fragmentation hypothesis was also applied [Barr07]. The above-mentioned p+C data, shown in Fig. 5.3, can indeed be claimed to display a qualitative similarity to the Pb+Pb reactions presented in Fig. 5.2a. This takes place in spite of the dramatic difference in participant system size ($\sim$3 participant nucleons in p+C reactions, relative to 54±11 in peripheral Pb+Pb collisions). This suggests that the increased depth of nuclear matter traversed by the projectile nucleon (multiple collisions, Section 2.3.5), an effect which is present already in p+C interactions, plays an important role also in Pb+Pb reactions.

4. In the particular context of 2. and 3., it is of course of great interest which part of the transverse momentum distribution is the region of applicability of notions developed for the description of "soft" processes (like the above-mentioned two-component fragmentation picture), and which should be ascribed to "hard" phenomena. Up to now, analyses based on the two-component fragmentation picture were applied to p_T distributions up to about 2 GeV/c [Fischer03, Chvala06, Barr07]. Also, theoretical explanations of the Cronin effect were based as much on "soft" as on "hard" dynamical mechanisms [Accardi02]. On the other hand, for a delimitation of a "hard" process, [Accardi02] claims "hard" scattering to occur for 1 GeV or more exchanged momentum. [Bartke09] gives the limit $p_T \geq 2-3$ GeV/c. [Barr07] gives a criticism of these notions, pointing also at the important role of resonances in building the p_T-spectrum (see Section 2.3.3, Figs 2.13b and 2.15b). The latter reference also indicates resonance decays as a potential source for the modification of p_T-distributions in nuclear reactions, via a shift in the parent resonance mass spectrum towards higher masses, induced by multiple collisions of the incoming nucleon.

5.5   Closing Comment

The set of very basic remarks given above can, at best, serve as a start-up for a more detailed assessment of the experimental information obtained in Chapter 3. It seems clear that such an assessment could contribute to the general discussion on the influence of the transition from the elementary (nucleon-nucleon) to the nuclear (heavy ion) environment on the spectra of produced particles. While limited to the region $p_T \leq 2$ GeV/c, it also seems clear from the above that the present dataset could bring valuable highlights on the interplay between the "soft" phenomena

---

[4]Note: measurements exist also off mid-rapidity but these correspond to quite a limited x_F range at top RHIC energy. For instance, the rapidity limit of 3.2 units for the BRAHMS experiment [Arsene04] corresponds to $x_F = 0.1$ at $p_T = 0.8$ GeV/c and to $x_F = 0.25$ at $p_T = 2$ GeV/c (see [Barr07]).

discussed in this paper and the region of presently very high interest in heavy ion collision studies, which is the region of nuclear suppression at high p_T.

On the other hand, it can nevertheless be said that the overall picture emerging from this Chapter, as well as from Chapter 4, is that of the Pb+Pb reaction being a "mixture" of different effects: participant fragmentation, spectator system, higher-p_T phenomena, electromagnetic interactions, etc. This is in particular valid also in the projectile fragmentation region which appears as a promising area for the delimitation and identification of these different effects.

Chapter 6

Summary and Conclusions

The aim of this paper was to give a comprehensive description of several phenomena present in the "soft" sector of particle production in elementary and nuclear reactions at high energies. Particular attention was devoted to peripheral heavy ion collisions in the SPS energy regime which, in the author's opinion, constitute a valuable "laboratory" for studies of specific effects induced by the strong and the electromagnetic interaction. These peripheral reactions were analysed in the context of various earlier findings on different characteristics of hadron-hadron, hadron-nucleus and nucleus-nucleus interactions.

The specific choice of kinematic variables used in most of this study (x_F, p_T), the phase space coverage of the considered experimental datasets, and finally the nature of the investigated phenomena, placed the main interest of this analysis in the projectile fragmentation region of particle production (say, $x_F > 0.1$). However, the central region $(x_F = 0)$ was, as a rule, an inherent part of this analysis. Usually, the considered trends in the data displayed a continuous evolution between the central and the fragmentation regions.

Finally, attempts were made to isolate general as well as specific similarities in particle production in different reaction types, in particular between elementary and nuclear collisions. This was inspired by the general belief that the presence of such similarities may indicate specific general features of the non-perturbative process, which may serve as a valuable input for future analyses.

Attempts at a partial synthesis of the presented results were made in the Chapters of this paper. Below, a set of more general remarks will be made, limited to the subjects which the author thinks most interesting for consideration in view of future studies.

(1a) Various studies on elementary and nuclear reactions suggest the possibility of formulating a two-component picture of longitudinal spectra of baryons and produced particles. Here, a certain similarity can be claimed between the studies of RHIC data made by means of the Wounded Nucleon and "Wounded Quark-Diquark" Models, and the comparative experimental analyses of proton- and pion-induced elementary and nuclear reactions made in the SPS energy regime. Following this general picture, a basic connection would exist between the initial and final state of the reaction: the regions of high absolute x_F in the projectile and target hemispheres would correspond respectively to the projectile and target fragmentation, while the central region at $x_F \approx 0$ would be the region of overlap between these two.

(1b) As far as the fragmentation of the projectile in nucleus-nucleus reactions is concerned, the above picture would imply the presence of isospin effects resulting from a summed proton and neutron participant fragmentation, with a predictable influence on final state π^+/π^- ratios. Also, the increased thickness of nuclear matter traversed by the projectile might modify the spectra resulting from its fragmentation relative to elementary nucleon-nucleon

collisions. Seen in this context, the double differential analysis of pion production ratios in Pb+Pb over p+p collisions ($R_{PbPb/pp}$) made at SPS energies in Chapter 5 shows that the transition from the elementary to the heavy ion reaction results in an x_F-dependent pattern of "transverse activity", with some similarity between Pb+Pb and p+C reactions. The same analysis suggests a specific difference in the longitudinal evolution of symmetric Pb+Pb relative to asymmetric proton-nucleus interactions. In the latter case of a single projectile nucleon colliding with many target nucleons, a depletion of particle production is known to be present at high x_F. No sign of such depletion is visible for Pb+Pb reactions, where the numbers of colliding projectile and target nucleons are equal.

(2a) An important item in this paper was the hope to exploit the presence of the spectator system in the peripheral heavy ion reaction to obtain new information on the non-perturbative process of particle production. In the author's opinion, this hope is at least partially fulfilled. Once visualized as the (x_F, p_T)-dependence of π^+/π^- ratios, the experimental data can be reasonably described by a superposition of two effects: a smooth decrease with x_F induced by the excess of neutrons in the Pb nucleus, and a spectator-induced electromagnetic distortion. The latter distortion can be fairly described by an extremely simple relativistic model (which may seem quite surprising in view of the potential complexity of the nuclear reaction).

(2b) On the basis of **(2a)**, some confidence can be attributed to the general phenomenological conclusions drawn on the basis of the very simple model mentioned above. Specifically, this model clearly predicts a sensitivity of final state π^+/π^- ratios, distorted by the spectator charge, to the initial conditions imposed on pion emission like the pion emission time or the position of the pion formation site relative to that of the spectator system. As such, the electromagnetic effect could indeed provide new information on the space-time evolution of the pion production process. This is particularly valid for pions at high x_F (e.g., $x_F \approx 0.4$), which are most sensitive to the imposed initial conditions.

(2c) There is also good reason to believe that the spectator-induced electromagnetic effect on final state π^+/π^- ratios will be sensitive to the fragmentation of the spectator system. As such, it could provide information about this process on time scales characteristic to pion propagation in its vicinity. Additionally, the basic kinematical characteristics of the same effect on final state ratios of charged kaons have been analysed. As follows from this introductory study, a qualitative similarity of the main features of the latter effect to the effect shown for pions is to be expected, but the bulk of the distortion of K^+/K^- ratios and the region of main sensitivity to initial conditions will both be shifted in the direction of very large $|x_F|$.

(2d) Account taken of the extremely simple phenomenological approach applied to study the spectator-induced electromagnetic effect in Chapter 4, it is still difficult to state whether the latter effect can be used to obtain fully model-independent information on the space-time evolution of the nuclear reaction. While the construction of a more detailed Monte Carlo apparatus can surely be considered, it also seems clear that the latter effect could provide valuable constraints for "microscopic" Monte Carlo generators, in particular in the fragmentation region at high $|x_F|$.

(3) On top of the electromagnetic effect discussed above, another important aspect of the space-time evolution of the particle production process is the problem of hadronic resonances. Several studies in hadron-hadron collisions indicate that resonance decays constitute an important, dominant mechanism directly underlying the production of final state particles, and playing its role also in e.g. baryon stopping effects. As such, also in nuclear

reactions, the role of resonance production calls for a closer scrutiny. This specifically applies to the longitudinal and transverse evolution of particle production in proton-nucleus and nucleus-nucleus reactions discussed in this paper. Issues such as the influence of multiple collisions on baryonic resonance production in view of baryon stopping processes, or multi-step resonance cascading decays, also require further investigation at both theoretical and experimental levels. Finally, the hypothesis of low-mass excitations of spectator nucleons as source of the low-p_T enhancement of pion production in the fragmentation region of peripheral Pb+Pb collisions, proposed in [Fischer07, Chvala05], calls for a detailed verification in view of future studies.

(4) Following the methodological postulates **1.**, **2.**, **3.**, formulated in Chapter 1, the various analyses presented in this paper attempted to make full use of the extended coverage and versatility of the available datasets. In view of the discussions of experimental aspects made in Chapters 2 and 3, it would seem that the studies discussed here would favour fixed target experiments at relatively moderate collision energies (of the type of NA49 at the SPS). Ensuring the simultaneous combination of extended x_F coverage, good acceptance at low p_T, and precise particle identification seems easier for such experiments. It should however be remembered that the ability of collider experiments to measure simultaneously the projectile and target hemispheres of the collision, like PHOBOS at RHIC, gave a very important advantage in specific studies made in Chapter 2. In view of future experimental studies of the effects discussed in this paper, various suggestions (high x_F acceptance, centrality dependence, etc) were already presented in precedent Chapters. It should however be added that a statistics decisively higher than the relatively moderate event sample available for the present analysis of peripheral Pb+Pb collisions, Chapter 3, would evidently give the possibility of a much more detailed scrutiny of the interplay between the strong and the electromagnetic interaction.

As a final remark, the author wishes to point at the "cross-connected" character of the present study, which was continuously faced with the interplay of different effects acting in the high energy nuclear reaction. This specific feature seems to be a common aspect of the soft sector of multiparticle production in hadronic and nuclear interactions. In the author's personal opinion, this is exactly what makes soft hadronic physics so much exciting. It is only to be hoped that the analysis presented in this paper may be of some help in future studies in this field.

Acknowledgements

I wish to express my deep gratitude to Dr Hans Gerhard Fischer for his inspiring guidance and continuous scientific support over many years of collaboration, as well as for his decisive role in the experimental effort of soft hadron studies. Together with him, I wish to acknowledge all the other people involved in the experimental analysis of peripheral Pb+Pb reactions: Dr Latchezar Betev, Dr Ondrej Chvala, Dr Michal Kreps, Dr Martin Makariev, Dimitar Panayotov, Victor Trubnikov, Dr Dezso Varga, and Dr Siegfried Wenig.

Equally warmly, I wish to thank Prof. Antoni Szczurek for our common phenomenological work on electromagnetic effects, as well as for his moral support and useful practical advice. I also wish to thank Dr Andrzej Górski and Dr Ewa Kozik for their help in specific parts of this work.

I am most indebted to all the people who helped with the realization of this paper by their attention, discussion, encouragement, and friendly advice. Most of all, I wish to thank Prof. Jerzy Bartke, Prof. Helena Białkowska, Dr Piotr Bożek, Prof. Wit Busza, Dr Adam Bzdak, Prof. Jan Figiel, Prof. Roman Hołyński, Prof. Marek Jeżabek, Dr Marek Kowalski, Prof. Leonard Leśniak, Prof. Adam Maj, Beata Murzyn, Dr Grażyna Nowak, Prof. Maria Różańska, Prof. Jan Styczeń, Dr Agnieszka Trzcińska, Dr Adam Trzupek, Prof. Jacek Turnau, and Prof. Barbara Wosiek. I also wish to thank Prof. Johanna Stachel, whose critical remark after one of my talks proved most inspiring for this analysis.

A large part of the study presented here has been realized within the framework of the NA49 experiment. I wish to thank the Collaboration for the possibility to use NA49 data. I am also very grateful to all its members for the pleasure I had in working with them, and for the help which I have received. In particular, I would like to thank the NA49 spokesperson, Prof. Peter Seyboth, for his continuous friendly attitude, as well as Prof. Christoph Blume for his very valuable help in specific parts of this analysis.

Finally, I wish to thank my family: my parents, for all their love, my brother, for his proof-reading effort, my daughter Hania and my son Antoni for their powerful moral support. Most of all, I wish to thank my wife Elżbieta for her love, understanding and patient encouragement.

Bibliography

[Aamodt10]   ALICE Collab., K. Aamodt, (A. Rybicki) *et al.*, arXiv:1006.5432 [hep-ex].

[Accardi02]   A. Accardi, arXiv:hep-ph/0212148.

[Adams05]   STAR Collab., J. Adams *et al.*, Nucl. Phys. A **757** (2005) 102.

[Adcox05]   PHENIX Collab., K. Adcox *et al.*, Nucl. Phys. A **757** (2005) 184.

[Afanasiev99]   NA49 Collab., S. Afanasiev, (A. Rybicki) *et al.*, Nucl. Instrum. Meth. A **430** (1999) 210.

[Afanasiev02]   NA49 Collab., S. V. Afanasiev, (A. Rybicki) *et al.*, Phys. Rev. C **66** (2002) 054902.

[Aguilar-Benitez91] LEBC-EHS Collab., M. Aguilar-Benitez *et al.*, Z. Phys. C **50** (1991) 405.

[Ahle98]   E802 Collab., L. Ahle *et al.*, Phys. Rev. C **57** (1998) R466.

[Aivazian89]   NA22 Collab., V. V. Aivazian *et al.*, Z. Phys. C **42** (1989) 533.

[Alessandro06]   ALICE Collab., G. Alessandro, (A. Rybicki) *et al.*, J. Phys. G **32**, 1295 (2006).

[Alt06]   NA49 Collab., C. Alt, (A. Rybicki) *et al.*, Eur. Phys. J. C **45**, 343 (2006).

[Alt07]   NA49 Collab., C. Alt, (A. Rybicki) *et al.*, Eur. Phys. J. C **49** (2007) 897, and references therein.

[Alt08]   NA49 Collab., C. Alt, (A. Rybicki) *et al.*, Phys. Rev. C **77** (2008) 034906.

[Ambrosini99]   NA52 Collab., G. Ambrosini *et al.*, New Jour. Phys. **1** (1999) 23.

[Ambrosini99a]   NA56/SPY Collab., G. Ambrosini *et al.*, Eur. Phys. J. C **10** (1999) 605; Phys. Lett. B **420** (1998) 225.

[Amsler08]   C. Amsler *et al.*, Phys. Lett. B **667**, 1 (2008), available on the PDG WWW pages (URL: http://pdg.lbl.gov/)

[Anticic09]   NA49 Collab., T. Anticic, (A. Rybicki) *et al.*, Phys. Rev. C **80** (2009) 034906.

[Anticic10]   NA49 Collab., T. Anticic, (A. Rybicki) *et al.*, Eur. Phys. J. C **65**, (2010) 9.

[Anticic10a]   NA49 Collab., T. Anticic, (A. Rybicki) *et al.*, Eur. Phys. J. C **68**, (2010) 1.

[Antreasyan79]   D. Antreasyan *et al.*, Phys. Rev. D **19**, 764 (1979).

[Appelshäuser98] NA49 Collab., H. Appelshäuser, (A. Rybicki) *et al.*, Eur. Phys. J. A **2** (1998) 383.

[Arsene04]   BRAHMS Collab., I. Arsene *et al.*, Phys. Rev. Lett. **93**, 242303 (2004).

[Arsene05]   BRAHMS Collab., I. Arsene *et al.*, Nucl. Phys. A **757** (2005) 1.

[Ayala97]   A. Ayala, J. Kapusta, Phys. Rev. C **56** (1997) 407.

[Ayala99]   A. Ayala, S. Jeon, J. Kapusta, Phys. Rev. C **59** (1999) 3324.

[Babecki78]   J. Babecki and G. Nowak, Acta Phys. Pol. B **9**, 401 (1978).

[Back05]   PHOBOS Collab., B. B. Back *et al.*, Nucl. Phys. A **757**, 28 (2005).

[Back06]   PHOBOS Collab., B. B. Back *et al.*, Phys. Rev. C **74** (2006) 021902.

[Barr07]   G. Barr, O. Chvala, H. G. Fischer, M. Kreps, M. Makariev, C. Pattison, A. Rybicki, D. Varga, S. Wenig, Eur. Phys. J. C **49** (2007) 919.

[Barrette92]   E814 Collab., J. Barrette *et al.*, Phys. Rev. C **45** (1992) 819.

[Bartke09]   J. Bartke, "Introduction to Relativistic Heavy Ion Physics," Hackensack, USA: World Scientific (2009), and references therein.

[Barton83]   D. S. Barton *et al.*, Phys. Rev. D **27**, 2580 (1983).

[Barz98]	H. W. Barz, J. P. Bondorf, J. J. Gaardhoje and H. Heiselberg, Phys. Rev. C **57** (1998) 2536.
[Bächler99]	NA49 Collab., J. Bächler, (A. Rybicki) *et al.*, Nucl. Phys. A **661** (1999) 45c.
[Bearden03]	BRAHMS Collab., I. G. Bearden *et al.* Phys. Rev. Lett. **93**, 102301 (2004).
[Beneson79]	W. Beneson *et al.*, Phys. Rev. Lett. **43** (1979) 683.
[Białas76]	A. Białas, M. Bleszyński and W. Czyż, Nucl. Phys. B **111** (1976) 461.
[Białas05]	A. Białas and W. Czyż, Acta Phys. Polon. B **36**, 905 (2005).
[Białas07]	A. Białas and A. Bzdak, Phys. Lett. B **649**, 263 (2007).
[Białkowski71]	G. Białkowski, R. Sosnowski, "Cząstki elementarne", Państwowe Wydawnictwo Naukowe, Warszawa 1971 (*in Polish*).
[Białkowski72]	G. Białkowski, R. Sosnowski, "Reggego metoda", and G. Białkowski, R. Sosnowski, S. Gąsiorowicz, "Reggego model", in: "Encyclopaedia of Physics", Państwowe Wydawnictwo Naukowe, Warszawa 1972 (*in Polish*).
[Blume07]	C. Blume, NA49 Collab., J. Phys. G **34** (2007) S951.
[Blume07a]	C. Blume, Nucl. Phys. A **783** (2007) 65.
[Bnl05]	BNL-73847-2005 Formal Report, and references therein.
[Bobbink82]	G. J. Bobbink *et al.*, Nucl. Phys. B **204** (1982) 173.
[Bonasera87]	A. Bonasera and G. F. Bertsch, Phys. Lett. B **195** (1987) 521.
[Brahms10]	BRAHMS Collab., "The acceptance versus rapidity and transverse momentum", http://www4.rcf.bnl.gov/brahms/WWW/brahms.html
[Brandt64]	S. Brandt, Ch. Peyrou, R. Sosnowski and A. Wróblewski, Phys. Lett. **12** (1964) 57.
[Busza84]	W. Busza and A. S. Goldhaber, Phys. Lett. B **139**, 235 (1984).
[Busza88]	W. Busza and R. Ledoux, Ann. Rev. Nucl. Part. Sci. **38** (1988) 119.
[Bzdak08]	A. Bzdak, private communication, 2008.
[Capella94]	A. Capella, U. Sukhatme, C. I. Tan and J. Tran Thanh Van, Phys. Rept. **236** (1994) 225.
[Chekanov03]	ZEUS Collab, S. Chekanov *et al.*, Nucl. Phys. B **658** (2003) 3.
[Chemakin99]	E910 Collab., I. Chemakin *et al.*, Phys. Rev. C **60** (1999) 024902, and references therein.
[Chvala04]	O. Chvala, NA49 Collab., Eur. Phys. J. C **33** (2004) S615.
[Chvala05]	O. Chvala, NA49 Collab., Nucl. Phys. A **749**, 304 (2005).
[Chvala06]	O. Chvala, Ph.D. Thesis, Charles University, Prague, 2006.
[Cooper99]	G. E. Cooper, NA49 Collab., Nucl. Phys. A **661** (1999) 362c.
[Cronin75]	J. W. Cronin, H. J. Frisch, M. J. Shochet, J. P. Boymond, R. Mermod, P. A. Piroue and R. L. Sumner, Phys. Rev. D **11** (1975) 3105.
[Cugnon81]	J. Cugnon and S. E. Koonin, Nucl. Phys. A **355** (1981) 477.
[Daté85]	S. Daté, M. Gyulassy and H. Sumiyoshi, Phys. Rev. D **32**, 619 (1985).
[Dainese06]	A. Dainese *et al.*, NA57 Collab., Nucl. Phys. A **774** (2006) 51.
[Deines-Jones00]	P. Deines-Jones *et al.*, Phys. Rev. C **62** (2000) 014903.
[Drijard84]	D. Drijard *et al.*, Z. Phys. C **21** (1984) 321.
[Fermi51]	E. Fermi, Progr. Theor. Phys. **5** (1951) 570; Phys. Rev. **81** (1951) 683.
[Feynman69]	R. P. Feynman, Phys. Rev. Lett. **23** (1969) 1415.
[Fiałkowski83]	K. Fiałkowski and W. Kittel, Rept. Prog. Phys. **46** (1983) 1283.
[Fischer02]	H. G. Fischer, NA49 Collab., Acta Phys. Polon. B **33** (2002) 1473.
[Fischer03]	H. G. Fischer, NA49 Collab., Nucl. Phys. A **715**, 118c (2003), and references therein.

[Fischer05]	H. G. Fischer *et al.*, CERN/SPSC 2005-035, http://spshadrons.web.cern.ch/spshadrons/doc/SPSC2005talk.pdf.
[Fischer07]	H. G. Fischer *et al.*, CERN/SPSC 2007-031, http://spshadrons.web.cern.ch/spshadrons/doc/SPSC2007talk.pdf.
[Fredriksson84]	S. Fredriksson, G. Eilam, G. Berlad and L. Bergstrom, "High-Energy Collisions With Atomic Nuclei. Part 1," TRITA-TFY-84-06, May 1984.
[Fricke95]	G. Fricke, C. Bernhardt, K. Heilig, L. A. Schaller, L. Schellenberg, E. B. Shera and C. W. de Jager, Atom. Data Nucl. Data Tabl. **60** (1995) 177.
[Friedländer62]	E. M. Friedländer, Phys. Lett. **2** (1962) 38.
[Glauber06]	R. J. Glauber, Nucl. Phys. A **774** (2006) 3, and references therein.
[Geant5013]	"GEANT, Detector Description and Simulation Tool", CERN Program Long Writeup W5013.
[Grässler78]	H. Grässler *et al.*, Nucl. Phys. B **132** (1978) 1.
[Gyulassy81]	M. Gyulassy and S.K. Kauffmann, Nucl. Phys. A **362** (1981) 503.
[Gyulassy94]	M. Gyulassy and X.-N. Wang, Comput. Phys. Commun. **83** (1994) 307.
[Hagedorn84]	R. Hagedorn, Riv. Nuovo Cim. **6N10** (1984) 1, and references therein.
[Hegab81]	M. K. Hegab and J. Hufner, Phys. Lett. B **105**, 103 (1981); M. K. Hegab and J. Hufner, Nucl. Phys. A **384**, 353 (1982).
[Heinz00]	U. W. Heinz and M. Jacob, arXiv:nucl-th/0002042.
[Jackson64]	J. D. Jackson, Nuovo Cim. **34** (1964) 1644.
[Jancso77]	G. Jancso *et al.*, Nucl. Phys. B **124** (1977) 1, and references therein.
[Karnaukhov06]	V. A. Karnaukhov *et al.*, Phys. Atom. Nucl. **69**, 1142 (2006), and references therein.
[Koch86]	P. Koch, B. Müller and J. Rafelski, Phys. Rept. **142**, 167 (1986).
[Kowalski10]	ALICE Collab., M. Kowalski *et al.*, Proc. Cracow Epiphany Conference on Physics in Underground Laboratories and Its Connection with LHC, Kraków, 5-8 January 2010, to appear in Acta Phys. Polon. B.
[Kreps04]	M. Kreps, Ph.D. Thesis, Comenius Univ., Bratislava, 2004 *(in Slovakian)*.
[Lacasse96]	R. Lacasse *et al.*, E877 Collab., Nucl. Phys. A **610** (1996) 153c.
[Laszlo07]	A. Laszlo, Ph. D. Thesis, KFKI Research Institute for Particle and Nuclear Physics, Budapest, 2007.
[Li95]	B.-A. Li, Phys. Lett. B **346** (1995) 5.
[Libbrecht79]	K. G. Libbrecht and S. E. Koonin, Phys. Rev. Lett. **43** (1979) 1581.
[Makariev07]	M. Makariev, NA49 Collab., AIP Conf. Proc. **899** (2007) 203.
[Matyja09]	A. Matyja, PoS(EPS-HEP 2009) 128.
[Mizutori00]	S. Mizutori, J. Dobaczewski, G. A. Lalazissis, W. Nazarewicz and P. G. Reinhard, Phys. Rev. C **61**, 044326 (2000).
[Mrówczyński98]	S. Mrówczyński, Acta Phys. Polon. B **29** (1998) 3711.
[Nouicer04]	PHOBOS Collab., R. Nouicer *et al.*, J. Phys. G **30** (2004) S1133.
[Offermann91]	E. A. J. M. Offermann *et al.*, Phys. Rev. C **44** (1991) 1096.
[Osada96]	T. Osada, S. Sano, M. Biyajima and G. Wilk, Phys. Rev. C **54** (1996) 2167.
[Pawłowski04]	P. Pawłowski and A. Szczurek, Phys. Rev. C **70** (2004) 044908.
[Perkins89]	D. H. Perkins, "Introduction to High-Energy Physics," Polish edition: Państwowe Wydawnictwo Naukowe, Warszawa 1989 *(in Polish)*.
[Rafelski82]	J. Rafelski and B. Müller, Phys. Rev. Lett. **48**, 1066 (1982).
[Różańska91]	M. Różańska, Institute of Nuclear Physics Report 1524/PH, Kraków, 1991 *(in Polish)*.
[Rybicki00]	A. Rybicki, NA49 Collab., CERN Heavy Ion Forum, 18 Oct. 2000.

[Rybicki02]	A. Rybicki, Ph. D. Thesis, Institute of Nuclear Physics, Kraków, 2002, CERN-THESIS-2003-005.
[Rybicki02a]	A. Rybicki *et al.*, NA49 Collab., Acta Phys. Polon. B **33** (2002) 1483.
[Rybicki04]	A. Rybicki, J. Phys. G **30** (2004) S743.
[Rybicki04a]	A. Rybicki, J. Phys. G **30** (2004) S411.
[Rybicki04b]	A. Rybicki, Acta Phys. Polon. B **35** (2004) 145.
[Rybicki06]	A. Rybicki, Report no. 1976/PH, H. Niewodniczański Institute of Nuclear Physics, Polish Academy of Sciences, Kraków 2006.
[Rybicki07]	A. Rybicki, A. Szczurek, Phys. Rev. C **75** (2007) 054903.
[Rybicki07a]	A. Rybicki, Int. J. Mod. Phys. A **22** (2007) 659.
[Rybicki09]	A. Rybicki, PoS(EPS-HEP 2009) 031.
[Rybicki09a]	A. Rybicki, Int. J. Mod. Phys. A **24**, 385 (2009).
[Schmidt03]	R. Schmidt *et al.*, Phys. Rev. C **67** (2003) 044308.
[Sick82]	I. Sick, Phys. Lett. B **116** (1982) 212, and references therein.
[Strzałkowski78]	A. Strzałkowski, "Wstęp do fizyki jądra atomowego", Państwowe Wydawnictwo Naukowe, Warszawa 1978 *(in Polish)*.
[Sullivan82]	J.P. Sullivan *et al.*, Phys. Rev. C **25** (1982) 1499.
[Szczurek07]	A. Szczurek, A. Rybicki, A. Z. Górski, J. Phys. G **34** (2007) S827.
[Szymański06]	P. Szymański, Report SINS-31/II, Institute for Nuclear Studies, Świerk, 2006.
[Trzcińska01]	A. Trzcińska, Ph.D. Thesis, Heavy Ion Laboratory, Warsaw University, 2001 (*in Polish*).
[Trzcińska01a]	A.Trzcińska *et al.*, Phys. Rev. Lett **87** (2001) 082501.
[Trzupek06]	A. Trzupek, Report no. 1983/PH, H. Niewodniczański Institute of Nuclear Physics, Polish Academy of Sciences, Kraków 2006.
[Varga04]	D. Varga, NA49 Collab., Eur. Phys. J. C **33** (2004) 515.
[Werner93]	K. Werner, Phys. Rept. **232** (1993) 87.
[Xu96]	N. Xu *et al.*, NA44 Collab., Nucl. Phys. A **610** (1996) 175c, and references therein.
[Yagoda52]	H. Yagoda, Phys. Rev. **85** (1952) 891.